A Novel Approach for Rapid Metal Dissolution

Masters Thesis

Submitted to the Faculty of Graduate Studies in partial fulfillment of the requirements of the Degree of Master of Science

University of Manitoba
Winnipeg, Manitoba
Canada

Michael Richard Carlson Boileau

THE UNIVERSITY OF MANITOBA

FACULTY OF GRADUATE STUDIES

*****

COPYRIGHT PERMISSION

A Novel Approach for Rapid Metal Dissolution

BY

Michael Richard Carlson Boileau

A Thesis/Practicum submitted to the Faculty of Graduate Studies of The University of Manitoba in partial fulfillment of the requirement of the degree

Master Of Science

Dedicated to Spike and Banjo

Ship It!

Acknowledgments

I would like to thank everyone who helped me, especially my mother and father who stood by and supported me from the beginning and all my friends. In particular, I would like to thank my supervisor, Douglas Goltz from the University of Winnipeg who taught me to believe in myself and not to underestimate the difficulties in filling up a volumetric flask. I would also like to thank Dr. Mike Attas and Linda Brown from Atomic Energy of Canada Limited (AECL) for the SEM and ED-XRF images and spectra, Dr. Mike Hinds from the Royal Canadian Mint (Ottawa) for the Bullion Reference Material, and Gundars Reinfelds from the University of Winnipeg for instrument support. Finally, I would like to deeply acknowledge Ann McEachern for her skills in understanding me, even when I am speaking gibberish.

Table of Contents

List of Figures

List of Tables

Abstract

Electrocorrosion and spark ablation are described for rapid dissolution of metals in aqueous solution. When current is applied between two metal samples in de-ionized water at close proximity (0.5 mm), spark ablation occurs in a discrete area. Low-powered spark ablation was characterized using rates of ablation of various metal samples, demonstrating similar ablation rates for all metals, ranging from 20 $\mu g\ s^{-1}$ to 60 $\mu g\ s^{-1}$ over a period of 60 to 120 s. Low-powered spark ablation was also used as a method of Au analysis with experiments focusing on methodology and quantification of Cu and Ag in Au bullion reference material (BRM-1, BRM-2, BRM-3) from the Royal Canadian Mint. A method for dissolving Ag in gold samples was developed as an alternative to dissolution by aqua regia. Experimental results demonstrated that HNO_3 was sufficient to dissolve the small aliquots of ablated metal, without matrix interferences using GFAAS.

Electrocorrosion utilises a conductive solution to carry charge, preventing spark formation. As a result, the submerged portion of the metal is corroded rather than a discrete area. Electrocorrosion rates decreased from 120 to 30 $\mu g\ s^{-1}$ as the gap increased from 2 to 5 mm. Rates of corrosion in steel also increased significantly from 200 to 1000 $\mu g\ s^{-1}$ as solution conductivity increased from 0.01 to 0.05 M NaCl. Electrocorrosion rates for different metals ranged in steels (27 $\mu g\ s^{-1}$ for High Test steel #1 and 220 $\mu g\ s^{-1}$ for Ti Weld) to brass and aluminum (230 $\mu g\ s^{-1}$ for low Zn brass to 770 $\mu g\ s^{-1}$ for Al alloy AMS 4190). This suggested that a correlation exists between corrosion rates and sample composition. Electrocorrosion solution composition was also investigated (0.025 M NaCl, NaF, NaBr or NaI) and did not appear to have a significant effect on the rate of

dissolution of metals by electrocorrosion. Since redox processes are involved in the dissolution of the metal, the composition of the metal is an important parameter for predicting rate of corrosion. Most metals oxidize readily (e.g. Cu, Zn) and are well suited for electrocorrosion, however, a small number of metals that are difficult to oxidize (e.g. Au and Rh) may not be.

Scanning electron microscopy (SEM) images were taken of stainless steel after high and low-powered spark ablation as well electrocorrosion in order to compare the surface properties. The SEM images of spark ablated samples revealed crater formation in the sample as a result of metal ablation. Other surface irregularities associated with melting and sample re-deposition of the metals were observed. Electrocorrosion of the metal surface appeared to be less damaging in appearance, indicating a less heterogeneously sampled surface. Energy dispersive x-ray fluorescence (ED-XRF) spectra of the spark-ablated surfaces indicated some elemental variability when high-powered spark ablation was used but not for low-powered spark ablation or electrocorrosion.

1. Introduction

1.1 The Analysis Process – Sample Preparation

The purpose of a chemical analysis is to obtain information about a sample. The sample can take on different forms, and the information obtained about said substance can be just as varied. This variance can be due to shape, state, or other factors such as surface properties. One of the first and perhaps most important steps of an analysis is sampling. Sampling involves the removal of a smaller, representative sample from a bulk sample. Sample integrity must be conserved at this point or all following steps will be in vain. Sample preservation is also important during an analysis, as there may be a large amount of time in between sampling and analysis. The sample must be preserved in order to maintain its original chemical makeup or else representativeness may be lost. Metal samples can experience effects such as surface corrosion or sample contamination can readily occur.

Sample dissolution can be the final step before introduction of the sample to an instrument. Solid samples often need to be dissolved for aqueous nebulization in the instrument, though sample dissolution has many pitfalls. If the sample requires acid for dissolution, the acid may be a source of impurities, however human error is often the largest source of error due to handling mistakes, calculation errors, or simply contamination. In sample preparation, the fewer steps that are involved, the lower the risk for contamination due to reduced human error.

1.2 Metal Digestion

Metals, either contained within samples or as a whole, can be analyzed by a wide variety of methods. Elemental determination for bulk or trace quantities is often performed by spectroscopic methods such as flame atomic absorption spectrophotometry (FAAS), graphite furnace atomic absorption spectrophotometry (GFAAS), atomic emission spectrometry (AES), inductively coupled plasma-atomic emission spectrometry (ICP-AES), inductively coupled plasma-mass spectrometry (ICP-MS), and energy dispersive-x-ray fluorescence (ED-XRF).

Sample dissolution is required in order to achieve one or more of the following goals: to separate single or multiple metals from the parent sample; to concentrate a trace amount of sample; or to dilute the sample sufficiently for further analysis. The sample preparation approach used will usually depend on the analytical method as well as the sample itself. Many sample preparation techniques dissolve a sample by means of acid digestion. Simple wet ashing (acid digestion) can be performed in an open container. For example, a sample can be placed in a beaker that contains the appropriate acid and covered by a watch glass. The beaker can then placed on top of a hot plate and brought to a gentle boil to allow for quicker digestion. After digestion is complete, the solution is allowed to simmer in order to reduce the acid concentration due to evaporation. Filtration may then be required to remove any non-soluble impurities such as silica. The choice of acid is also important, as it depends on the sample of interest. Some Al alloys will require the addition of $HgCl_2$ to the acidic solution to digest the oxide layer that forms on its surface[1]. Other metals may simply require an oxidizing acid like HNO_3 for dissolution[1]. Problems such as contamination, analyte loss due to sample volatility,

vessel dissolution (HF and glass), and human error are factors that must be considered when using acid.

A major drawback to wet digestion is the time required for sample dissolution. For example, some tungsten steels may require several hours to fully dissolve[2,3]. With this in mind, methods have been developed in order to improve the speed of dissolution as well as to minimize other drawbacks associated with acid digestion. Microwave digestion[4-13] combines the dissolution properties of wet ashing but in a closed, container lowering the possibilities of contamination. There are several benefits to this method of digestion. The plastic container allows less chance for sample contamination common to glass containers, where metals and other contaminants may be leached out. Being a closed vessel, there is also less chance for airborne particulates to enter the solution, and less loss due to the volatilization of metal species. Another advantage is that this method can be automated, which requires less attention from the operator. Figure 1.1 shows the microwave digestion vessel.

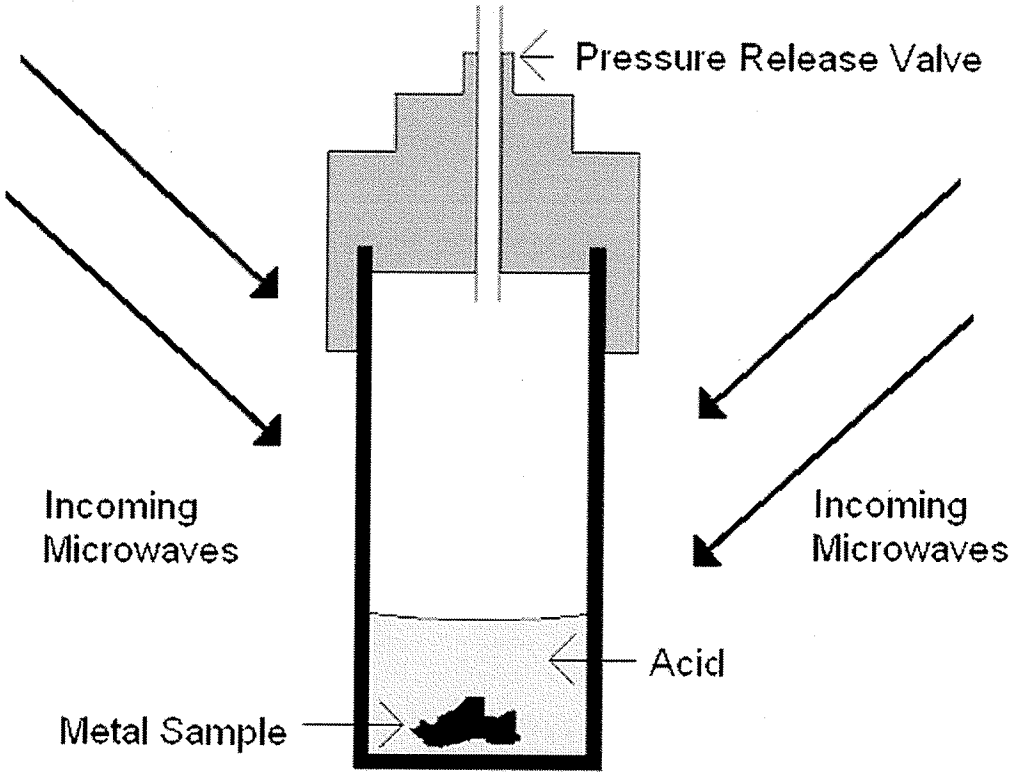

Figure 1.1: Microwave digestion apparatus

Fernando *et. al.*[11] used closed-vessel microwave digestion as a salt-free solution matrix in studying the complete digestion of Al in steel by ICP-AES. Traditional analysis procedures include fusions of Na_2SO_4 with the sample, though this method leaves Na in the matrix, inducing signal suppression in ICP-AES. Standard reference materials were evaluated for Al, Mn, P, Cu, Ni, Cr, V, Mo, Sn, Si, and Ti ranging in concentration from 0.0022% (Al) to 3.19% (Ti) with the technique demonstrating agreement with all certified values. The authors also noted that because of the closed nature of the vessel, volatile elements could also be analyzed by this technique. Kingston *et. al.*[13] used open-vessel microwave digestion in comparison to wet ashing for removal

and identification of different metals (Cd, Cr, Cu, Pb, Ni, and Zn) in environmental samples. Their work demonstrated that microwave digestion was able to achieve similar results compared to wet ashing, though with 60% shorter time periods.

Bombs[14-16] are used as an alternative to microwave and wet digestion. They comprise a Teflon® vessel surrounded by a steel jacket that is heated in an oven. This provides higher pressure and temperatures than is possible in open beaker acid digestion. Their main benefit is the speed in which digestion can take place versus wet digestion. Some inorganic materials do not dissolve in acids. For these samples, a fusion can be performed with acidic or basic flux to melt the sample[17-22]. Once the melt has cooled to a solid, it can then be easily dissolved by HNO_3. Fusions are created by mixing a 20 to 1 flux-to-sample ratio in the appropriate crucible which is then heated to melting temperatures. When the melt becomes clear, the fusion is complete. Table 1.1 shows different types of sample/flux combinations and what kind of crucibles should be used.

Table 1.1: Common fluxes[19].

Flux	Melting Point (°C)	Crucible	Types of Samples
Na_2CO_3	850	Pt	For silicates (e.g. rocks), sulfates, and phosphates.
$Li_2B_4O_7$ $LiBO_2$ $Na_2B_4O_7$	650 845 740	Pt, graphite Au-Pt alloy Au-Rh-Pt alloy	For aluminosilicates, carbonates, and high concentrations of basic oxides
Na_2O_2	675	Zr	Strong base, good for silicates not dissolved by Na_2CO_3
B_2O_3	450	Pt	For silicates and oxides. Main advantage is its ability to be completely removed

Electrical discharge or spark ablation spectroscopy[23-44] (spark source atomic emission spectroscopy) was one of the first techniques to truly challenge wet-chemical analysis in the early 1940's. It offered advantages such as avoiding the prolonged digestion and separation procedures of digestion methods, high sensitivity, and the capability of simultaneous, multi-element analysis (optical emission spectroscopy) making this the choice technique for metal analysis around the world. However, some drawbacks do exist, one of which is that spark ablation requires a conductive and homogenous sample. Non-conductive or heterogeneous samples such as minerals and rocks have been analyzed by grinding the sample to increase homogeneity and adding powdered graphite to enhance conductivity[23].

Electric discharge atomic emission spectroscopy is traditionally done in the gas phase. These methods typically include the spark as well as the direct current (DC) or alternating current (AC) arc. The DC arc is characterized by having two metal samples either initially touching or separated by a small gap (2-5 mm). Current is applied (1-30 A cm^{-2}, typically 8-14 A cm^{-2}), creating a discharge between the two metal samples. The metal tips are rapidly heated and volatilization and ionization of the sample begins. The ions increase in population to the point where they are able to sustain the arc (plasma) once the samples are separated[28]. The electrical plasma, sometimes referred to as the fourth state of matter consisting of ionized gases, is estimated to reach a temperature between 6000-6500 K, or enough to continually volatilize and excite ions from most samples. Photons from excited ions and atoms are then detected using a spectrometer where the amount of emr energy is proportional to sample concentration. High sensitivity is achieved with this technique, though reproducibility suffers[23]. This is because the plasma travels between the path of least resistance, traveling between two high points, from the sample to the reference electrode (Figure 1.2). When this occurs, the high point is rapidly ablated, and the plasma wanders to the next available point on the sample surface hampering reproducibility on a sample that may not be completely homogeneous[23].

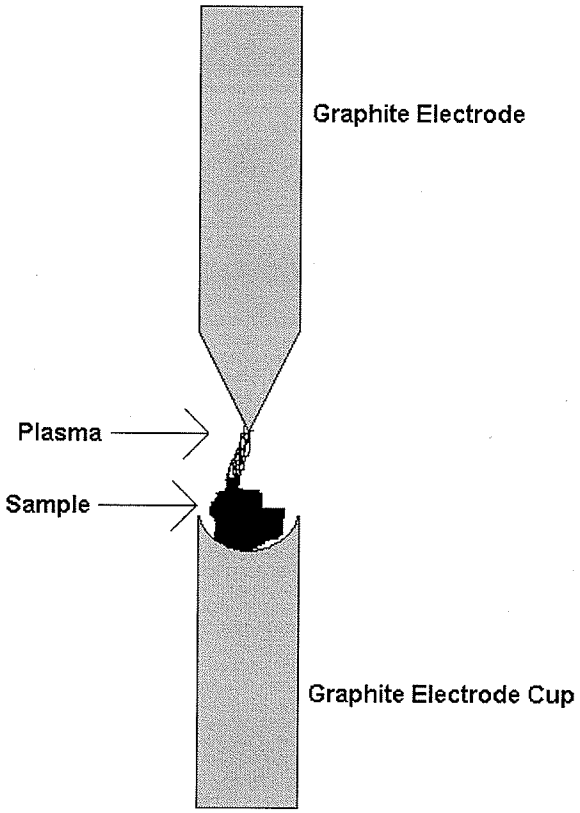

Figure 1.2: DC arc ablating sample at its highest point.

The AC arc is similar in principal to the DC arc except the current is formed in one direction then stopped, and then formed in the opposite direction at roughly 100-120 Hz. In general, currents in an AC arc are also lower by approximately 1-5 A cm^{-2}. The repeated formation and re-formation of the current reduces the temperature of the electrodes compared to electrodes in a DC arc[26]. High spot ablation is minimized due to the nature of the AC arc, which increases sample reproducibility with little loss in sensitivity[23].

Spark ablation is created by using a high voltage (15-40 kV) between two metal samples, with operating currents that are typically lower than arc sources[31]. The spark itself is also created in a different manner than arc discharges. Circuits are usually

designed using capacitors that only allow for an electrical discharge at maximum voltages. Therefore, the metal sample gap is not the determining factor in the formation of a spark. This allows for much higher precision, as the discharge does not depend on sample variations[28]. At the moment of electrical discharge, currents can run as high as 1000 A cm^{-2} with temperatures approaching 40000 K[31]. This high amount of energy is conducive to the formation of excited ions in the gas phase.

In this study, spark ablation was carried out in aqueous solution rather than in the gas phase (Figure 1.3-1.4). Figure 1.3 shows the ablation of two steel samples (308L) in a beaker. Current is supplied to the alligator clips, each one attached to a metal sample. Figure 1.4 illustrates how the spark ablation vessel can be run as an online device for ICP-MS. Traditionally, spark ablation in gaseous surroundings is often used for sample introduction (e.g. ICP-AES). Spark ablation in an aqueous solution is used for sample preparation, though spark ablation interfaced with an ICP has been reported[24]. Spark ablation of metal in water can produce colloids in solution that can be subsequently dissolved with a small amount of high purity acid to ensure solution homogeneity. The high degree of resistivity afforded by the use of de-ionized water (18 MΩ cm) means that sample gaps are typically much smaller (0.1-1 mm) than that in the gas phase. The high resistivity of the surrounding solution is necessary. If the solution were made conductive, a spark would not occur, as current would be carried by its spark ablation solution. Solution conductivity is also responsible for the ablation rate decrease over time due to ablated metal particles being introduced into solution, increasing conductivity.

There are many advantages of this technique versus that of spark ablation in a gaseous environment. The main advantage is the availability of many instruments that

require liquid nebulization (FAAS, GFAAS, ICP). Also, if post-ablation sample storage is required, solution storage is as easy and convenient as applying a top to the container.

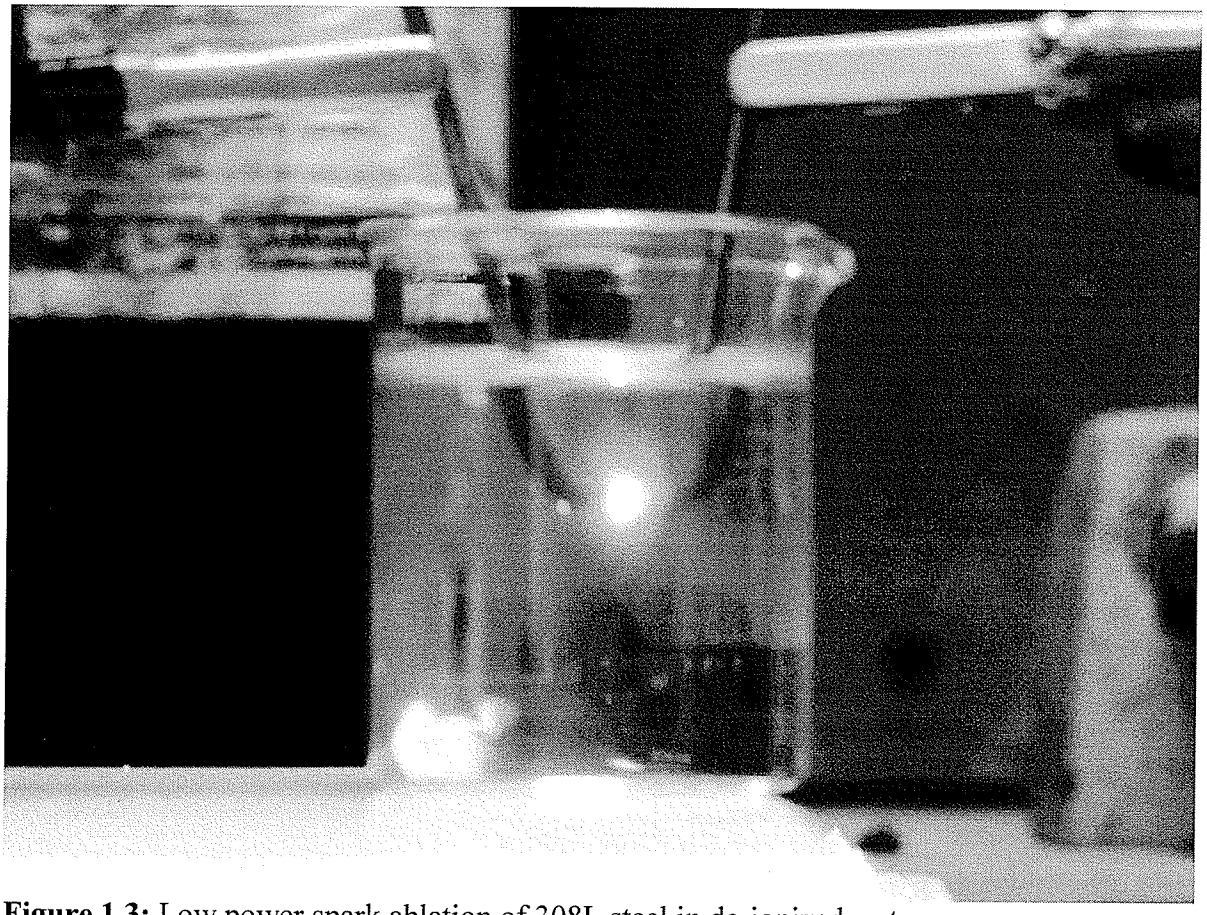

Figure 1.3: Low power spark ablation of 308L steel in de-ionized water.

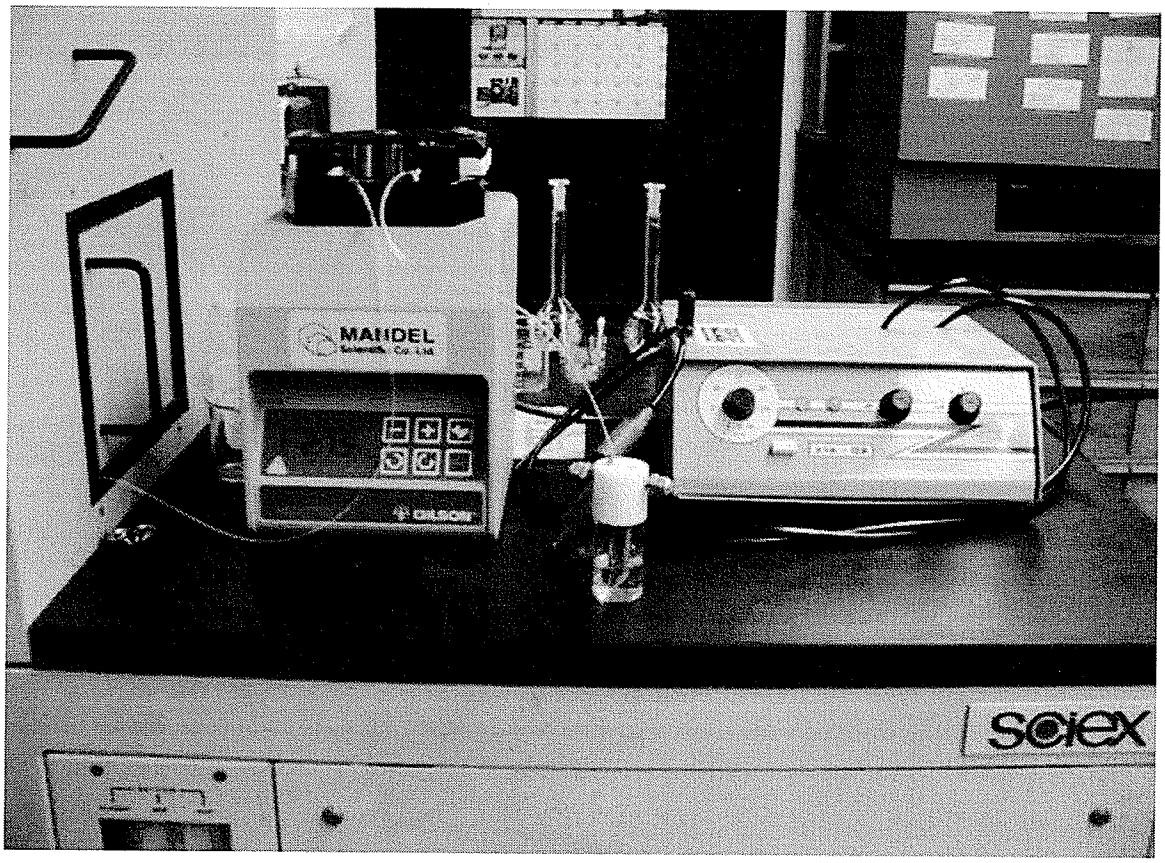

Figure 1.4: Spark ablation interfaced to an ICP-MS via peristaltic pump.

Both high power (275-1100 W)[24] and low power (20-300 W)[25] spark ablation in a liquid medium have been investigated for rapid dissolution of various metal samples prior to analysis by ICP-MS and GFAAS. Goltz *et al.*[25] found that during low powered spark ablation, rates of ablation of Fe in mild steel decreased over time due to the increased solution conductivity. This was followed by experiments dedicated to purposely increasing the conductivity of the solution. Various amounts of KCl were added to the solution until a spark was no longer able to form at a concentration of 0.02 M KCl. Similar experiments were performed by varying the pH of the solution, with results that demonstrate the highest rate of ablation was observed at a pH of

approximately 7, due to low concentrations of electrically conductive metals in solution. Temperature experiments were also investigated. As the temperature of the solution was increased, ablation rates decreased. A result of higher colloid solubility at elevated temperatures, reducing the amount of electrically neutral colloids in solution. High-powered spark ablation was also investigated by Goltz *et al.*[24]. Various current settings were explored with results that demonstrate an increase in ablation rates with higher applied currents supplied to the metal samples. Spark ablation was also considered for trace analysis by ICP-MS. In these experiments, a brass rod was ablated and mass scans over 5, 10 and 20 s of applied power were taken. Results show peaks at 58 and 60 amu appearing strongly at 20 s, demonstrating that accurate quantitative analysis is possible after short periods of time. This paper also explored high-powered spark ablation for quantitative analysis. A National Institute of Standards and Technologies (NIST) Cr-V steel sample was chosen because of its wide range of elemental concentrations (0.098 % Cu to 19.5 % Cr). L'vov *et al.*[36] performed low power spark ablation in the liquid phase on steels prior to analysis by GFAAS. They demonstrated that colloids were easily generated with minimal difficulty and little time, averaging in size of about 1 μm, which guarantees representativeness. Trace analysis was also performed with high purity Al and Ti. Experimental results were in agreement with certified values. Pchelkin *et al.*[37] used spark ablation in a liquid medium and compared it to chemical methods in the analysis of standard reference materials. Their results were in agreement with the certified values as well as the values established by chemical means. This paper also described a relationship between the variables of the spark ablation circuit and the particles it produced, relating the capacitance, the distance between the two metal

samples in the secondary discharge gap and input power in a final equation. Houk *et al.*[44] used arc ablation in the gas phase coupled to an ICP-MS for rapid metal determination, avoiding complications associated with the use of acids in the plasma, such as oxides ($^{35}Cl^{16}O^{+}$) possibly interfering with transition metals like $^{51}V^{+}$. Experiments were undertaken to test arc nebulization for detection limits, sensitivity, as well as precision and the ability to remove, or cleanout the sample from the instrument. Detection limits were explored via an ion monitoring system on the ICP-MS. Steel standard reference materials were analyzed with concentrations (%) varying from 0.001-0.225%. All results agreed within certified values, with calibration curves being linear ($r^2 > 0.995$). Sensitivity experiments focused on steel standard reference materials, where various elements were analyzed for signal intensity with concentrations ranging from 0.4-4 $\mu g\ g^{-1}$. With the exception of ^{60}Ni, which showed particularly poor sensitivity, all elements had favourable results. Houk *et al.*[44] believed that this was due to lower aerosol gas flow rates that were used. They also demonstrated that, when compared to aqueous sample introduction into an ICP-MS, the analyzed values obtained were quite low overall. This, was due to less sample being introduced into the ICP-MS overall, as rates of sample introduction were at least two orders of magnitude lower with arc ablation than with aqueous nebulization.

Electrocorrosion[45-53] or electrolytic dissolution, is achieved without an arc or spark. Electrocorrosion is able to corrode metal samples very rapidly; creating dense colloids in solution that can be dissolved by small amounts (e.g. 100 µl) of high purity acid. The main benefit of electrocorrosion is its gentle means of sample preparation where disfiguration or destruction is kept to a minimum.

Electrocorrosion can be done in water that is made conductive in order for the current to pass from one metal sample to another, purposely avoiding an arc or spark. Sample gaps are typically large (> 2 mm) in electrocorrosion in order to avoid a spark. Oxidation also occurs on the entire surface area of the submerged metal samples and not in discrete areas. In Figure 1.5, the power source is in the background and is attached to the electrocorrosion apparatus by two current carrying wires. Figures 1.6–1.7 demonstrate the electrocorrosion process over time. Here, two brass samples are corroded as colloid formation (the murky solution) occurs. After 20 s, the power is ceased and the metal samples can be removed and rinsed. Small amounts of HNO_3 can be added at this time to homogenize the solution.

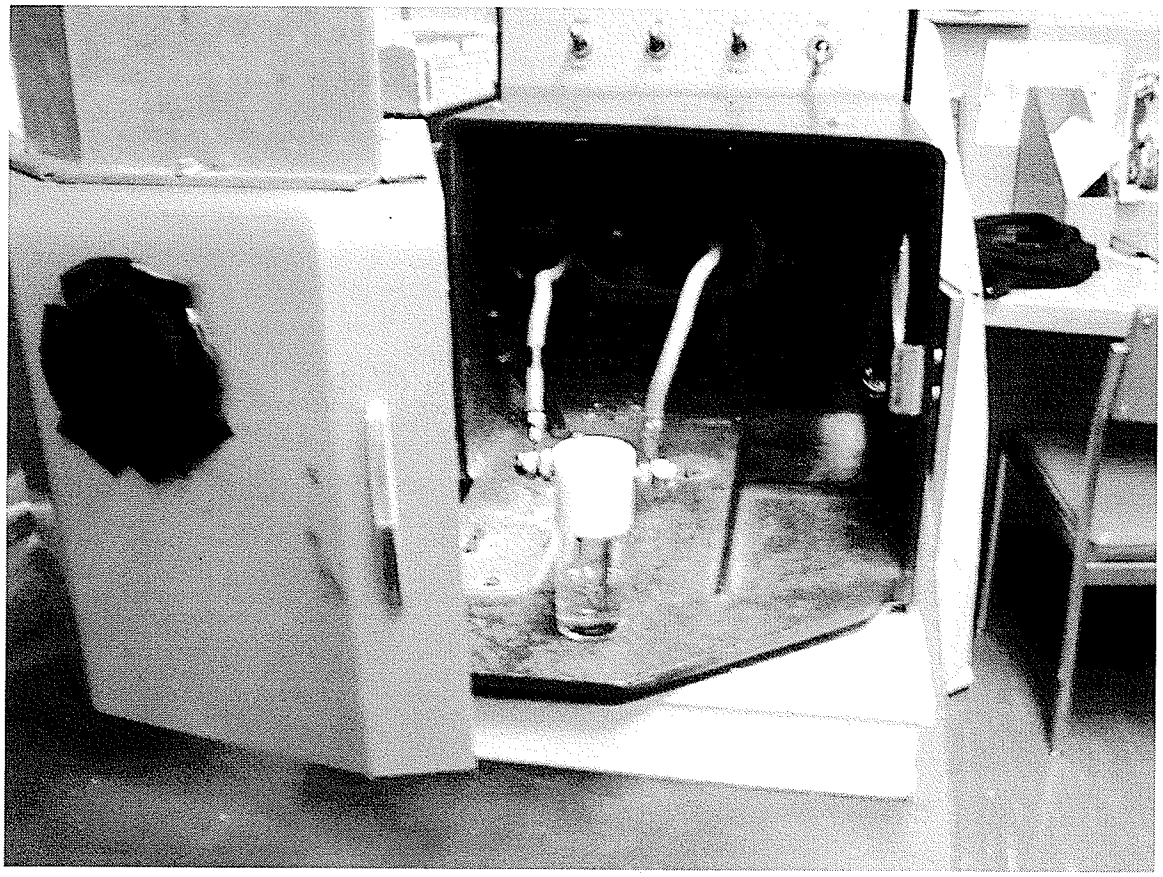

Figure 1.5: The electrocorrosion vessel attached to samples from ARL Spark Source power supply.

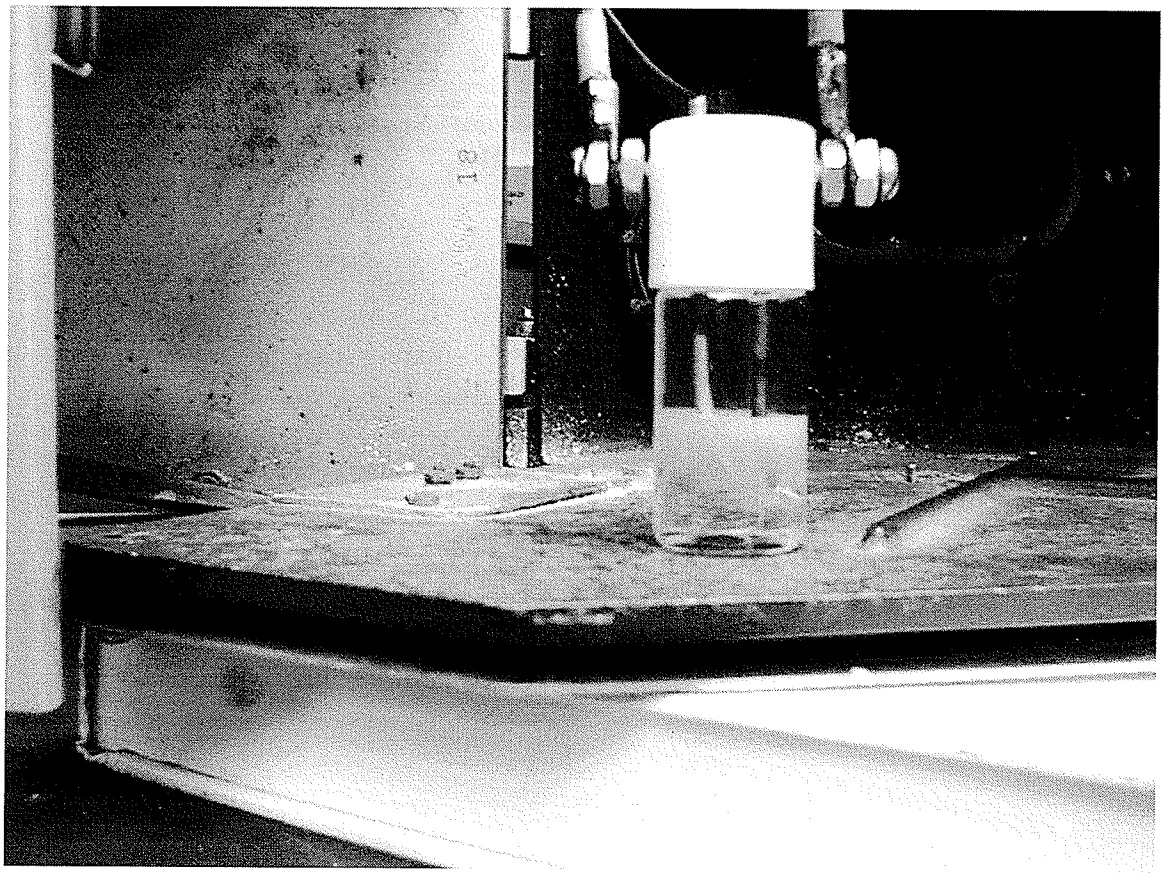

Figure 1.6: The electrocorrosion process at 2 s after corrosion has begun. Gas is evolving from the surface of the metal samples.

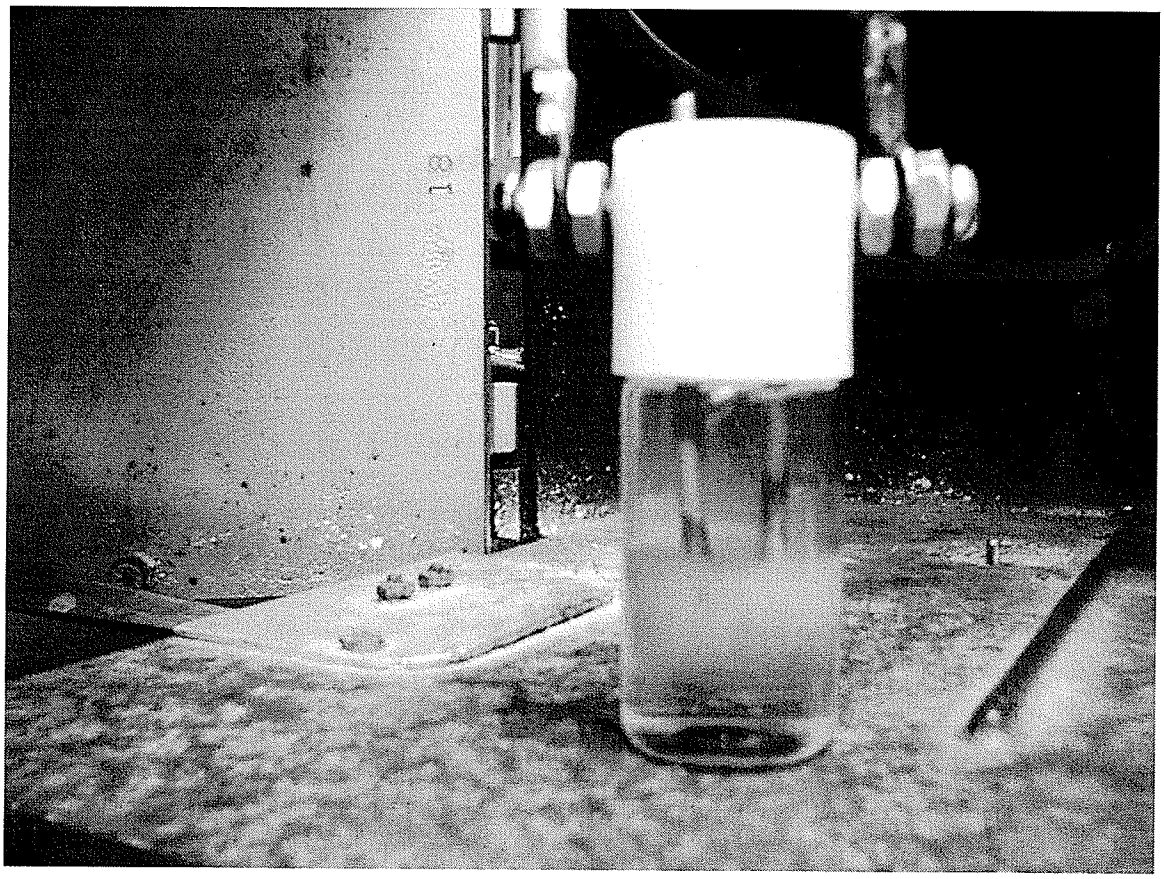

Figure 1.7: The electrocorrosion process at 20 s. Colloids are beginning to form a deep yellow colour in the vessel.

Other researchers have used electrolytic dissolution in various forms to quantify different elements in metals. Bergamin et al.[45] dissolved alloys for the determination of Al and Mn using flow injection analysis. Flock *et al.*[46] analyzed steel samples using electrolytic dissolution with FAAS. More recently, Gervaio et al.[48] used electrocorrosion for rapid dissolution of steel for on-line measurement with ICP-AES. Kondo et al.[59] have used electrolytic dissolution for rapid determination of metals in steel using ICP-AES. This group has developed a method for bulk and trace analysis of S in steel, showing a high degree of linearity ($R^2 = 0.9941$) between S and the S/Fe ratio in steel. In contrast,

standard solutions containing SO_4^{-2} were analyzed and plotted on the same graph. These results show that, with electrolytic dissolution, sensitivity increased one order of magnitude due to an increased amount of material being introduced into the instrument. To create the electrolytic solution, Kondo used a 6 M HCl solution lowering the pH of the solution as a result. When using electrolytic dissolution for quantitative analysis of S in steel standards, experimental results demonstrated a high degree of agreement with certified steel values of elements ranging in concentration from 21.3 $\mu g\ g^{-1}$ to 198.0 $\mu g\ g^{-1}$.

2.0 Experimental

2.1 Chemicals

All solutions were made with de-ionized water (18 MΩ Milli-Q). Sodium fluoride, sodium chloride, sodium iodide (all supplied by Aldrich), and sodium bromide (Sigma), were reagent grade and used without purification. Standard solutions were prepared by appropriate dilutions of 1000 μg mL^{-1} standards (SCP Science) and all solutions were made with high purity AR Select® Plus HNO_3 (Mallinckrodt).

2.2 Metal Samples

Standard reference materials (SRMs) were used for quantitative analysis purposes. Selected elemental concentrations can be seen in Table 2.1. Steel and non-steel (e.g. Al, Brass) welding rods were used as samples in various experiments. Bulk and trace elemental composition can be found in Tables 2.2 through 2.3. Gold bullion reference material (BRM) was used in the characterization of Ag and Cu. Compositional values of the BRMs can be found in Table 2.4. Table 2.5 provides the various metal sample diameters and tensile strengths of different sample welding rods.

Table 2.1: National Institute of Standards & Technologies SRM 663 Cr-V Steel

Element	**% by Wt.**
Copper	0.098
Nickel	0.32
Lead	0.0022
Cobalt	0.048
Aluminum (total)	0.24
Silver	0.0038

Table 2.2: Welding rod samples

Metals	Supplier	Elemental Composition
High test steel #1*	Union Carbide	Mn (1.0%) Si (0.2%) C (0.15%)
Ti Weld #65*	Lincoln Electric	Ti (10.0%) Cr (5.0%) Co (0.5%)
ER308L*	Lincoln Electric	Cr (19.5-22.0%) Ni (9.0-11.0%)
ER316*	Lincoln Electric	Cr (18.0-20.0%) Ni (11.0-14.0%)
E6013*	Lincoln Electric	Mn (0.60%) Si (0.40%) C (0.10%)
E7018*	Lincoln Electric	Mn(2.0-3.0%) Si (2.0%) C (2.0%)
E2100*	Lincoln Electric	Ti (5.0%) Cr (10.0-12.0%) Co (0.5%)
E11018*	Lincoln Electric	Mn (1.3-1.8%) Ni (1.25-1.5%) Si (0.6%)
AMS 4190^	Lincoln Electric	Si (4.5-6.0%) Fe (0.8%) Zn (0.1%)
ER4043^	Lincoln Electric	Si (9.3-10.7%) Fe (0.8%) Cu (0.3%)
ER5356^	Lincoln Electric	Mn (4.5-5.5%) Zn (0.1%) Cu (0.1%)

* Denotes steel welding rods, bulk element is Fe.
^ Denotes aluminum welding rods, bulk element is Al.

Table 2.3: Non-welding rod metal samples

Metals	Supplier	Elemental Composition (%Wt.)
Low Zn Brass	Alfa Aesar	Zn (30%)
High Zn Brass	Alfa Aesar	Zn (70%)
Gold	Alfa Aesar	Au (99.9%)
Nickel	Alfa Aesar	Ni (99.9%)
Rhodium	Alfa Aesar	Rh (99.9%)
Silver	Alfa Aesar	Ag (99.9%)
Copper	Alfa Aesar	Cu (99.9%)
Zinc	Alfa Aesar	Zn (99.9%)

Table 2.4: Gold Bullion Reference Material (BRM) samples

Metals	Supplier	Elemental Composition (% by Wt.)
BRM 1*	Royal Canadian Mint	Au (94.847%±0.064) Ag (4.15%± 0.36)
BRM 2*	Royal Canadian Mint	Au (89.928%±0.050) Ag (8.03%± 0.20)
BRM 3*	Royal Canadian Mint	Au (84.905%±0.062) Ag (12.08%±0.33)
BRM 4*	Royal Canadian Mint	Au (79.962%±0.050) Ag (15.09%±0.34)
BRM 5*	Royal Canadian Mint	Au (74.988%±0.107) Ag (15.04%±0.24)

*BRM 1-5 contains a Cu percent balance to 100% (i.e. Cu is not certified)

Table 2.5: Diameter and tensile strength of selected welding rods

Metals	Diameter (mm)	Tensile Strength (kpsi)
High test steel #1	1.53	70
Ti Weld #65	1.53	110
ER308L	2.60	79
ER316	2.60	75
E6013	2.60	60
E7018	2.60	70
E2100	2.60	118
E11018	2.60	110
ER4043	1.53	25
ER5356	1.53	50
High Zn Brass	2.60	N/A

Many welding rods use a common name (*e.g.* High test steel #1) while other rods follow the American Welding Society (AWS) naming procedures (*e.g.* E7018). The AWS requirements for the identification of welding rods are found as a number, stamped at the base of the rod, while the letter indicates the type of welding the rod is used for. The first two digits (or three digits in the case of a 5 digit number) indicate the tensile strength of the rod, where the rod should meet or exceed the tensile strength of the welded material. The third digit (or the fourth digit in the case of a 5 digit number) indicates the preferred position of the weld. The final digit refers to the type of flux used on the rod itself.

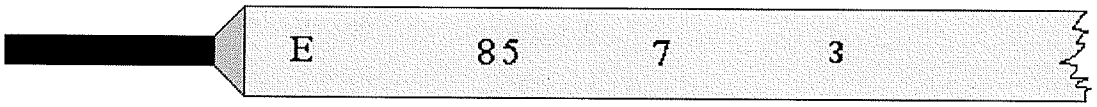

Figure 2.1: Example of AWS identification

2.3 Electrocorrosion Vessel

The metal sample carrying cap, made of Teflon® for ease of machine-ability and for its thermal and conductive resistivity, was constructed to fit the top of a 20 mL scintillation vial (Figure 2.2).

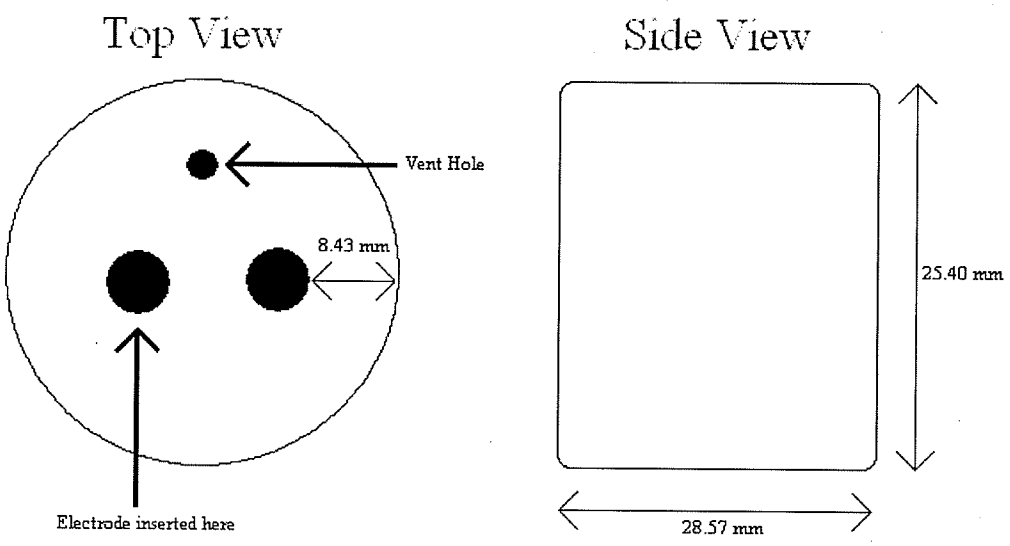

Figure 2.2: Top and side views of the metal sample carrying cap

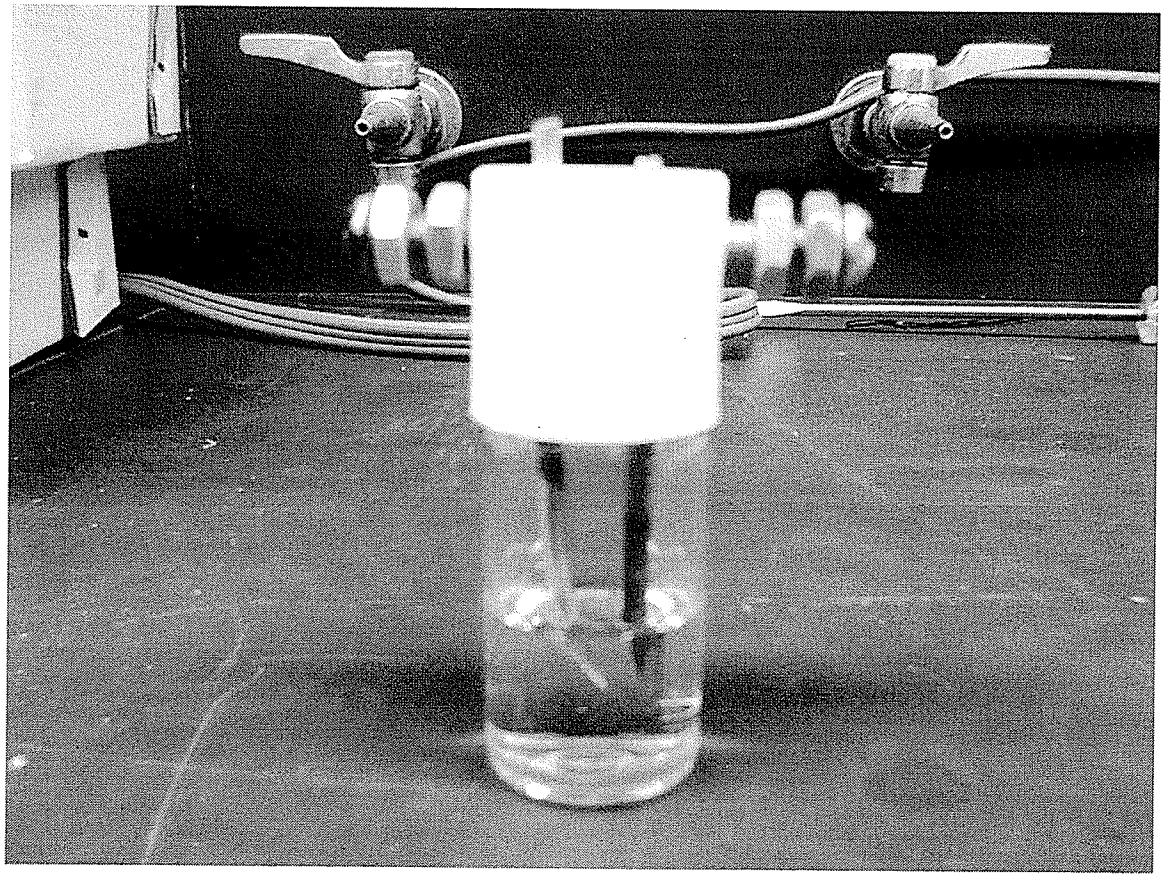

Figure 2.3: The electrocorrosion vessel with brass metal samples in 0.05 M NaCl.

2.4 Electrocorrosion and Spark Ablation Apparatuses

(i) Electrocorrosion

The power source used for electrocorrosion was an Applied Research Laboratories (ARL) Model 26000 spark source unit from a spectrographic analyzer. A summary of the electrocorrosion parameters can be found in Table 2.6. In brief, the spark source has a power requirement of 115 V at 50 or 60 Hz AC and 20 A. The metal samples have an output from a 14 kV transformer and two 0.5 mF capacitors (in series), which are in parallel to the high voltage transformer. Two parallel inductors (50 mH) in series with capacitors and a rectifier circuit control the output current. Therefore, the output current of the discharge can be full-wave rectified at 5 and 10 A or half-wave rectified at 2.5 and 5 A. The spark source unit was modified by removing the graphite electrode holders and the wires attached to them from the output transformer. Longer wires were connected from the output transformer to allow an easy and removable connection to the electrocorrosion vessel. Preparation of the metal samples for electrocorrosion involved bending of the two metal samples with pliers to facilitate gap variation. Contact between the metal sample surface and pliers was kept to a minimum by insertion of Kim Wipes®. Both metal samples were filed and finally rinsed with de-ionized water.

Table 2.6: Operating conditions for the ARL 26000 spark source unit

Power Requirement (V):	115 (60 Hz frequency)
Current settings (A):	2.5, 5.0, 10.0
Electrode Polarity:	positive or negative
Waveform:	Half: 2.5 and 5.0 A
	Full: 5.0 and 10.0 A
Metal Sample Gap (mm):	2.5 – 8.0

(ii) Spark ablation

The spark ablation device that was used had a power requirement of 220 V at 50 or 60 Hz. The input voltage is stepped up using a transformer with three tap settings that are controlled with a switch. In this fashion, the input power has settings of 100, 200, or 300 W, which control the output voltage of this transformer. The output voltage (2 kV) of this transformer supplies power to a circuit containing a high frequency transformer, three capacitors (4.7 μF) and a secondary spark discharger. Resistance in the high frequency part of this circuit can be controlled by adjusting the spark gap, where the larger the gap, the higher the resistance. Controlling the resistance in this circuit allows for control of the voltage to the high frequency transformer. The high frequency transformer has an output voltage of 0 – 10 kV to the metal samples with an applied power of 100, 200, or 300 W. Unless otherwise stated, power settings were kept to 100 W. A circuit diagram can be seen in Figure 2.3. Preparation of the metal samples for spark ablation was minimal as sample gap was less of a problem, therefore allowing them to be kept straight. The metal samples were cleaned with a gentle abrasive then washed and rinsed with de-ionised water.

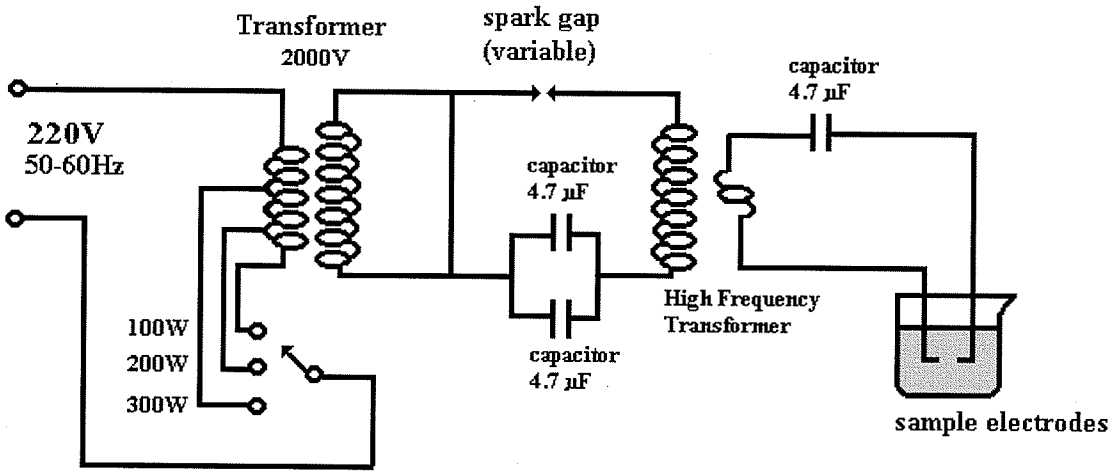

Figure 2.4: Schematic circuit diagram of spark source.

2.5 Instrumentation

The Flame Atomic Absorption Spectrophotometer (FAAS) used was a Perkin-Elmer Atomic Absorption Spectrophotometer 460 (Table 2.7). Trace analysis was performed using a Perking-Elmer AAnalyst 800 Graphite Furnace Atomic Absorption Spectrophotometer (GFAAS), and a Perkin-Elmer Sciex Elan 500 Inductively Coupled Plasma Mass Spectrometer (ICP-MS). Instrumental parameters for the ICP-MS and GFAAS can be found in Table 2.8 and 2.9 respectively. A JEOL JSM-6300V with VISIONS instrument control and image capture software (Table 2.10) was used for Scanning Electron Microscopy (SEM). Energy dispersive-x-ray fluorescence (ED-XRF) was performed using an Oxford Instruments LINK ISIS Microanalysis Tower System with Si/Li Category "C" Pentafet slide-mounted ATW detector. Unless indicated otherwise, standard conditions were used for all instruments.

Table 2.7: Instrumental operating parameters for FAAS.

Flame	Air-acetylene		
Element	Cr	Ni	Cu
Wavelength (nm)	357.9	232.0	324.8
Slit (nm)	0.7	0.2	0.7
Flame Type	rich (reducing)	lean (oxidizing)	lean (oxidizing)

Table 2.8: Instrumental operating and data acquisition parameters of ICP-MS

ICP	
RF power	1100 W
Coolant Ar flow	15.0 L $minute^{-1}$
Auxiliary Ar flow	1.4 L $minute^{-1}$
Carrier Ar flow	1.0 L $minute^{-1}$
ICP-MS Data Acquisition	
Dwell Time	50 ms
Scan mode	peak hopping
Number of masses (m/z) monitored	3-8
Signal measurement	average counts
Resolution	0.9 a.m.u. at 10% peak height

Table 2.9: Instrumental operating parameters of GFAAS

Element	Cu	Ni	Ag	Cr	Zn
Pyrolisis (°C)	1200	1100	800	1500	700
Atomization (°C)	2000	2300	1700	2300	1800
Wavelength (nm)	324.8	232.0	328.1	357.9	324.8
Slit (nm)	0.7	0.2	0.7	0.7	0.7

3.0 Results and Discussion:

3.1 Electrocorrosion - Characterization of the Electrocorrosion Process

When high current (1-10 A cm^{-2}) is applied between two conductive samples in an aqueous solution, electrocorrosion occurs on the surface of the metal samples as a result of electrolysis and possibly collisions of dissolved ions with the metal surface. As long as a large enough current is used, corrosion will occur at one (unipolar) or both (bipolar) metal surfaces in aqueous solution. A spark may form if the gap between the conducting samples is too small. A number of properties influence the amount of material that is corroded from the metal surface including the gap, applied current (or power) and the conductivity of the electrocorrosion solution. Other researchers[51-52] have looked at electrolysis under different conditions (e.g. pH < 3) than those described in this study. An examination of electrocorrosion properties is useful for understanding both the limitations of the electrocorrosion device as well as to provide clues about the mechanism of the dissolution process for different metals.

The first property investigated was the mass of metal removed and the rate of corrosion of metals in an aqueous solution for a given power setting. Figure 3.1 shows the mass of Cu and Zn corroded from a sample of brass over time. For these measurements, the electrocorrosion process was carried out at 2.5 A cm^{-2} in a known volume (~10 mL) of a 0.01 M NaCl solution. After fixed periods of time, small volumes (0.5 mL) of liquid media were removed, diluted to 20 mL and analyzed using FAAS. Since the concentration and volume were known, the mass of metal corroded was readily calculated. Figure 3.1 shows that the mass of Cu and Zn in the electrocorrosion solution increases with time, as would be expected, but the mass of metal appears to corrode at an

increasing rate over time. Using the same data, the rate of metal corrosion was also calculated and plotted as a function of time as shown in Figure 3.2. This experiment illustrates that the rates of corrosion of Cu and Zn are not constant; and increase significantly over time. For example, after 30 s the rate of corrosion of Cu and Zn in brass doubled over 5 s. This suggests that physical or chemical properties of the electrocorrosion process are changing over time. During the corrosion process at least two parameters change constantly with respect to time. One parameter is the gap between the metal samples, which must increase slightly as metal is removed from the surface of the sample. A second is the chemical composition of the aqueous solution. It is possible that the corroded metal in the aqueous solution could increase the overall conductivity of the electrocorrosion solution, particularly between the metal samples. It is worth noting that if high concentrations of NaCl (0.05 M) are used, the contribution of ions from the corroded metal should be minimal. Another property that also changes in the electrocorrosion solution is temperature. The temperature of the solution changes significantly with respect to time, depending on the applied current. Usually the temperature in the solution can reach a boiling point in less than 1 minute at 2.5 A cm^{-2}. For electrolyte solutions, molar conductivity generally increases with increasing temperature.

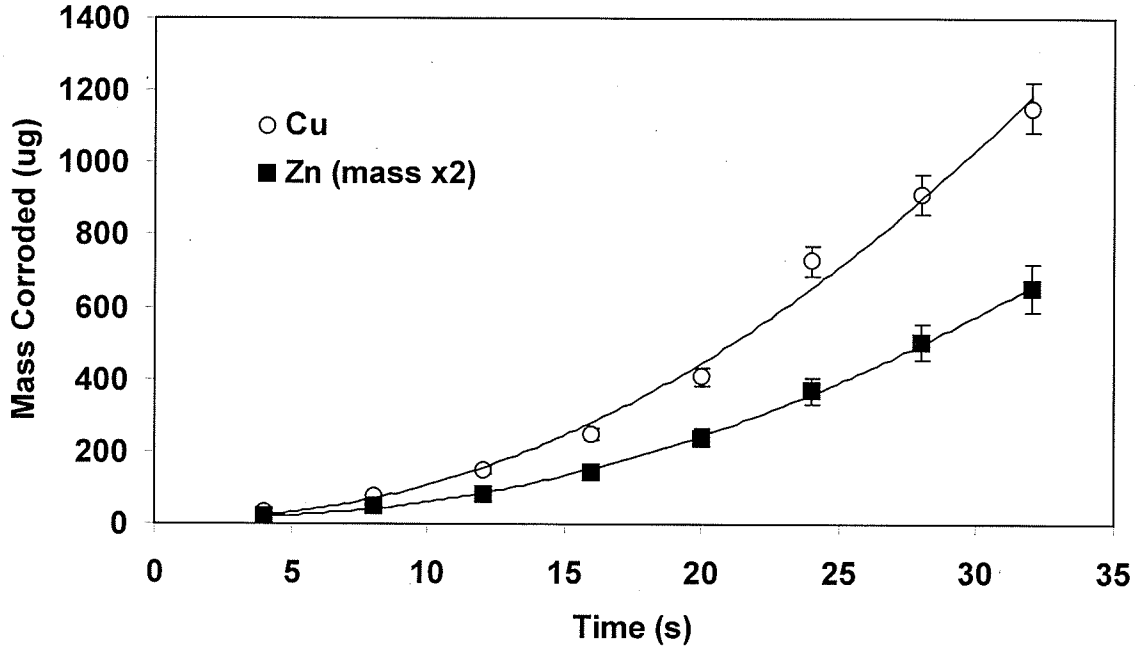

Figure 3.1: Mass of Cu and Zn removed from brass over time in 0.01 M NaCl and a metal sample gap of 5.0 mm.

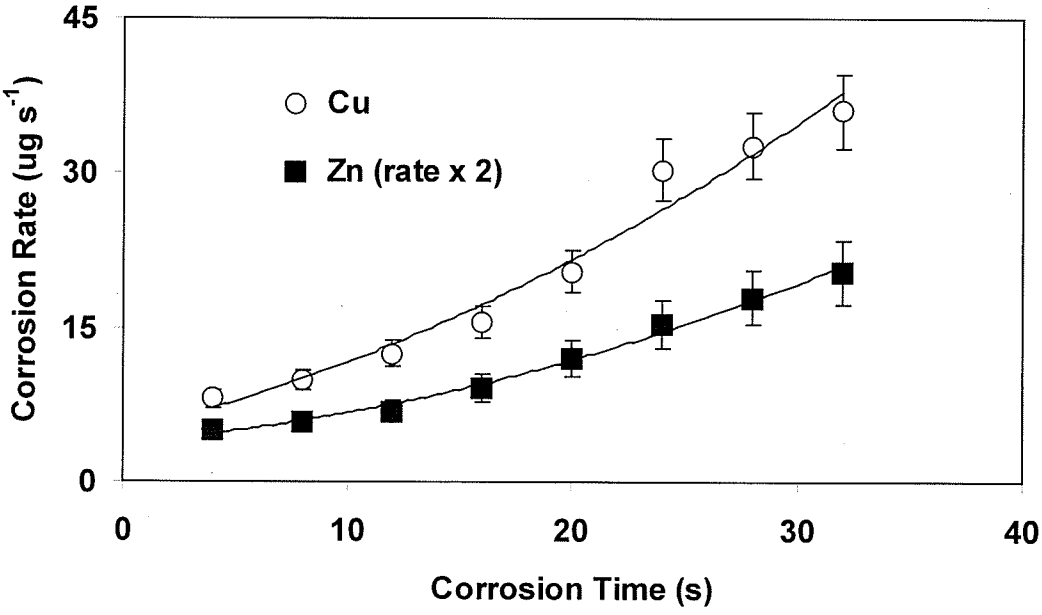

Figure 3.2: Rate of electrocorrosion of Cu and Zn from brass over time in 0.01 M NaCl and a sample gap of 5.0 mm.

Experiments were carried out to determine the effect of the sample gap and the conductivity of the electrocorrosion media on the rate of corrosion. The effect of increasing the sample gap on the rate of corrosion is illustrated in Figure 3.3. A corrosion time of 15 s was used at 2.5 A cm^{-2} in 0.01 M NaCl. Figure 3.3 illustrates that increasing the gap between the conductive samples will decrease the rate of metal corrosion. This suggests that changes in the gap have greater effects on rates of corrosion when a small gap (1-2 mm) is used. During a typical experiment, the change in gap is quite small (< 0.1 mm) so it is unlikely to have any noticeable effects on the electrocorrosion rate over short periods of time.

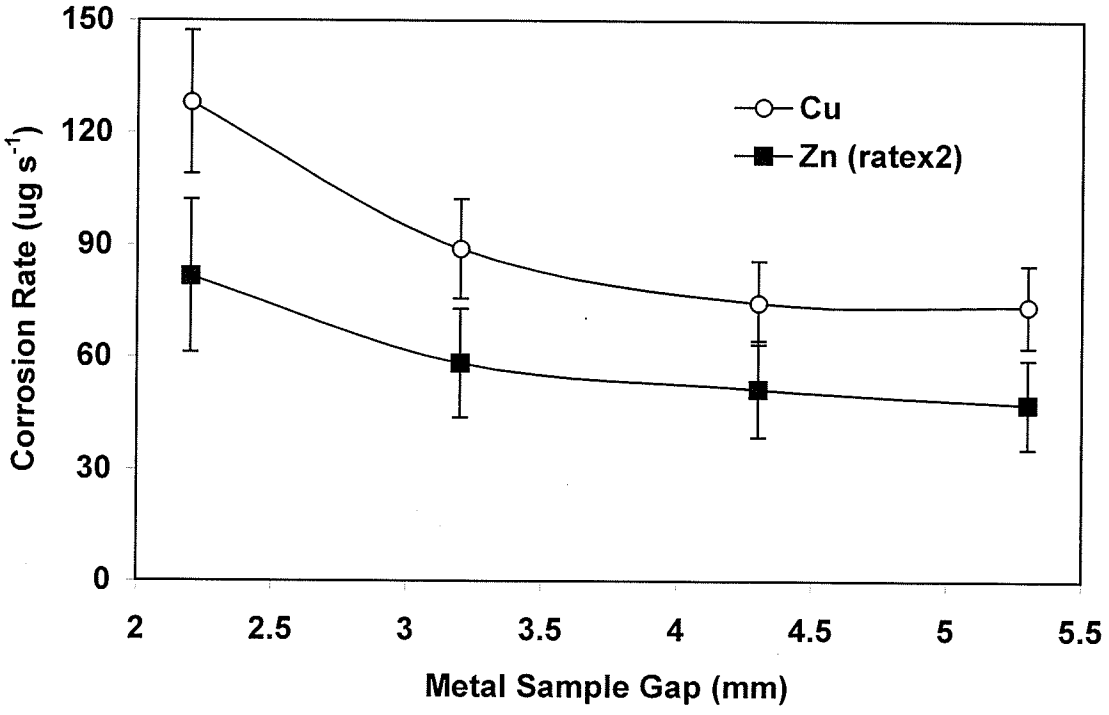

Figure 3.3: Effect of gap on the rate of corrosion of Cu and Zn from brass in 0.01 M NaCl (n=5).

The effect of conductivity as shown in Figure 3.4 illustrates that the higher the concentration of NaCl in the electrocorrosion solutions, the greater the rate of corrosion of metal. For the large gaps (2 mm) used in these studies, the effect of conductivity appears to be a more important consideration than the sample gap. One reason that the rate of corrosion increases is because the conductivity between the metal samples increases as more ionic species form in the aqueous solution between the metal samples. It may be logical to minimize the role of the gap at this stage. However, it should be noted that as the gap increases, the effect of conductivity on the rate of corrosion decreases significantly. It should also be noted that if the conductivity of the solution is high (0.05 M NaCl), the relatively small contribution of corroded metal to overall solution conductivity should be negligible (increasing solution molarity by 0.46 M for Cu and 0.16 M for Zn).

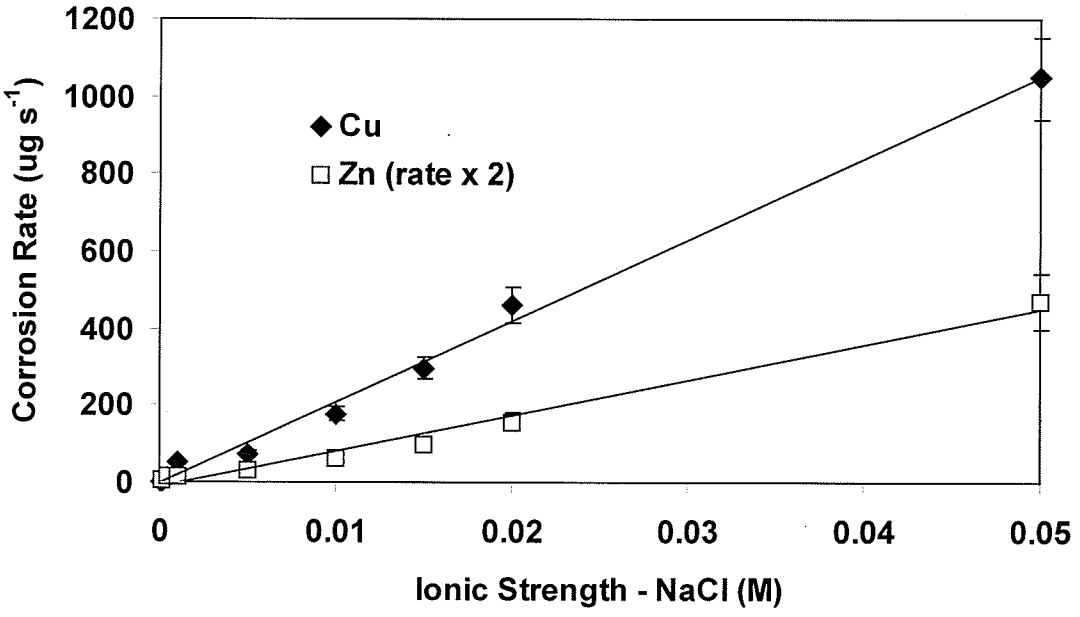

Figure 3.4: Effect of solution ionic strength on the rate of corrosion of Cu and Zn in brass and using a sample gap of 5 mm (n=5).

A question that requires further examination is whether one metal is preferentially corroded relative to another in an alloy. If one element is preferentially removed, then erroneous analysis will result and the overall effect will be the same as an incomplete acid digestion. One way to demonstrate whether preferential corrosion of one metal is occurring in an alloy is to plot the mass of one metal with respect to another. Experiments were carried out using Cu and Zn from a brass metal sample. Figure 3.5 shows a plot of mass of corroded Cu with respect to corroded Zn in a sample of brass. For these experiments, a single sample of brass was corroded over time at 2.5 A cm^{-2} in 0.01 M NaCl, with a metal sample gap of 2 mm. At fixed intervals, a small amount of liquid was removed (0.1 mL), diluted, and the corroded masses of Cu and Zn were quantified. The ratio of Cu:Zn in this brass sample is approximately 3:1. Each data point in this graph represents a different time interval (from 0 to 32 s) when the solution was sampled. The high degree of linearity ($r^2 = 0.996$) in Figure 3.5 strongly suggests that in an alloy such as brass, neither Cu nor Zn is removed preferentially over time.

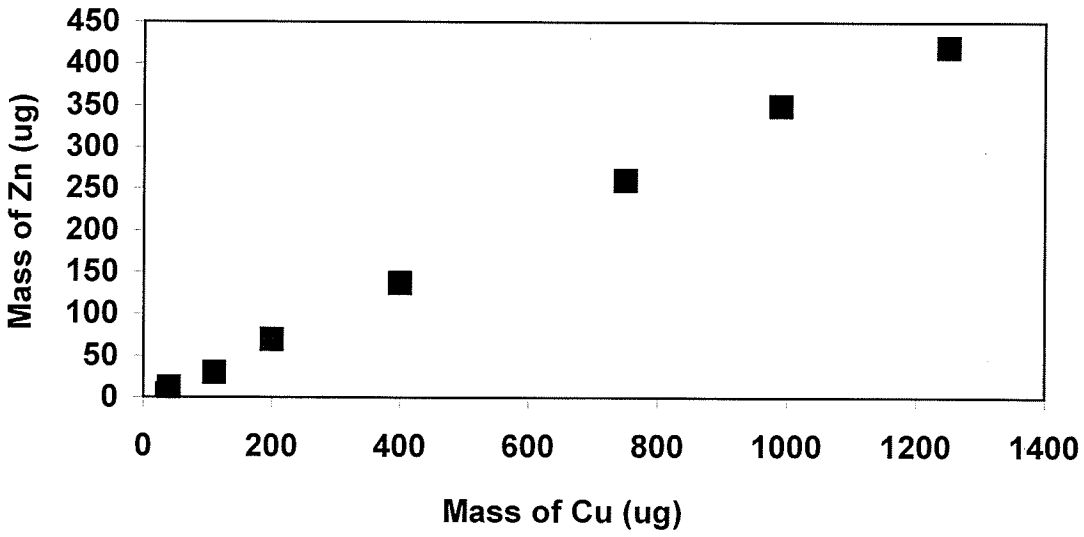

Figure 3.5: Comparison of the masses of Cu to Zn corroded over time from brass in 0.01 M NaCl and a sample gap of 5.0 mm.

To establish whether electrocorrosion can be used as a sample preparation tool, it is important to know if all metals have uniform corrosion rates. One general property that was investigated is whether different alloys have different rates of electrocorrosion. Figure 3.6 shows the corroded mass of a variety of metal samples including steel, brass, and aluminum after 10 s when 2.5 A cm^{-2} is applied in 0.025 M NaCl. Figure 3.6 shows the difference in masses corroded, and hence corrosion rates for various metals under identical experimental conditions. In general, lower rates of corrosion are observed with higher tensile strengths (e.g. stainless steel) versus softer alloys (e.g. aluminum). This general trend can be found within any particular type of alloy (e.g. brass). The mass corroded and the rate of dissolution varied from 27 $\mu g\ s^{-1}$ for High Test Steel #1 to 770 $\mu g\ s^{-1}$ for the aluminum alloy AMS 4190. This result may not be unexpected, however, it is of interest to understand why different metals corrode at different rates in order to establish the use of electrocorrosion for routine sample preparation. These results also illustrate the difficulty in trying to correlate rates of corrosion to tensile strength when looking at alloys of different composition. Other factors such as the surface area of the metal and the presence of an oxide coating on the metal surface are also important considerations with regard to corrosion rates. A direct result of this chemical property is that lower rates of corrosion were observed in metals with such oxide layers. Solubility of the corroded metals in aqueous solution should also have a noticeable effect on the rates of corrosion as an increase in metal concentration increases solution conductivity. This would depend to an extent on the role of dissolved oxygen, or the ability for the metal to form other complexes in aqueous solution such as MO or MO_2 metal oxides which may or may not be prone to corrosion.

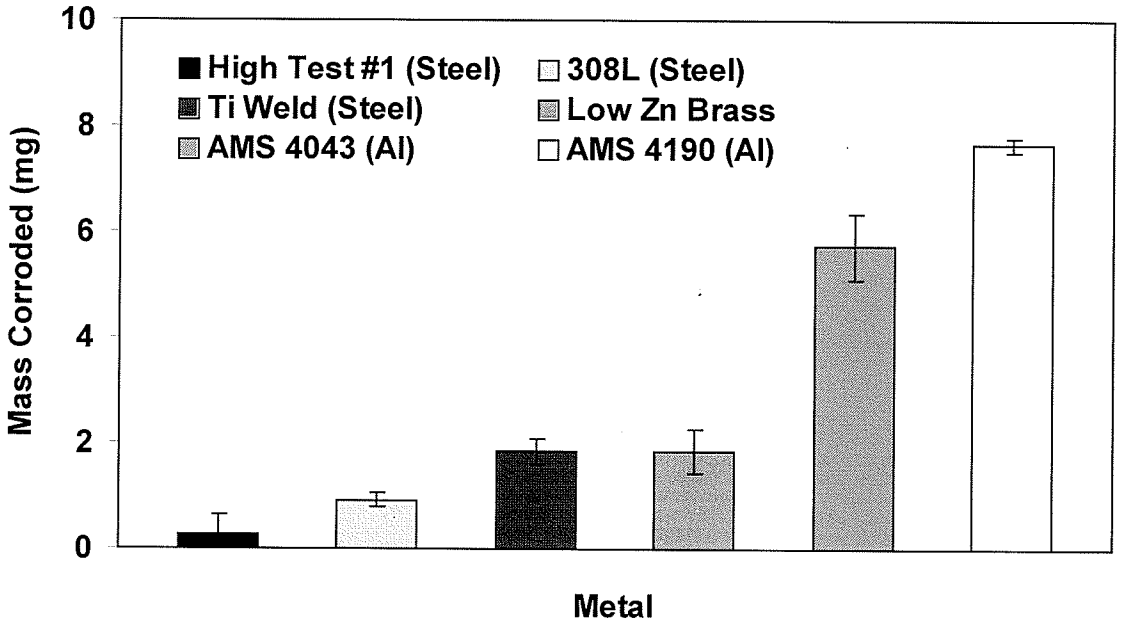

Figure 3.6: Corrosion of different metals using 2.5 A for 10 s in 0.025 M NaCl (n=7).

Experiments were carried out to determine if tensile strength had an effect on the rate of electrocorrosion of different metals. For this experiment, a series of steel samples were used. These steel samples were chosen because of their availability, similar composition and documented values for their tensile strength. Figure 3.7 shows the mass of corroded metal for a series of stainless steel samples that ranged in tensile strength from 60 to 118 kpsi. In general, it could be hypothesized that if a relationship existed between tensile strength and corrosion rates, then the softest steel should corrode at the highest rate. Figure 3.7 shows some degree of relationship between the two properties. However, the stainless steel with the highest tensile strength, Blue Max 2100® (118 kpsi), did not corrode at the highest rate. Stainless steel 11018-M, which had the highest amounts of Mn (1.6%), Cr (0.09%) and Ni (2.0%), had the highest corrosion rates, whereas alloy 6013, which had the lowest concentrations of Mn (0.6%), Cr (<0.01%) and

Ni (<0.01%), had the lowest corrosion rates. This suggests that elemental composition of the steel, rather than tensile strength, is more useful for predicting the rate of electrocorrosion.

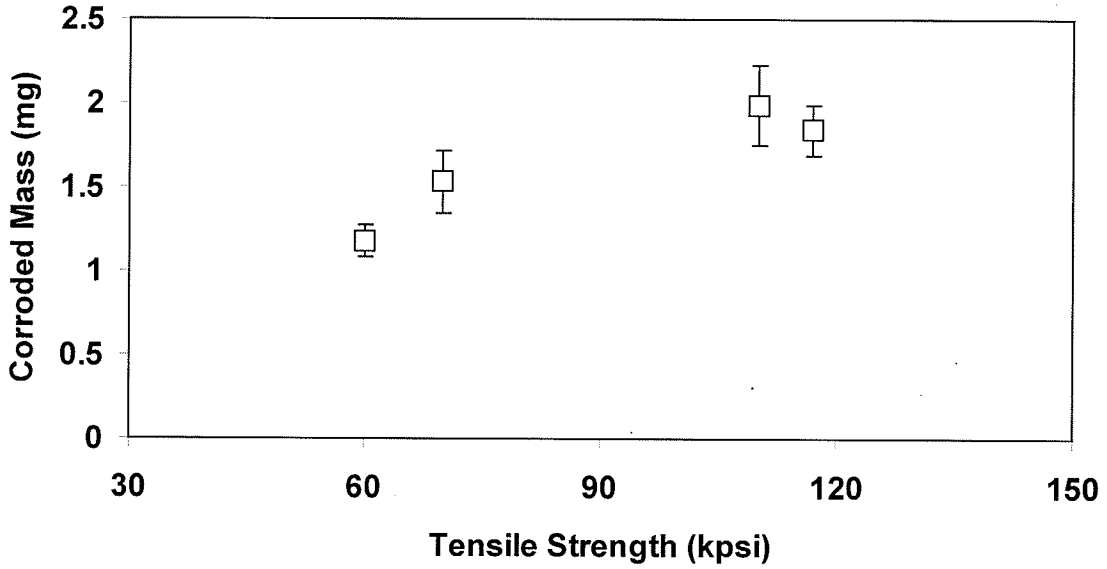

Figure 3.7: Correlation of the mass of corroded steels with tensile strength for various steel samples: 11018-M (110 kpsi), Blue Max® 2100 (118 kspi), E7018 (70 kspi), E6013 (60 kpsi). Electrocorrosion was achieved using 2.5 A cm^{-2}, for 10 s in 0.025 M NaCl (n=7).

To evaluate the possible effect of the composition of the aqueous solution on corrosion rates for different metals, several experiments were performed using salt solutions of various aqueous anions. For these experiments, 0.025 M solutions of NaF, NaCl, NaBr and NaI were prepared for electrocorrosion of pure Zn, Ni, Cu, Ag, and Au. These metals were chosen in order to provide a range of standard reduction potentials (E^{o}). Metals that have very high reduction potentials (Table 3.1), are more difficult to corrode. Some electrocorrosion reactions favor H_2O electrolysis rather than redox reactions with the metals, decreasing the rates of corrosion considerably.

Table 3.1: Standard reduction potentials[18].

	Reaction	$E°$ (V)
Gold		
	$Au^{+} + e^{-} \leftrightarrow Au(s)$	+1.69
Iodine		
	$I_2(s) + 2e^{-} \leftrightarrow 2I^{-}$	+0.620
Silver		
	$Ag^{+} + e^{-} \leftrightarrow Ag(s)$	+0.799
Copper		
	$Cu^{+2} + 2e^{-} \leftrightarrow Cu(s)$	+0.339
Nickel		
	$Ni^{+2} + 2e^{-} \leftrightarrow Ni(s)$	-0.236
Zinc		
	$Zn^{+2} + 2e^{-} \leftrightarrow Zn(s)$	-0.76

Figure 3.8 shows the electrocorroded mass of each of these metals in 0.025 M NaCl after 10s at 10 A cm^{-2} of applied current. For comparison, the electrocorroded mass of each metal in 0.025 M NaBr after 10 s at 10 A cm^{-2} is shown in 3.9. Some general observations can be made from these experiments. For example, the mass corroded (rate of corrosion) of each metal in a Cl^{-} matrix is similar, within experimental error, to that in a Br^{-} matrix. When Au was the target metal, oxidation or electrocorrosion did not occur. For all of the halides except F^{-}, this can be explained by the fact that they are easier to oxidize than Au[18]. Therefore, under these conditions, Au could not be oxidized and is not included in the figures. These experiments also illustrate that E° of the pure metal alone may not be useful for predicting relative rates of corrosion since Ag was found to corrode at a much higher rate than the other metals. In the case of Ag, it may be better to describe

the oxidation in terms of AgCl formation and recognize that the AgCl layer on the surface of the Ag (s) is not necessarily passive, as it is still conductive.

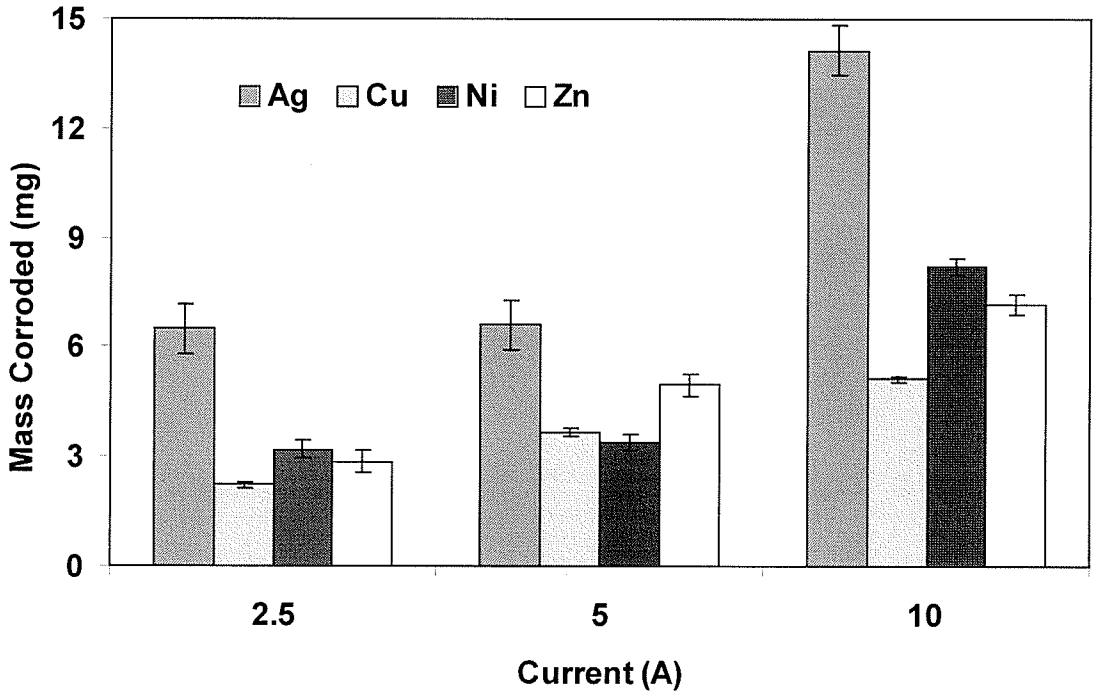

Figure 3.8: Mass of corroded metals for 10 s in 0.025 M NaCl (n=7).

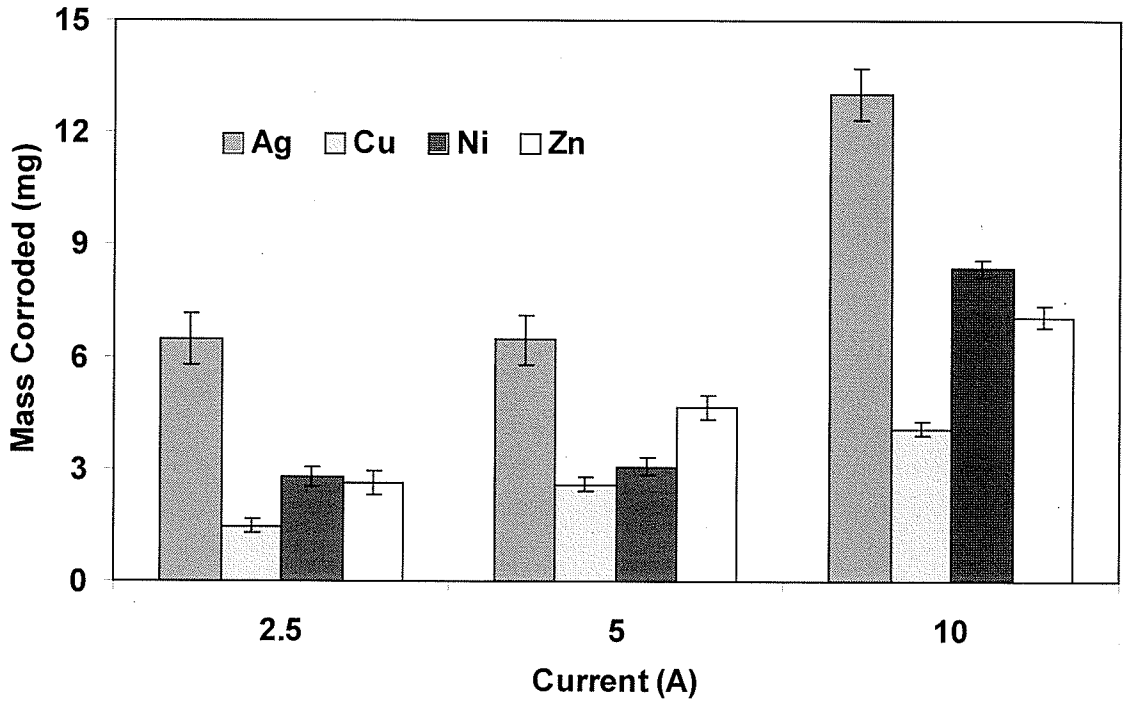

Figure 3.9: Mass of corroded metals for 10 s in 0.025 M NaBr as a function of applied current (n=7).

In similar experiments the relative rates of corrosion for pure metals was examined in different halide solutions, primarily to determine if different anions would affect the rate of electrocorrosion. It is hypothesized that anions of different mass will have different kinetic energy if an ion-metal collision process were occurring on the sample metal surface. In terms of mass, F^- is the lightest and therefore, one might expect the lowest rate of corrosion to be associated with this ion. For these experiments, Ag, Cu, Ni and Zn were electrocorroded in 0.025 M solutions of NaF, NaCl, NaBr and NaI. Figure 3.10 shows the effect of different halides on the corrosion of Zn. This behavior is representative of each of the metals except for Ni. One can conclude that the effect of halide on the rate of corrosion is minimal, which strongly suggests that a kinetic or

collision type of process is not likely and that electrolysis is the likely mechanism for the dissolution of metals. Other than Au, which is difficult to oxidize in aqueous solution, Ni is an interesting exception to this general trend. The electrocorrosion of Ni in different halide solutions is shown in Figure 3.11. Nickel has comparable corrosion rates to other metals such as Zn when 0.025 M NaBr or NaCl are used. When 0.025 M NaF and NaI are used, electrolysis or oxidation of Ni occurs at a very low rate relative to when Cl^- and Br^- are used.

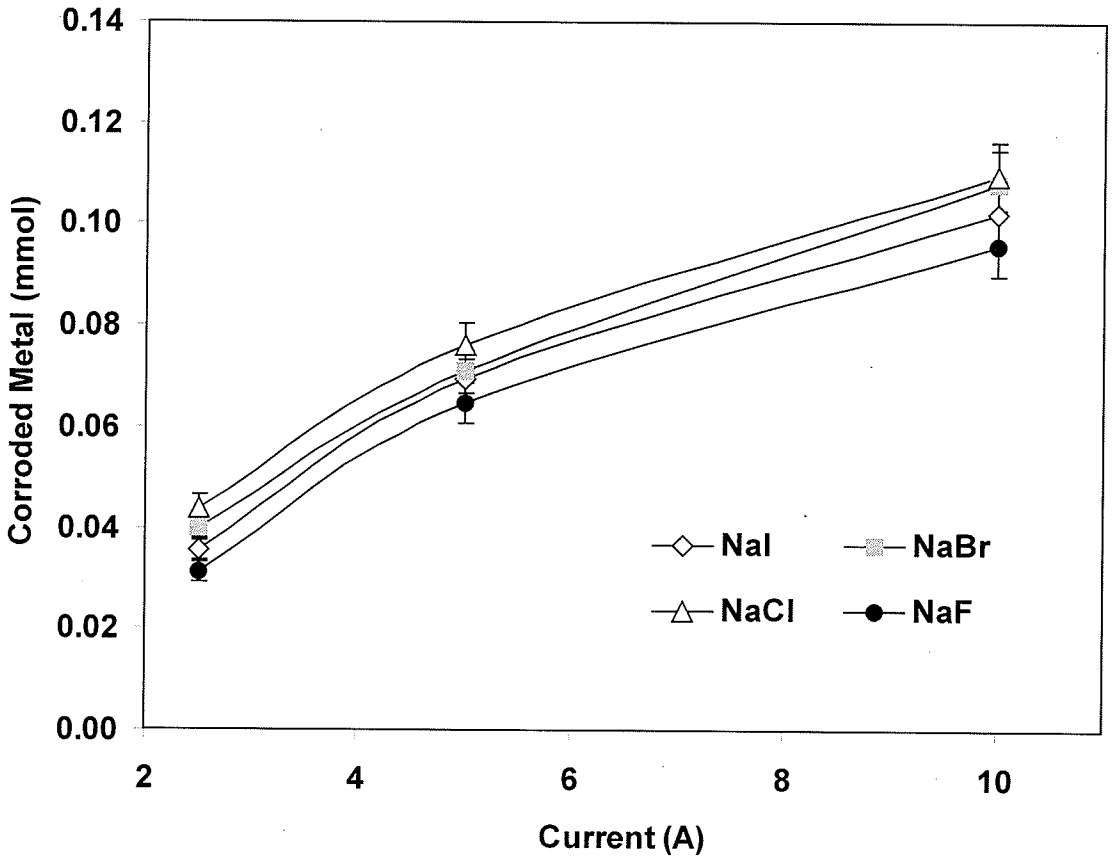

Figure 3.10: Electrocorrosion of Zn (E° = -0.76 V) at 2.5, 5 and 10 A cm^{-2} in 0.025 M solutions for 10 s (n=7).

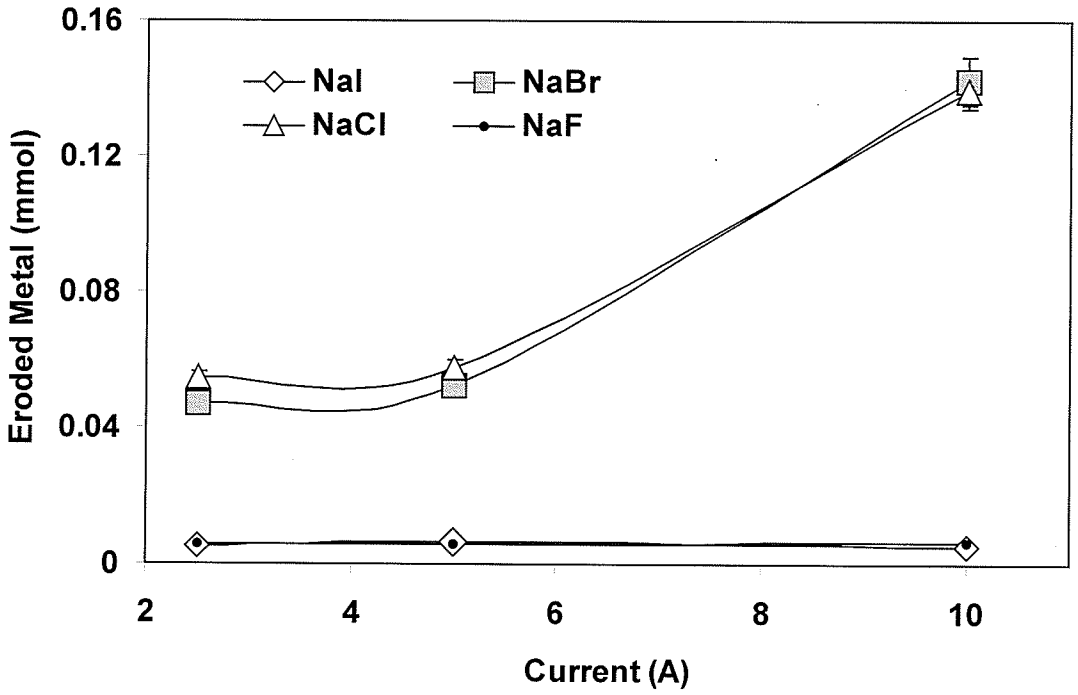

Figure 3.11: Electrocorrosion of Ni (E^o = -0.25 V) at 2.5, 5 and 10 A cm^{-2} in 0.025 M solutions for 10 s (n=7).

It is important to understand what is occurring with the solution as electrocorrosion is occurring as certain halides seem to allow corrosion while others do not. An experiment was devised in order to see if the resultant solution remained neutral (pH of 7) or if another effect was taking place. Measurements of pH were taken before and after electrocorrosion in various solutions and the results are shown in Table 3.2.

Table 3.2: The effect of electrocorrosion on pH of the sample solution over 20 s at 2.5 A cm^{-2}.

Element	Aqueous Solution	Initial pH	Final pH
Ag	NaCl	6.6	11.1
	NaBr	7.0	10.5
	NaF	7.3	9.6
	NaI	7.3	11.1
Au	NaCl	6.5	9.6
	NaBr	7.3	9.3
	NaF	7.1	10.1
	NaI	7.0	10.0
Cu	NaCl	6.9	11.0
	NaBr	7.2	10.5
	NaF	7.1	10.2
	NaI	7.1	10.7
Ni	NaCl	6.5	10.3
	NaBr	6.7	9.2
	NaF	7.1	9.0
	NaI	6.9	9.9
Zn	NaCl	7.1	9.2
	NaBr	7.1	9.6
	NaF	7.0	10.3
	NaI	6.8	7.9

For all the metals in each halide solution, pH was found to increase significantly from a pH of approximately 7 before current was applied to 10 after current was applied. The change in pH occurred rapidly and is consistent with the following mechanism that has been described for many metals in the literature[61]:

$$M + nH_2O \rightarrow M^{n+} + nOH^- + n/2H_2$$

and

$$M^{n+} + nOH^- \rightarrow M(OH)_n\ (s)$$

One might expect, by Table 3.1, that the electrocorrosion of Cu would be higher than Ni, however, this is only true if Ni is oxidizing directly to Ni^{+2}. Nickel oxidation resulting in the formation of a $Ni(OH)_2$ passive layer on the metal surface greatly affects the conductivity of the metal surface, in some cases will cease conductivity all together[22]. In 0.025 M NaI, the I^- oxidizes more readily than Ni. This was easily observed, since a dark brown color quickly formed in the solution, indicating that I_2 (aq) or I_3^-(aq) was forming. When NaF was used, a different situation likely occurs on Ni. As with I^-, pH increases and corrosion of the Ni surface does not occur. Oxidation of F^- (aq) to F_2 (g) does not appear to occur at this point, and there is no experimental evidence to suggest that F_2 (g) is formed. This is likely because F^- (E^o= +2.8V) is a much harder ion to oxidize than I^-(aq) (E^o = +0.54V). Nickel has been described as one of the least corroding metals in F^- media and in liquid HF, Ni is the only anode material of choice for electrochemical perfluorination of organic compounds with anhydrous HF[24].

Pourbaix diagrams are useful for determining the condition that a metal might be susceptible to corrosion or oxidation at various pH levels. Pourbaix diagrams overlay the stability or dissociation diagram of water with the redox and acid-base chemistry of metals. The Nernst equation (Equation 3.1) is used in the construction of the diagrams, relating the thermodynamic stability of specific products at various pH levels.

Equation 3.1:

$$\mathbf{E = E^{\circ} - ((0.05916\ V) \times (n)^{-1}) \times \log((A^{B}_{B}) \times (A^{A}_{A}))}$$

Where E is the half cell potential, E° is the standard reduction potential of the half cell, n is the number of electrons transferred in the half cell reaction and A^{B}_{B} and A^{A}_{A} are activity coefficients of the reduced and oxidized species respectively. These coefficients are unity for pure solids, while liquids, solvents and solutes are expressed in concentration (moles L^{-1}), and gases as partial pressures (bar).

The Pourbaix diagram (Figure 3.12) indicates if a metal is in a region where corrosion is more favourable or whether the metal is resistant to corrosion. There is another case where there is a potential for passive film formation. These areas may slow oxidation or prevent it, though the formation of these films is still a source of controversy. Pourbaix diagrams[54] for Ni indicate that a passive layer consisting of $Ni(OH)_2$ and possibly NiO can form at a pH of 10. This passive layer may be enough to prevent corrosion and oxidation of Ni. It is interesting to note that ions such as Cl^- actually delay the formation of the passive layer[54-57] and can cause pitting on the surface of Ni, which is why electrocorrosion occurs readily in 0.025 M Cl^- or Br^- media, but not in 0.025 M F^-.

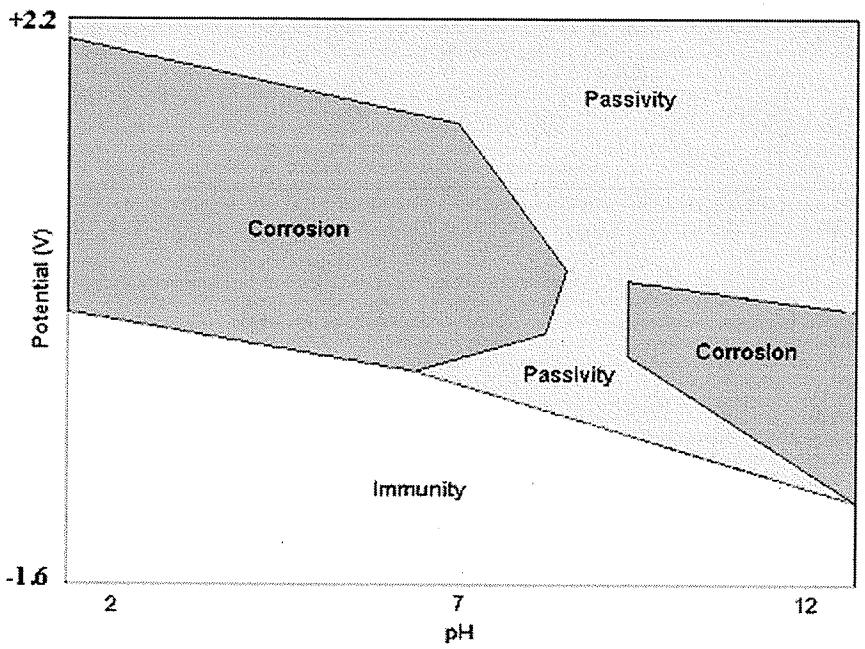

Figure 3.12: Pourbaix diagram for Ni [54].

The rate of electrocorrosion of an alloy with a high concentration of Ni was also examined to determine if it would behave in a similar manner as pure Ni. The alloy stainless steel 308L was chosen because it contained a fairly high percentage of Ni (9-11%) with Fe and Cr as the predominant elements. Figure 3.13 shows the mass of Ni corroded from stainless steel 308L at 10 A cm^{-2} in 0.025 M NaCl, NaBr, NaF or NaI over a period of 10s. It is interesting to observe that the rate of corrosion of this alloy was similar in 0.025 M Cl^-, Br^-, and F^-. However, in 0.025 M I^-, the rate of dissolution of metal was much less. When 0.025 M NaI was used, the rate of dissolution of the alloy 308L with 9% Ni was 10-20 $\mu g\ s^{-1}$, which is similar to the low rate of dissolution of pure Ni. Iodine or $I_2(aq)$ or $I_3(aq)$ formed readily, indicating that oxidation of I^- occurred preferentially over oxidation of the alloy surface. When 0.025 M NaF was used, the rate

of dissolution of the alloy 308L with 9% Ni was 800-1000 μg s^{-1}, which was not similar to pure Ni. When Ni is in an alloy, F^- may attack Fe and Cr and coincidentally allow Ni corrosion. Therefore, if the main components of the alloy were attacked by F^-, then Ni would also be more readily available for corrosion due to surface area.

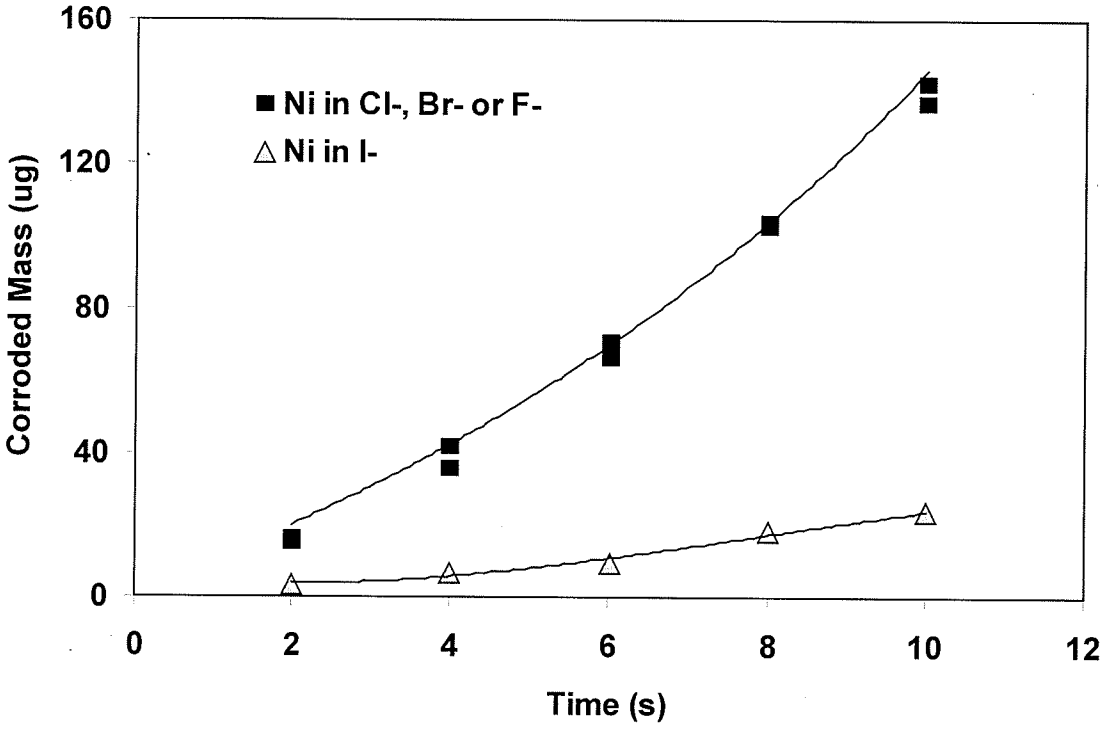

Figure 3.13: Mass of dissolved Ni from stainless steel 308L over time. Electrocorrosion was carried out at 10 A cm^{-2} in 0.025 M NaCl, NaBr, NaF and NaI (n=7).

These experiments strongly suggest that the use of I^- in the electrocorrosion solution is not recommended if the target metal contains significant amounts of Ni. For most metals, 0.025 M Cl^-, (as NaCl), is likely the preferred anion of all the halides. Additional experiments were carried out to determine whether preferential removal of metals such as Cr occurs during electrocorrosion of a sample that is high in Ni. If preferential oxidation and corrosion of one or more elements occurs in an alloy, then the

application of electrocorrosion for sample preparation is compromised. This experiment was carried out by applying 2.5 A cm^{-2} to the stainless steel 308L in 2 s intervals starting from 4 to 14 s in 10 mL of 0.025 M NaCl. After each interval, 1 mL was removed for analysis using FAAS. Figure 3.14 shows the mass of Cr and Ni in the NaCl solution over time as a 2.03: 1 ratio. The nominal composition of Cr is 18-21% and Ni is 9-11 %, which indicates that the expected relative amounts of metals were measured. Furthermore, since the ratio of Cr to Ni did not change significantly over time, it can be concluded that preferential elemental removal did not occur for these elements in steel.

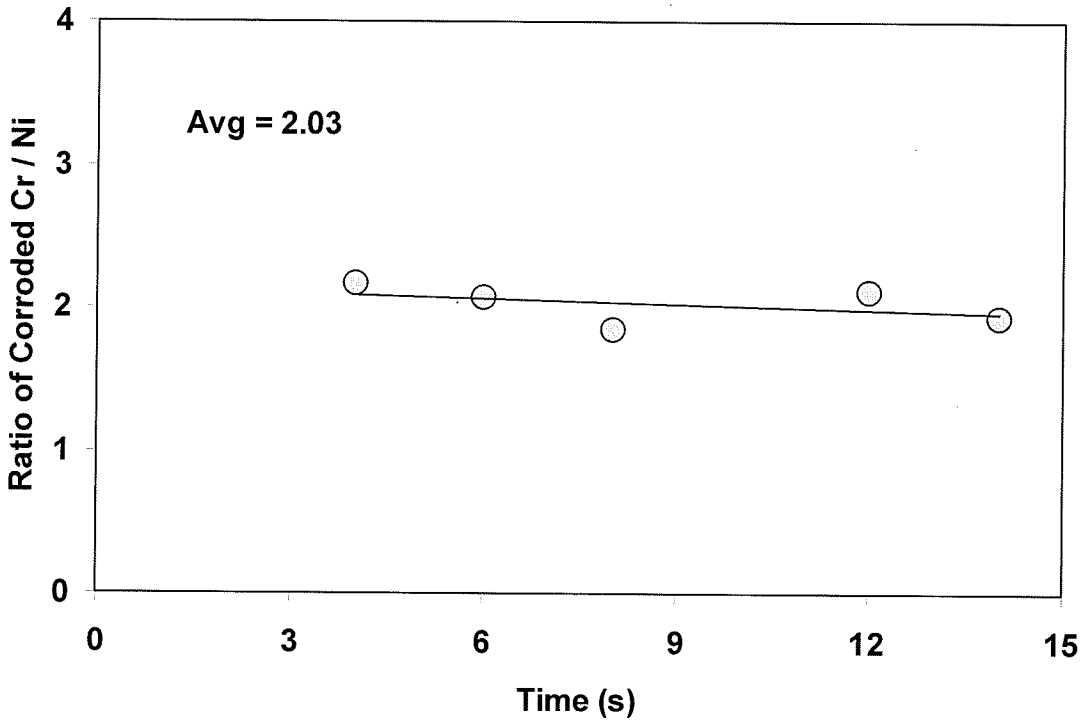

Figure 3.14: Electrocorrosion of Cr and Ni in stainless steel 308L in 0.025 M NaCl, at 2.5 A cm^{-2}.

Introduction of the solutions containing electrocorroded metals into an ICP-MS was carried out using stainless steel 308L in 0.01 M NaCl. Figures 3.15-17 show the mass scans of over 0-15 s. In terms of signal intensity, these Figures illustrate the length of time required for detecting trace levels of metals such as Ni and Mn in stainless steel (the peak at 56 amu is $^{56}Fe^{+}$ and $^{40}Ar^{16}O^{+}$). When an electrolyte such as NaCl is used, some practical considerations regarding its use should be noted. For example, although the addition of the electrolyte is essential for carrying charge in the electrocorrosion solution, it is a possible source of metal contamination as well as a spectral interference due to the formation of $^{35}Cl^{16}O^{+}$, which interferes with $^{51}V^{+}$. A number of simple solutions can be used to overcome these types of chemical or spectral interferences such as using an alternative salt (e.g. NH_4NO_3). Trace levels of transition metals can also be removed easily by running the salt solution through an ion-exchange resin such as 8-hydroxyquinoline.

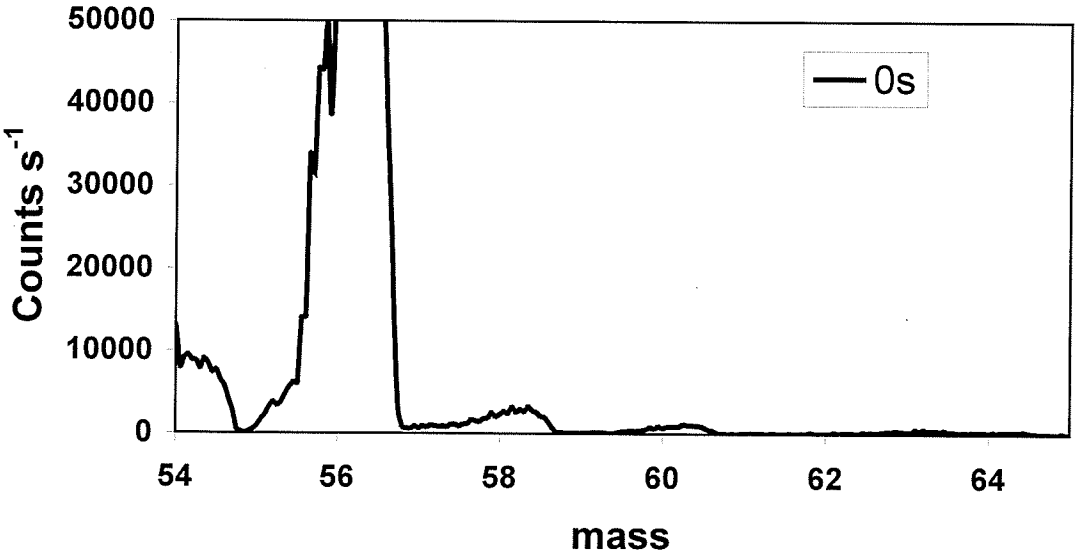

Figure 3.15: ICP-MS mass scans showing the formation of $^{58}Ni^{+}$, $^{60}Ni^{+}$ and $^{55}Mn^{+}$ in stainless steel for 0 s in the electrocorrosion solution.

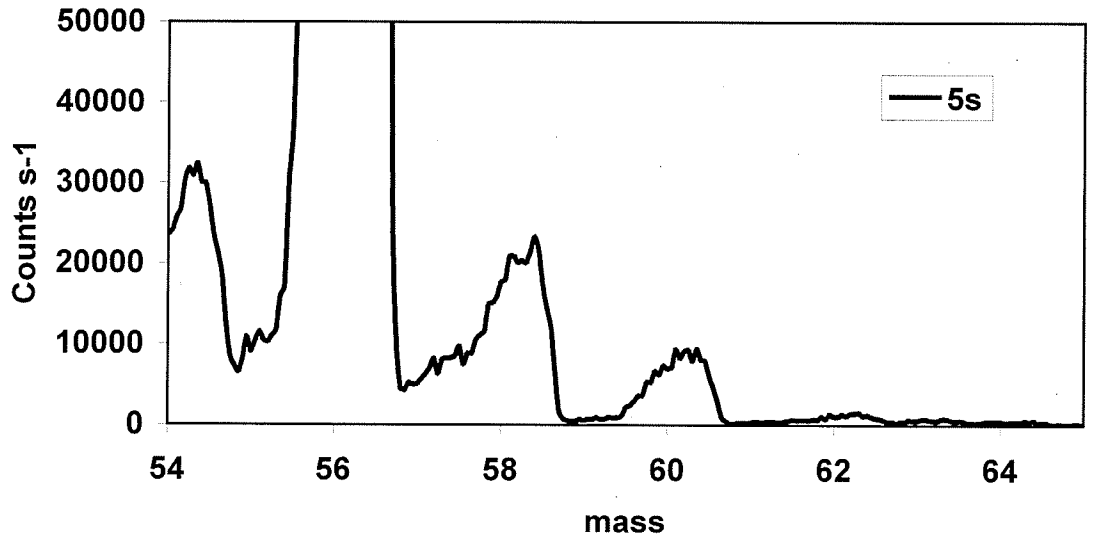

Figure 3.16: ICP-MS mass scans showing the formation of $^{58}Ni^{+}$, $^{60}Ni^{+}$ and $^{55}Mn^{+}$ in stainless steel for 5 s in the electrocorrosion solution.

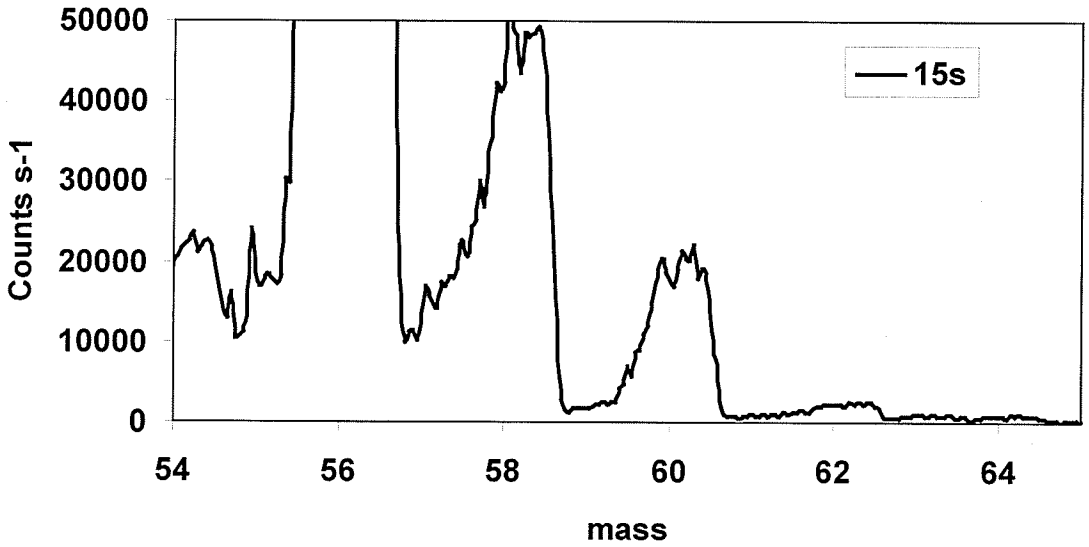

Figure 3.17: ICP-MS mass scans showing the formation of $^{58}Ni^{+}$, $^{60}Ni^{+}$ and $^{55}Mn^{+}$ in stainless steel for 15 s in the electrocorrosion solution.

Figures 3.18 and 3.19 show time profiles of $^{52}Cr^{+}$, $^{55}Mn^{+}$ and $^{60}Ni^{+}$ from the electrocorrosion of stainless steel-308L. The composition of 308L is 19.5-22% Cr, 9-11% Ni and 1-2.5% Mn as well as other trace metals and Fe. The argon dimer $^{80}Ar_2^{+}$ was also monitored to qualitatively determine if drifting, or possibly, loading of the plasma occurred, shifting or reducing the overall signal as the electrocorrosion solution was introduced. Metal in high concentration ($^{52}Cr^{+}$) was monitored as shown in Figure 3.18 and for clarity the behavior of metals that were lower in concentration ($^{55}Mn^{+}$ and $^{60}Ni^{+}$) is shown in Figure 3.19. In these experiments the electrocorrosion solution was continuously introduced into the ICP. A small stir bar was used to keep the electrocorrosion solution as homogeneous as possible. At approximately 45 s, and again at 160 s current was applied to the metal samples resulting in the increased signal after approximately 25-30 s when the solution reached the nebulizer. Sample was introduced directly into the plasma and no further treatment of the solution was performed. Since the Ar_2^{+} was not suppressed, it appeared that plasma effects such as loading were minimal. Time profiles illustrate that sample introduction of Cr was reasonably well behaved, relative to the metals of lower concentration (e.g. Mn and Ni). The %RSD of the signals between 130 s and 180 s was 5.04% for Cr, 10.78% for Ni, and 8.38% for Mn. The high %RSD is probably due to the heterogeneity of the electrocorrosion solution, which contains a disperse colloidal suspension. All of the ICP-MS signals appeared to be somewhat noisy, particularly when low levels of metals ($^{55}Mn^{+}$) are monitored. The noisy signals encountered are also likely a result of the heterogeneity of the colloidal suspension allowing for inconsistent sample introduction. At no point did the glass concentric nebulizer clog, however, some flicker of the plasma was observed.

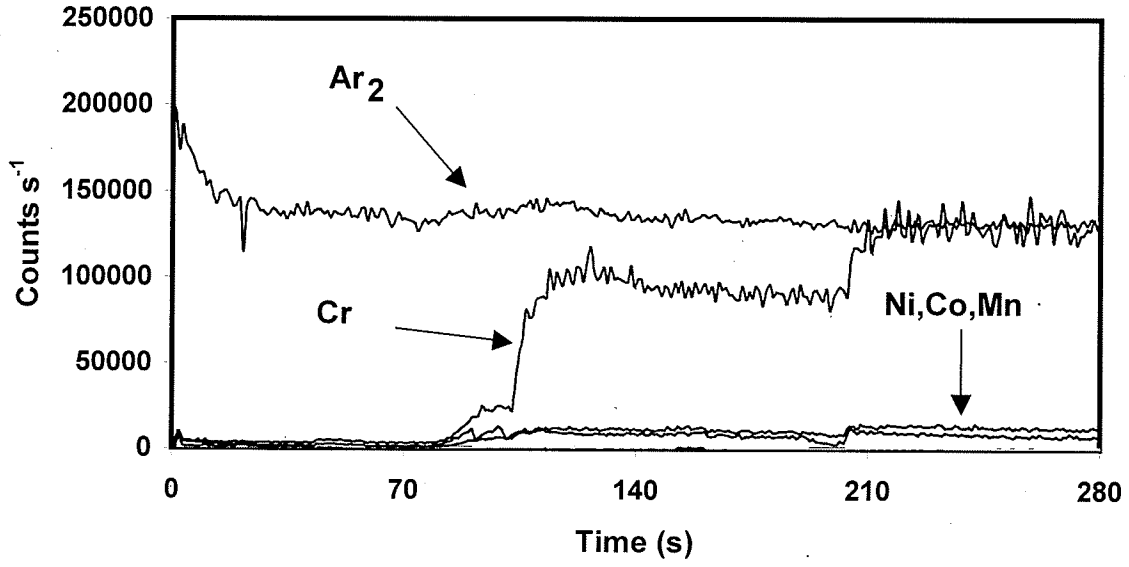

Figure 3.18: Continuous monitoring of $^{52}Cr^{+}$ in the electrocorrosion solution over time using ICP-MS.

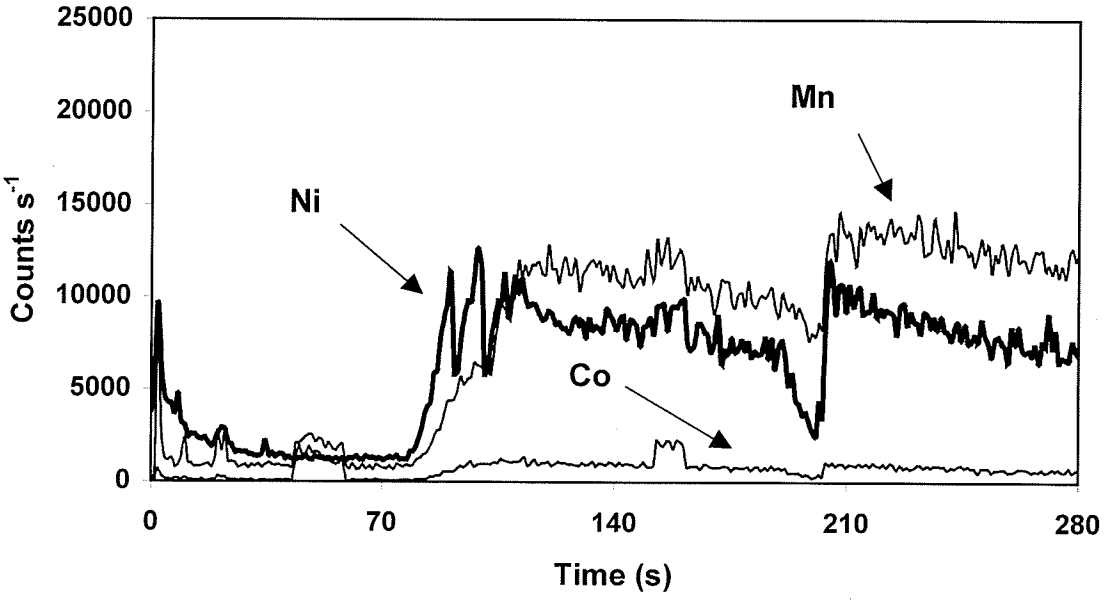

Figure 3.19: Continuous monitoring of $^{58}Ni^{+}$ and $^{55}Mn^{+}$ in the electrocorrosion solution over time using ICP-MS.

To illustrate the effects of solution heterogeneity on signal reproducibility, an experiment was carried out to compare signals of $^{52}Cr^{+}$, $^{60}Ni^{+}$ and $^{55}Mn^{+}$ before and after the addition of 100 μL of concentrated HNO_3 to a 20 mL sample containing the colloidal suspension. The colloidal suspension was prepared with an applied current of 2.5 A cm^{-2} using stainless steel 308L in 0.01 M NaCl for different time intervals. The results of these experiments, which are summarized in Table 3.3, illustrate how addition of 100 μL of concentrated HNO_3 improved the signal reproducibility regardless of corrosion time. Addition of HNO_3 did not increase signal intensity but did improve the signal reproducibility for shorter corrosion times (5 s) and smaller signals. The slight decrease in signals at shorter corrosion times indicates that when acid was added some additional loading or cooling of the plasma may have occurred, especially when large concentrations of Na^{+} and Cl^{-} are already in the solution. Addition of acid increased both signal intensity and reproducibility for a longer corrosion time (40 s). Addition of HNO_3 dissolved the colloidal material and improved the ionization efficiency of the ICP. For all corrosion times, dissolution of the colloidal material improved the sample heterogeneity and ultimately signal reproducibility.

Table 3.3: Signal reproducibility (%RSD) before and after addition of concentrated HNO_3

	Signal (Counts s^{-1})			
	$^{55}Mn^+$	$^{52}Cr^+$	$^{60}Ni^+$	$^{40}Ar_2^+$
100 ppb std.	3129 ± 5.63	840 ± 4.71	163 ± 4.34	87860 ± 3.39
5s no acid	32320 ± 12.8	11070 ± 9.55	3983 ± 15.8	87140 ± 2.44
5s + HNO_3	34270 ± 4.28	9975 ± 5.23	3621 ± 9.19	61410 ± 2.14
20s – no acid	175800 ± 5.60	53350 ± 4.26	20170 ± 6.69	56600 ± 3.00
20s + HNO_3	240800 ± 2.29	76480 ± 3.86	28580 ± 4.43	61360 ± 2.02
40s – no acid	343500 ± 5.52	128700 ± 4.83	45540 ± 5.53	64990 ± 2.00
40 + HNO_3	398900 ± 3.59	133600 ± 3.60	52000 ± 4.20	62240 ± 2.44

To test the feasibility of electrocorrosion for quantitative analysis, the determination of Ni, Cu, Co, Al, Pb and Ag was carried out on a sample of known composition. A Cr-V steel standard from the National Institute of Standards and Technology (NIST 663) was electrocorroded for 10 s at 2.5 A in a 0.01 M NaCl solution. The elements were chosen to specifically demonstrate the feasibility of the electrocorrosion apparatus to perform sample preparation of trace elements over a range of concentrations. Metal determination was carried out by GFAAS using the method of standard addition. The results of this experiment are summarized in Table 3.4. All of the determined concentration values with corresponding standard deviations overlap those of the reference material values and associated confidence intervals.

Table 3.4: Determination of trace elements in Cr-V Steel (NIST SRM 663). Standard deviation was calculated from four trials.

	Concentration (%)		
	Ag*	**Cu**	**Pb**
Certified	0.0038 ± 0.001	0.098 ± 0.005	0.0022 ± 0.0001
Found	0.003 ± 0.001	0.098 ± 0.010	0.0022 ± 0.0001
	Ni	**Al**	**Co**
Certified	0.32 ± 0.01	0.24 ± 0.01	0.048 ± 0.05
Found	0.33 ± 0.01	0.25 ± 0.07	0.048 ± 0.01

* not certified.

3.2 Spark Ablation

Spark ablation is similar in principal to electrocorrosion, though differences exist. In spark ablation, current is carried via a high-voltage electric discharge (spark) where electrons accelerate to neighboring metal samples. Conversely, electrocorrosion depends on solution conductivity to carry electrons. The sample gap is critical in spark ablation. Due to high solution resistivity (18 MΩ De-ionized water), the sample gap must be sufficiently small to overcome the solution barrier. If the metal samples are placed far apart from each other, a spark will not form.

Many properties of high-powered[24] and low-powered[25] spark ablation in aqueous solutions have been previously described. This research was dedicated to the characterization of low-power ablation of metals that are difficult to oxidize such as Au and Rh.

Wide ranges of metals were chosen to see if ablation rates varied for different metals. Another goal for this particular experiment was to see if Rh and Au would be

ablated into solution. The graphs were created by weighing the metal samples before and after ablation, with the change in mass being plotted over a range of ablation periods from 60 to 120 s. As expected, there is an increase in mass lost over time. Figures 3.20-3.22 demonstrate that not only are all metals ablating at similar rates, but that difficult to oxidize metals (e.g. Rh and Au) can be rapidly ablated into solution by spark ablation.

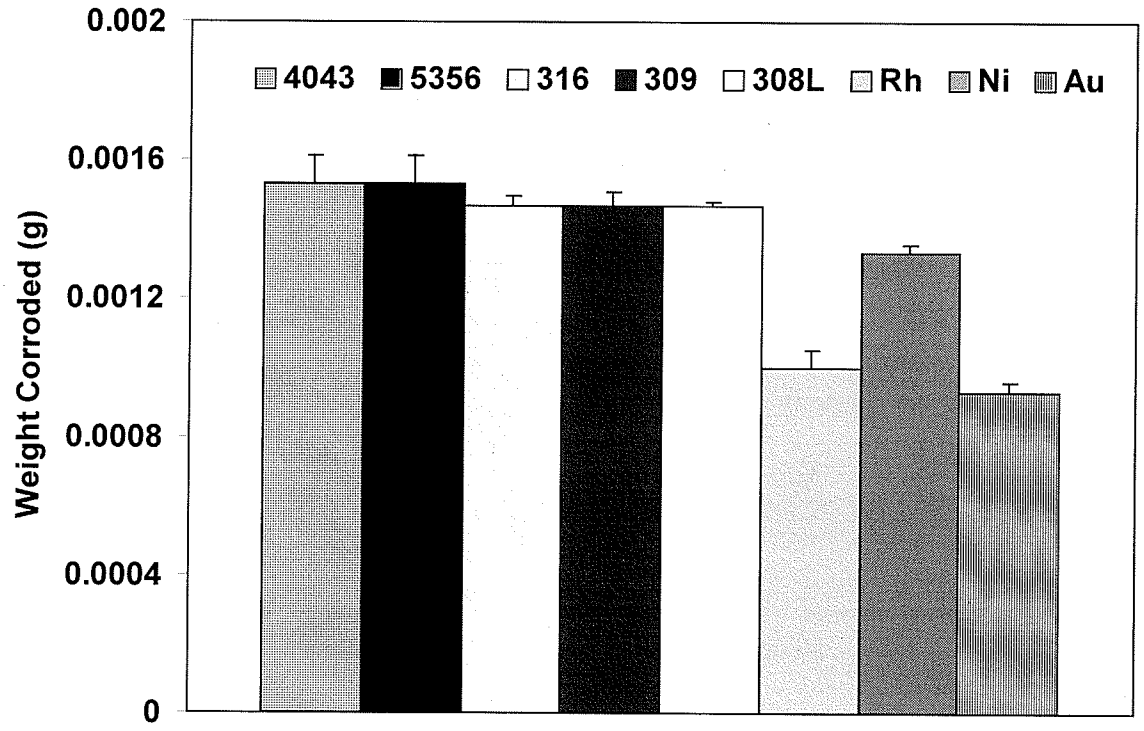

Figure 3.20: Spark ablation of different metals over a period of 60 s.

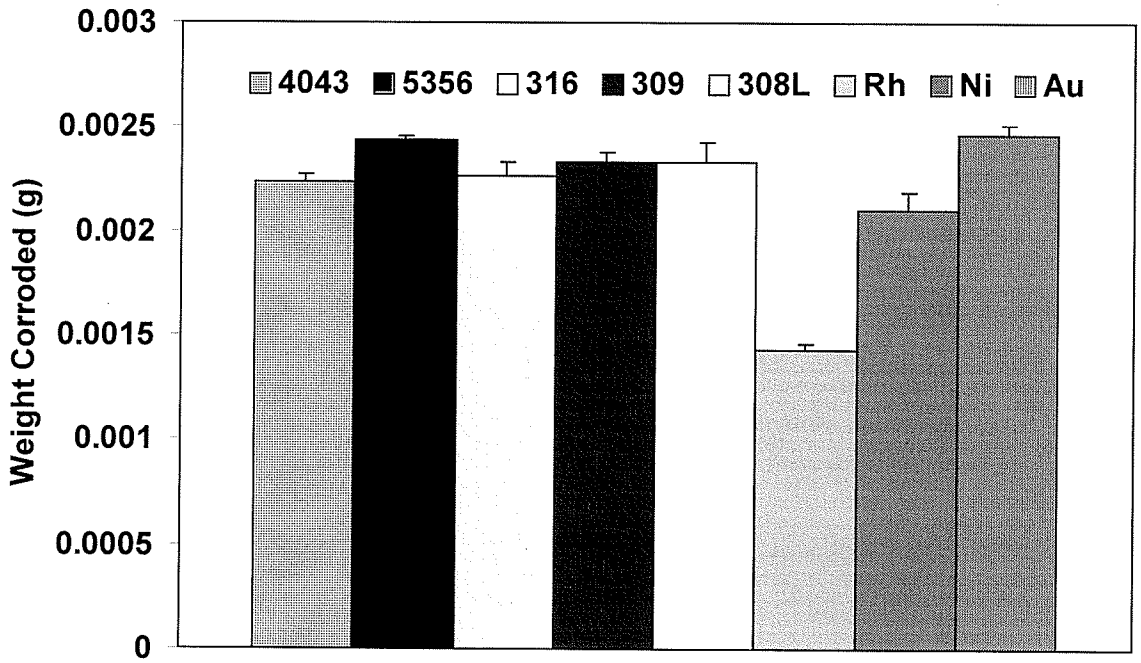

Figure 3.21: Spark ablation of different metals over a period of 90 s.

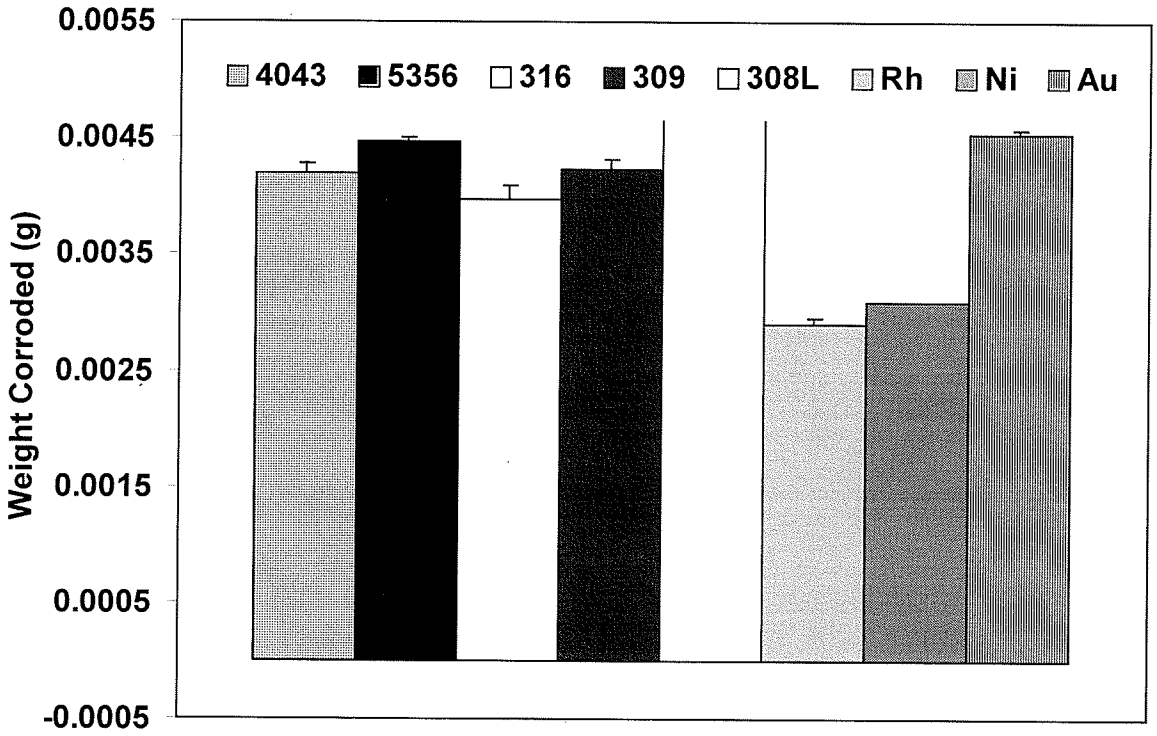

Figure 3.22: Spark ablation of different metals over a period of 120 s.

The solution in which spark ablation occurs plays a crucial role as it creates the resistance through which the spark can occur. If the solution were to become conductive, the spark may become weak. This may decrease the rate, or cease ablation all together. The effect of volume and ablation time on signal intensities was investigated to understand this principal more completely. Iron in stainless steel 308L was monitored by FAAS for a period of 30 to 150 s at volumes of 10 mL and 50 mL, the results are plotted in Figure 3.23. Here, the rate of ablation is decreasing in the smaller volume more rapidly than in the larger volume sample. This is due to the total conductivity of the solution increasing at a much higher rate compared to the larger volume. This increase in solution conductivity reduces the energy of the spark directed to the metal samples, therefore reducing the total rate of ablation over time. The larger volume requires significantly more metal in solution in order for the conductivity of the solution to increase significantly. This factor is important to understand if analysis for trace elements is to be conducted which will require longer ablation periods to extract the lower concentration elements.

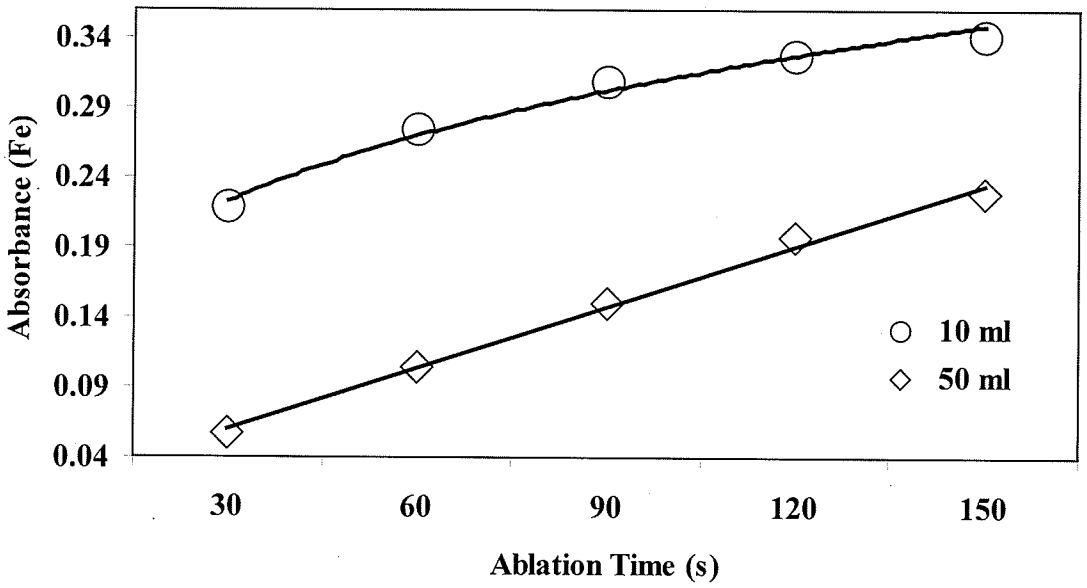

Figure 3.23: Effect of volume and ablation time on signal intensity of Fe in alloy 308L.

The effect of ablated material in solution on conductivity was also investigated with two different metals to observe the correlation between solution conductivity and signal intensity. Steel alloy 308L and a brass sample were ablated over a period of 30 to 300 s with the resulting solution analyzed for conductivity (S cm^{-2}). Figure 3.24 shows how increasing ablated mass in solution increases the conductivity. This effect will ultimately reduce the rate of ablation over time.

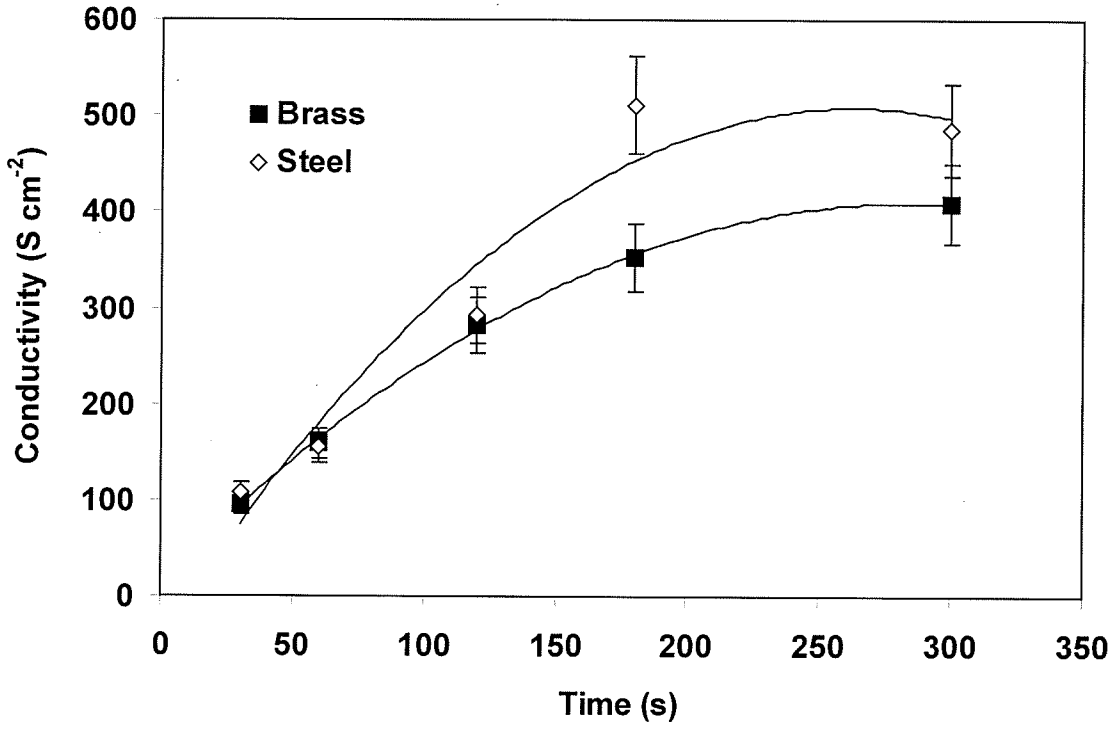

Figure 3.24: Effect of conductivity on the ablated mass in solution.

The analysis of Cu and Ag in Au standards obtained from the Royal Canadian Mint was investigated by spark ablation. These experiments were performed to determine if spark ablation in the liquid phase could be used for quantitative analysis of trace metals in Au. One of the properties associated with spark ablation is the heterogeneous nature of the post-sparked solution. In many cases, colloids can be dissolved by small amounts (50 μL) of acid, creating a homogeneous solution ready for sample introduction to an ICP. Typically, Au is dissolved with a strong oxidative acid such as aqua regia (3:1 HCl to HNO_3) because weaker oxidative acids such as HNO_3 alone are not strong enough dissolve Au. Difficulties can emerge when analyzing for Ag in Au due to precipitate formation upon addition of aqua regia. Thus, experiments were designed to see if analysis without the addition of acid is feasible. Cu, which has a 1%

balance in bullion reference material (BRM-1), was analyzed over several different time periods. The solution was sparked and colloids were allowed to settle for 5 to 70 s before introduction into the GFAAS for final analysis. All trials (n =6) were run in a set volume of 25 mL. Results are represented by percent relative standard deviation (%RSD) over time. Figure 3.25 shows that at 5 s, the %RSD is high relative to the rest of the results due to little sample available versus the larger volume. As ablation time increases, so does the amount of colloid in solution, therefore the solution is more homogeneous with respect to the colloids. This means that with techniques such as GFAAS, set volumes are being introduced into the furnace. If the solution is more densely populated by colloidal material, the likelihood of receiving a similar amount of sample in the furnace each time is relatively high over multiple trials versus the likelihood of the same situation occurring with fewer colloids. These results demonstrate that at longer ablation times, acid is not necessarily needed, though analysis for bulk elements may mean that highly sensitive instruments such as GFAAS are no longer required. Problems may arise when consistency is needed for analyzing bulk and trace elements concurrently while using a similar volume and instrument, therefore considerations like volume and time must be made.

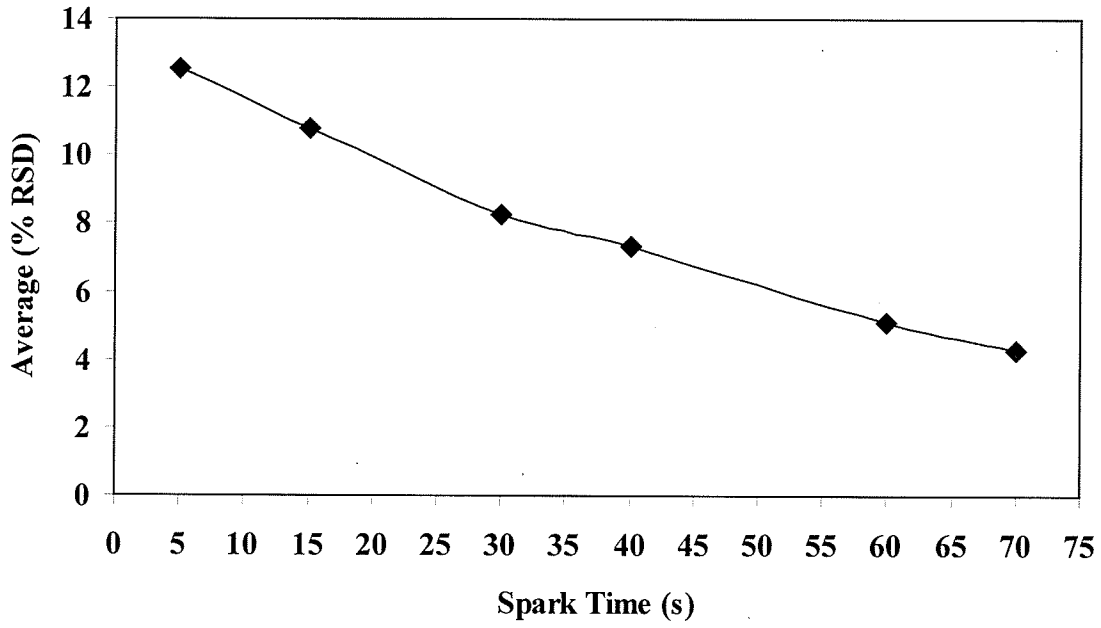

Figure 3.25: Relationship of %RSD of Cu in BRM-1 with respect to spark time.

In the case of BRMs, Cu and Ag percentages varied from 1-10% and 4-15% respectively, therefore a need for ablation times shorter than 70 s is required so that signals are not too high. Acid must now be considered to create a homogeneous solution. Acid addition experiments were constructed in order to find out which acid would be suitable for Cu and Ag analysis in BRM samples. Ultra pure HNO_3, HCl, aqua regia were compared with controls to see if any method would produce low sample deviations. All volumes and samples were fixed as were ablation times in order to focus on colloidal dissolution effects and not effects from sample gap or conductivity. All trials were run in multiples of 10 ablated over a period of 60 s and results recorded with respect to %RSD for Cu (Figure 3.26) and Ag (Figure 3.27). Figure 3.26 demonstrates little to no problems associated with the addition of acid to Cu signals. In fact, all of the % RSDs are lower with acid than without. Figure 3.27 indicates higher % RSD values when using

HCl containing acids showing a possible interaction between Cl and Ag as AgCl. This can be contrasted with the relatively low % RSD with use of HNO_3. Therefore, HNO_3 addition of over 300% can be used to digest and stabilize the small amount of colloids (50 μL) in solution so Ag determination in Au can proceed.

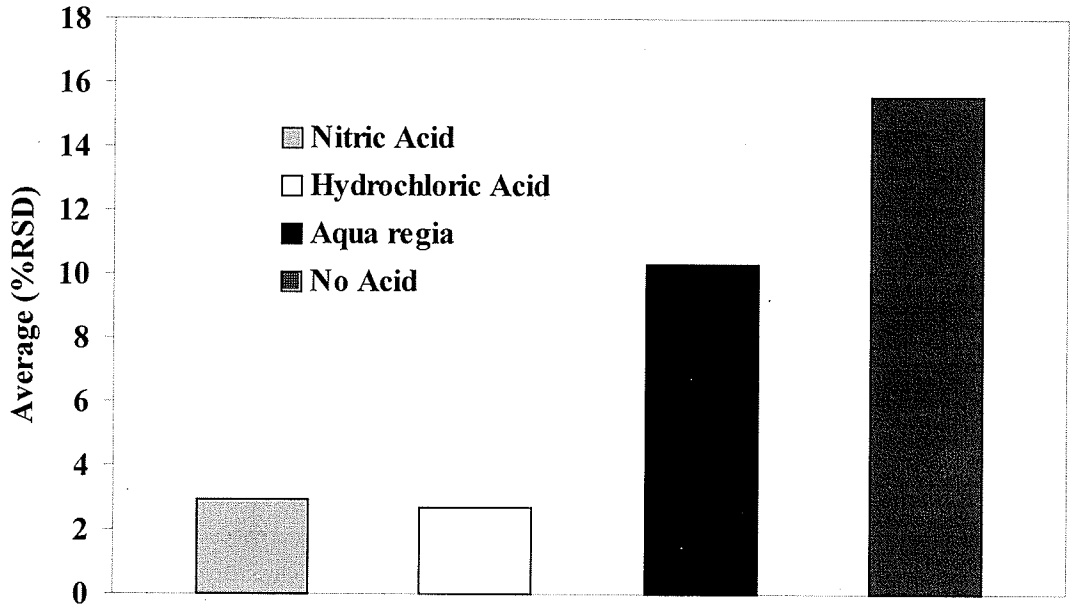

Figure 3.26: %RSD of Cu in BRM-1 using various acids.

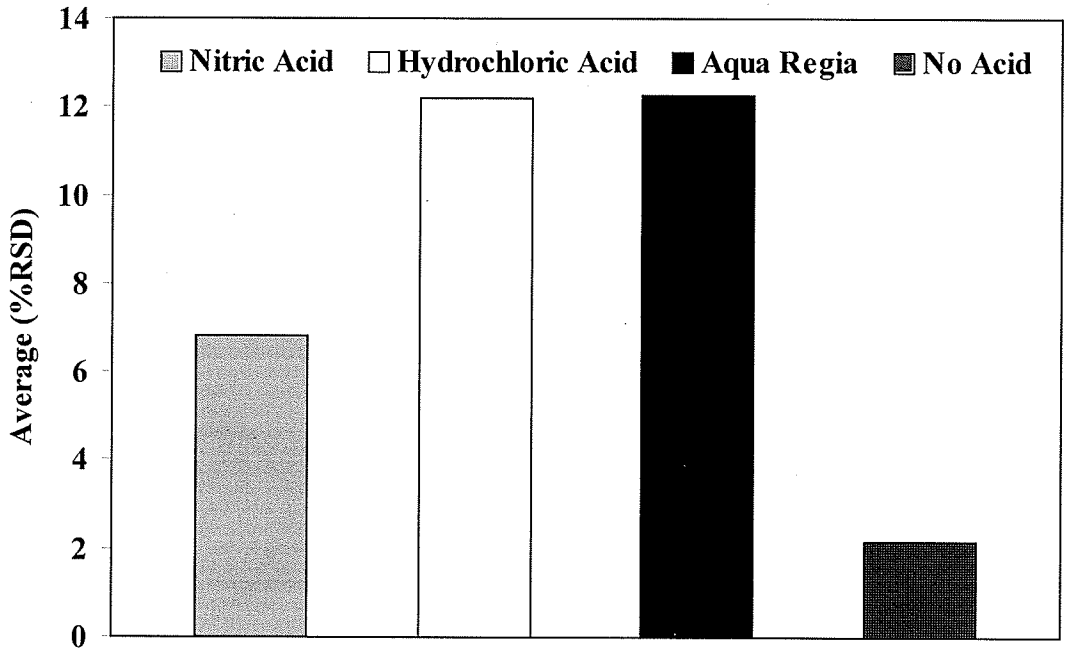

Figure 3.27: %RSD of Ag in BRM-1 using various acids.

Quantitative analysis of Cu and Ag in BRM-1, BRM-2, BRM-3 is possible, as a method for Ag determination has been established. In these experiments, the BRMs were ablated in GFAAS plastic cups and the analysis was performed by the method of standard addition. A spark time of 90 s was used in a volume of 6 mL. A 50 μL aliquot was then removed and digested in 200 μL of HNO_3, then diluted to 25 mL and introduced directly into the GFAAS without any further preparation. Values for all BRM's show excellent reproducibility and accuracy compared to certified values, as seen in Table 3.5-3.7

Table 3.5: Quantitative analysis of Cu and Ag in BRM-1.

	Ag	Cu
Found (%)	**3.85**	**0.91**
	4.48	**1.06**
	4.35	**0.84**
	3.72	**0.82**
	3.90	**0.93**
	4.07	**0.92**
	3.89	**0.97**
	3.80	**1.03**
Average (%)	4.01 ± 0.27	0.94 ± 0.09
Certified (%)	4.15 ± 0.36	1*

***Cu values are not certified, but percent balanced to 100%**

Table 3.6: Quantitative analysis of Cu and Ag in BRM-2.

	Ag	Cu
Found (%)	**8.21**	**2.16**
	7.87	**2.07**
	8.01	**1.79**
	8.87	**2.11**
	8.15	**1.84**
	8.01	**1.92**
	8.43	**1.97**
	7.69	**1.90**
Average (%)	8.16 ± 0.37	1.97 ± 0.13
Certified (%)	8.03 ± 0.20	2*

***Cu values are not certified, but percent balanced to 100%**

Table 3.7: Quantitative analysis of Cu and Ag in BRM-3.

	Ag	Cu
Found (%)	**12.27**	**2.63**
	12.15	**3.14**
	12.10	**3.34**
	12.05	**3.11**
	12.50	**3.23**
	11.71	**3.04**
	12.14	**3.14**
	11.90	**3.38**
Average (%)	12.10 ± 0.24	3.13 ± 0.23
Certified (%)	12.08 ± 0.33	3*

***Cu values are not certified, but percent balanced to 100%**

3.3 Scanning Electron Microscopy (SEM) and Energy Dispersive-X-ray Fluorescence (ED-XRF) of Electrocorrosion and High and Low-Powered Spark Ablation

Qualitative comparison of spark ablation and electrocorrosion by SEM and ED-XRF can provide information about chemical and physical properties that are occurring on the surface of the metal samples. An illustration of high-powered spark ablation, low-powered spark ablation, and electrocorrosion approaches that were performed for these experiments can be seen in Figure 3.28.

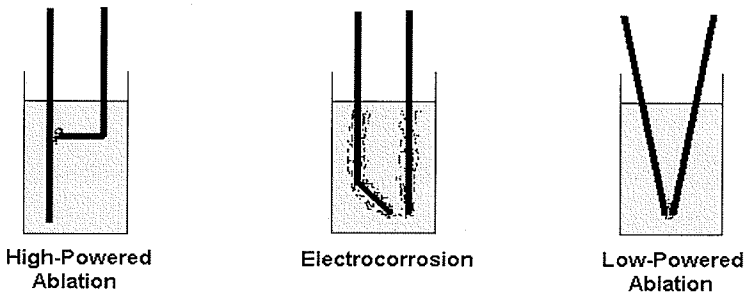

Figure 3.28: Sample positions of the different techniques. Sample gaps for high-powered ablation, low-powered ablation and electrocorrosion being 1 mm, 3 mm, and 0.5 mm respectively

SEM images of stainless steel 308L were taken after the metal sample was ablated under high power (10 A cm^{-2}) for 2 s. Figure 3.29 shows a large pit in the side of the metal sample. Here, areas A through C were chosen as spots of interest as they represent

different characteristics of the ablation crater, and subsequent magnification was performed.

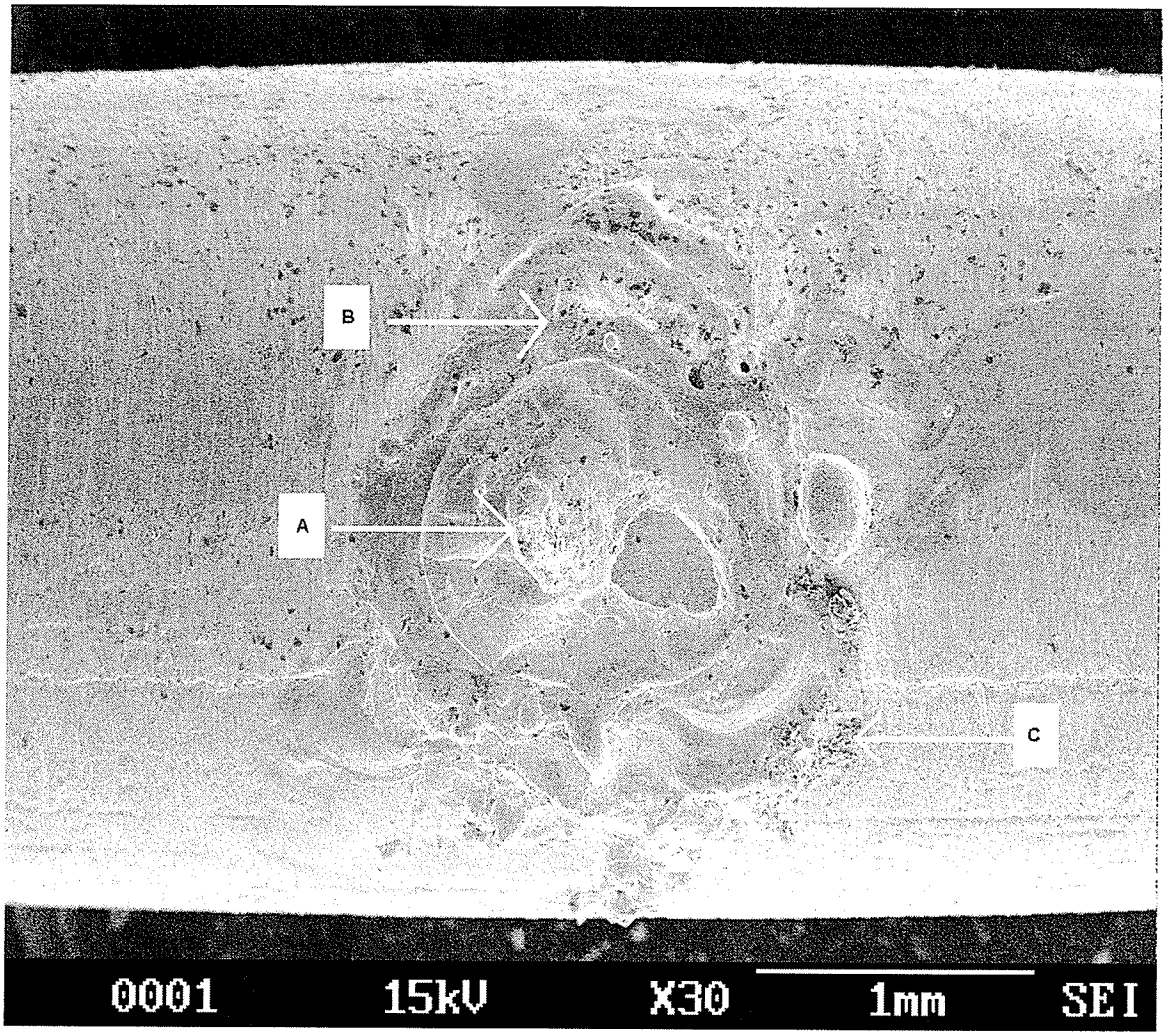

Figure 3.29: SEM image of alloy 308L after high-powered (10 A cm^{-2}) spark ablation

Area A was the area of highest impact and the deepest part of the crater, which can be seen by higher magnification in Figure 3.30. Energy dispersion-XRF spectra were also taken from Areas 1 and 2. These spectra demonstrate an important characteristic of high-powered spark ablation, which are the difficulties associated with excessive damage to the surface.

An ED-XRF spectrum of Area 1 (Figure 3.31) shows the presence of Si (1% in 308L). When compared to the ED-XRF spectra of Area 2 (Figure 3.32), the lack of an Si peak demonstrates that a high-powered spark may be more difficult to control, meaning possible problems with representative sampling.

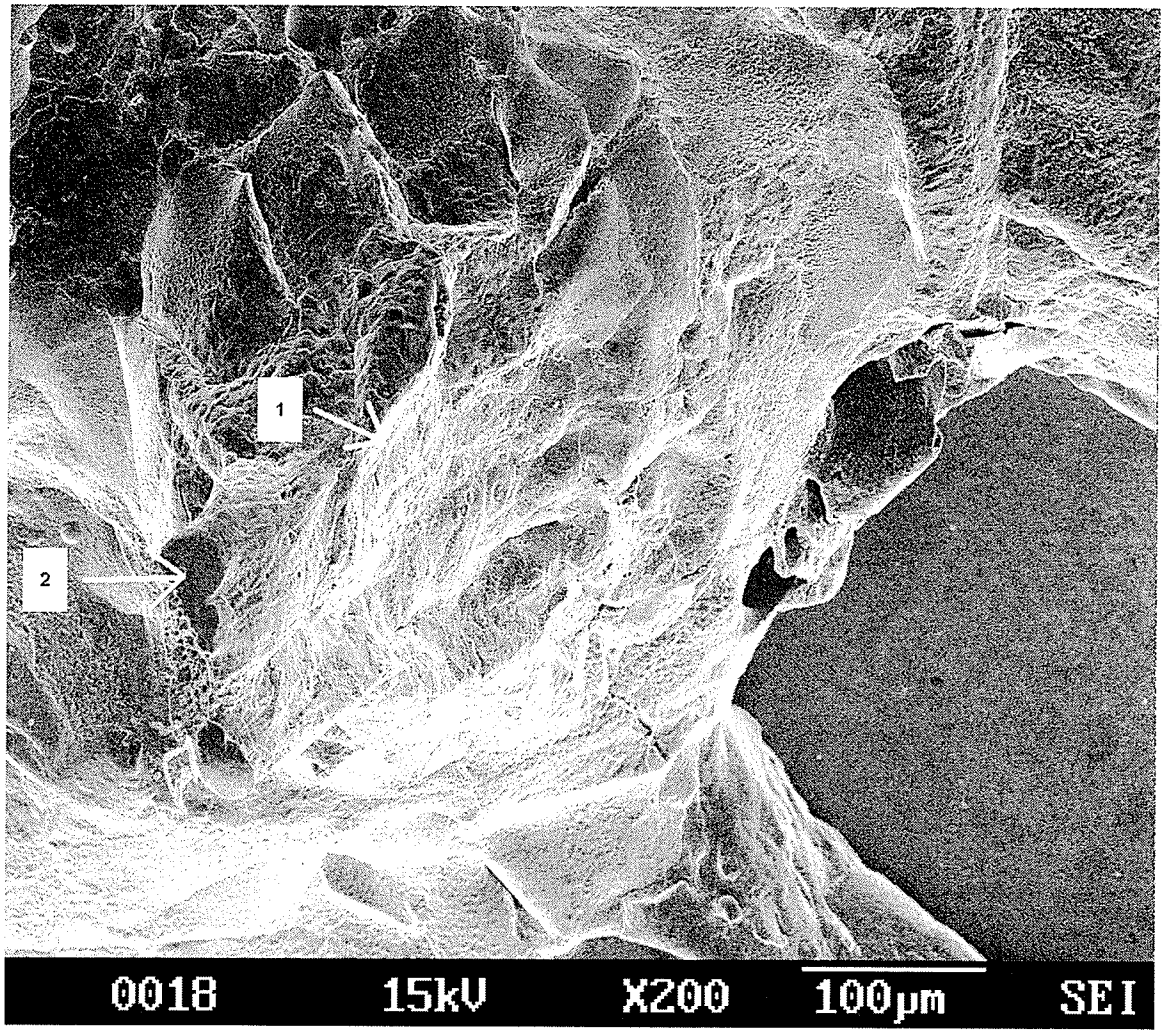

Figure 3.30: Higher magnification of Area A of Figure 3.29.

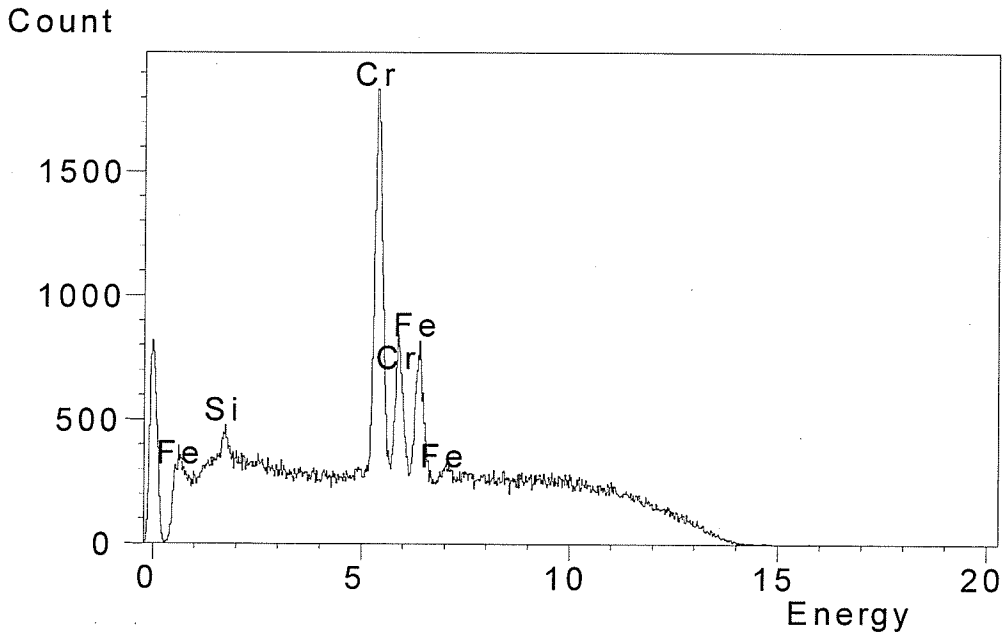

Figure 3.31: ED-XRF spectra of Area 1 from Figure 3.29.

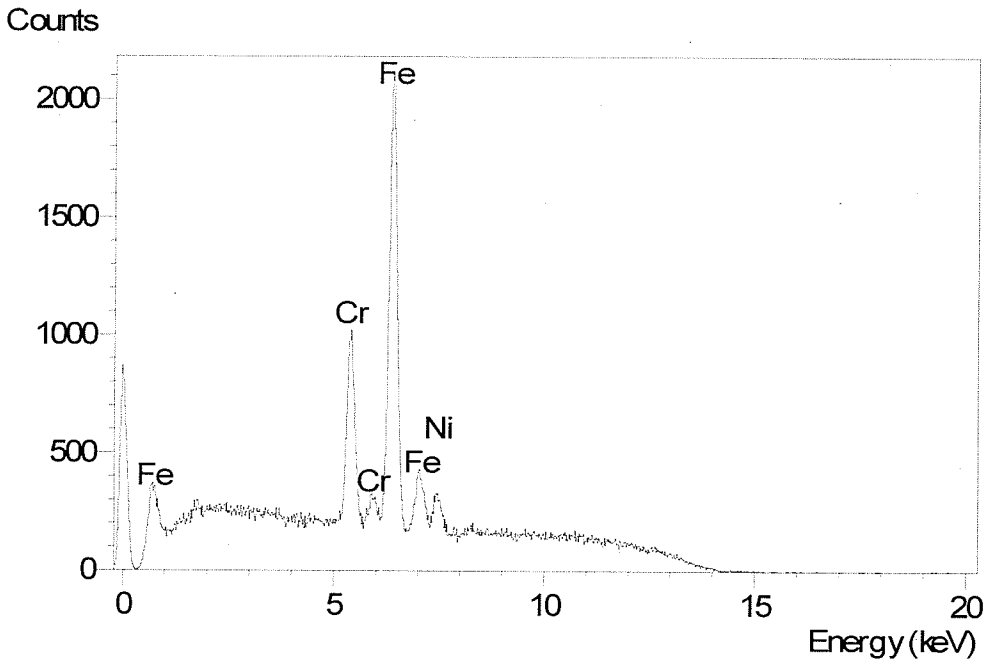

Figure 3.32: ED-XRF spectra of area 2 from Figure 3.29.

Figures 3.33 and 3.34 are higher magnification images from Areas B and C from Figure 3.29 respectively. Both Figures demonstrate the high-energy which was impacted at the metal sample surface, as molten metal had formed and hardened. ED-XRF spectra of areas 3 through 6 confirm the difficulties in maintaining a consistent spark with high-powered spark ablation, as peaks for Cr, Fe, and Mn fluctuate significantly. The Si peak may be an impurity derived from the glass vessel as the peak is only observed in two discrete areas.

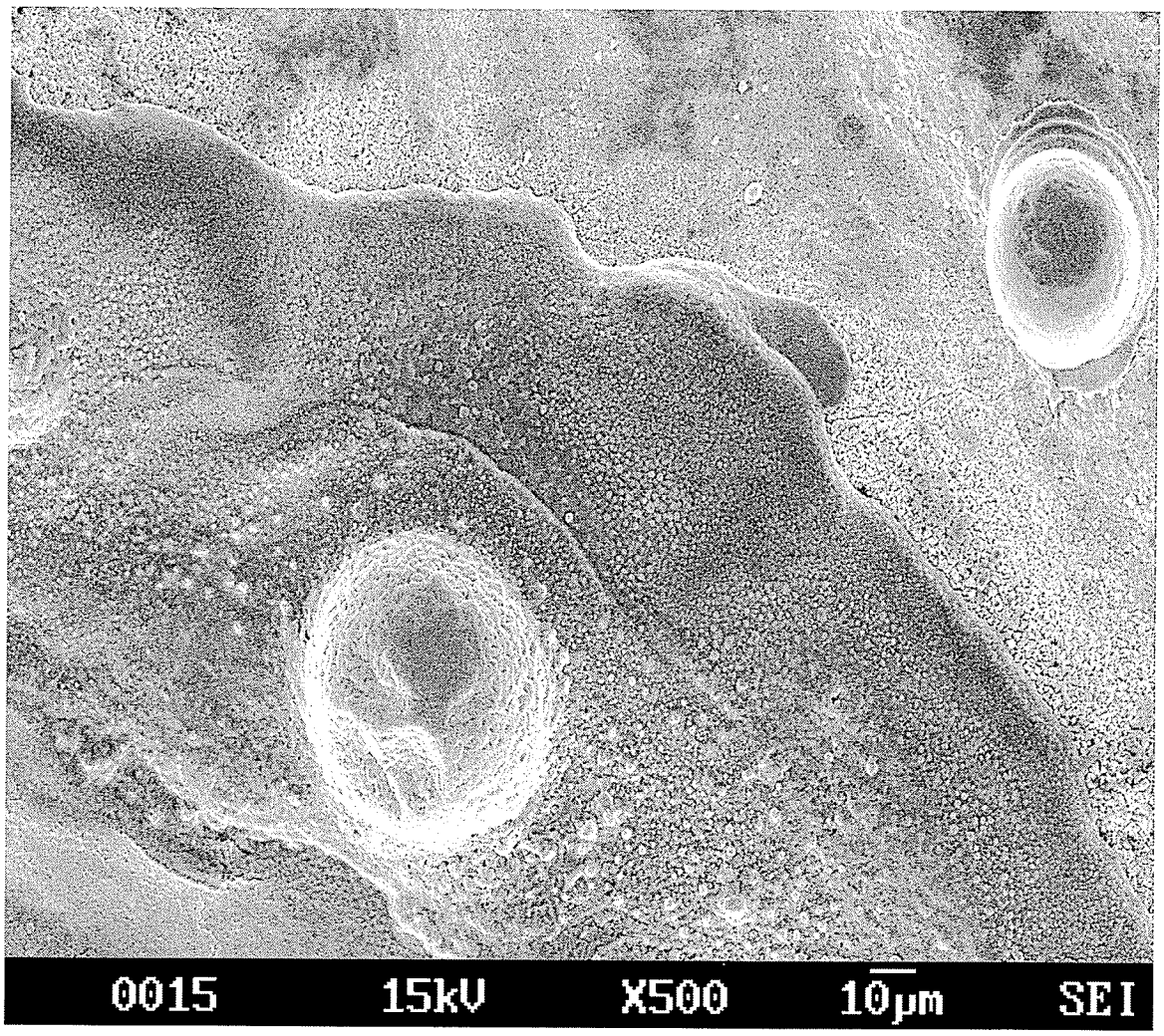

Figure 3.33: High resolution (10 μm) of Area B from Figure 3.29.

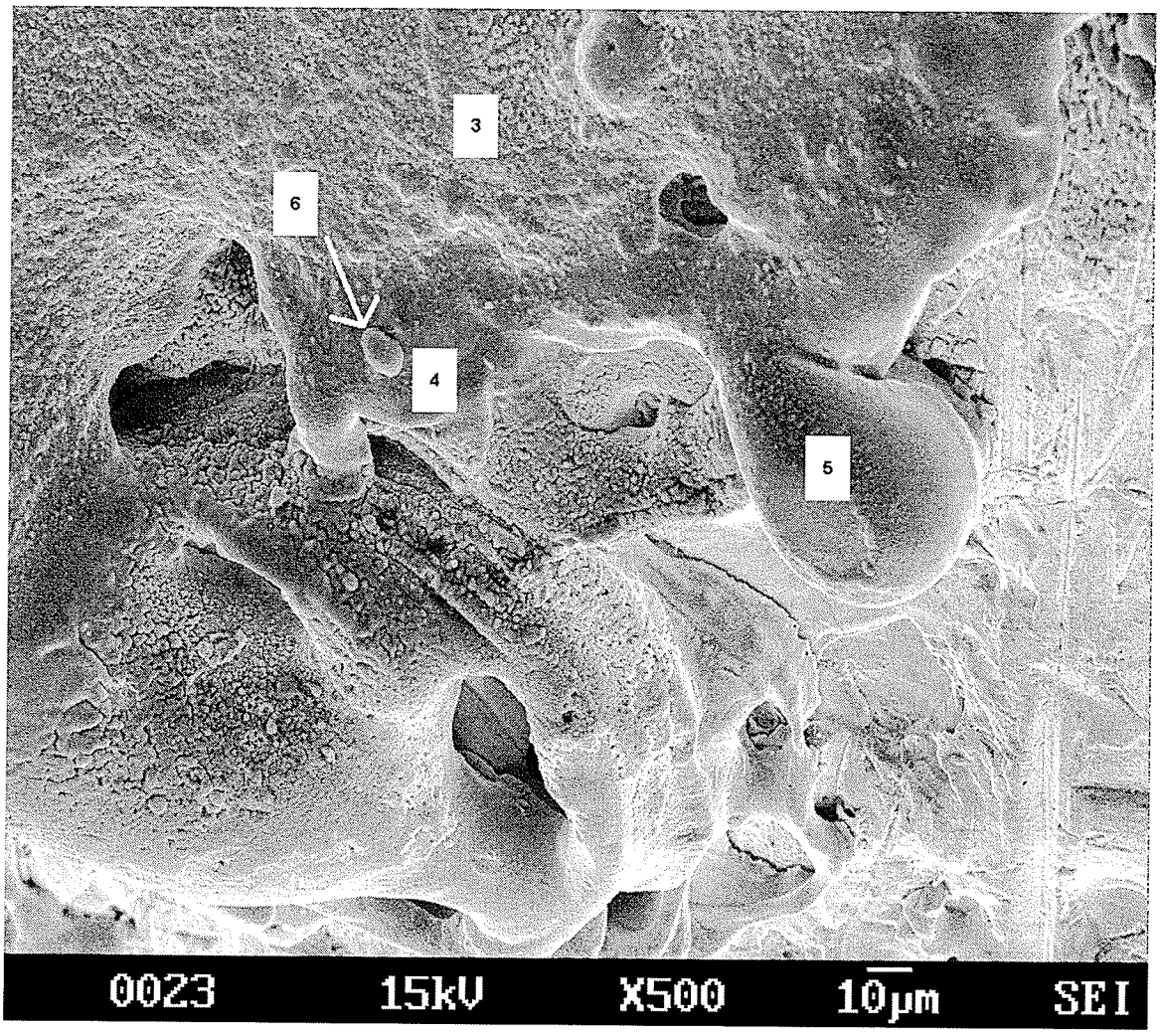

Figure 3.34: High resolution (10 µm) of Area C from Figure 3.29.

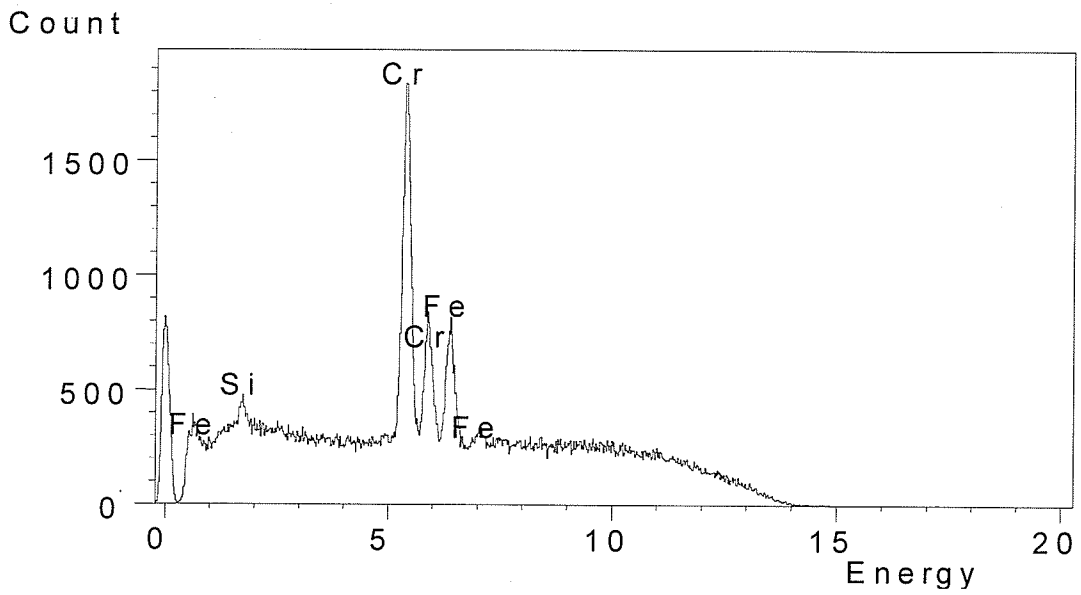

Figure 3.35: ED-XRF spectra of Area 3 from Figure 3.34.

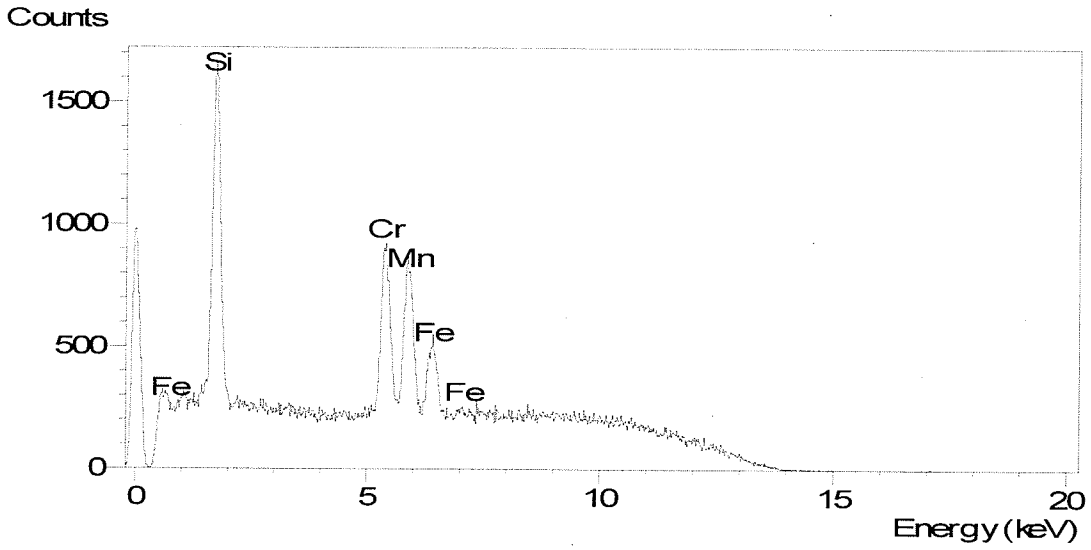

Figure 3.36: ED-XRF spectra of Area 4 from Figure 3.34.

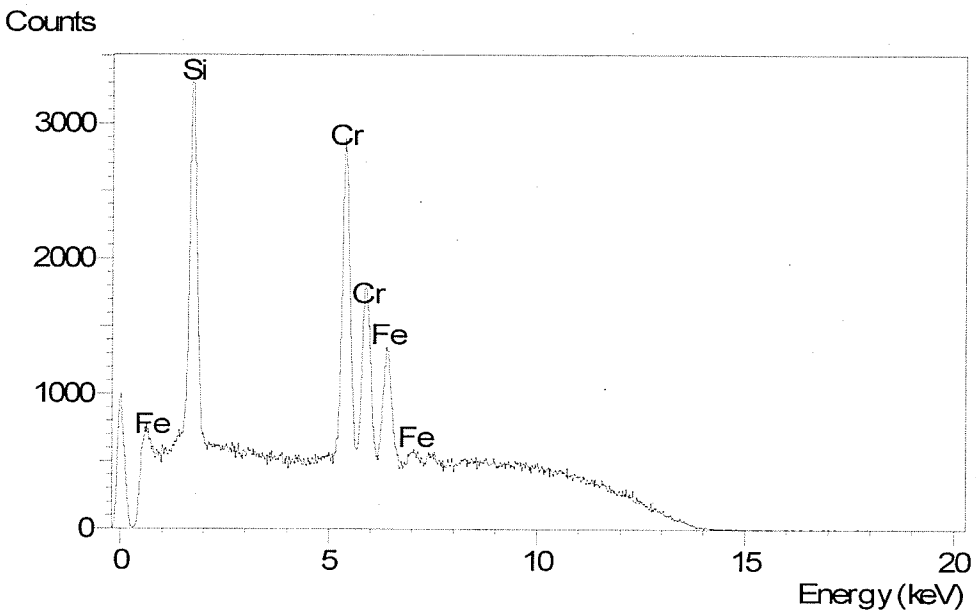

Figure 3.37: ED-XRF spectra of Area 5 from Figure 3.34

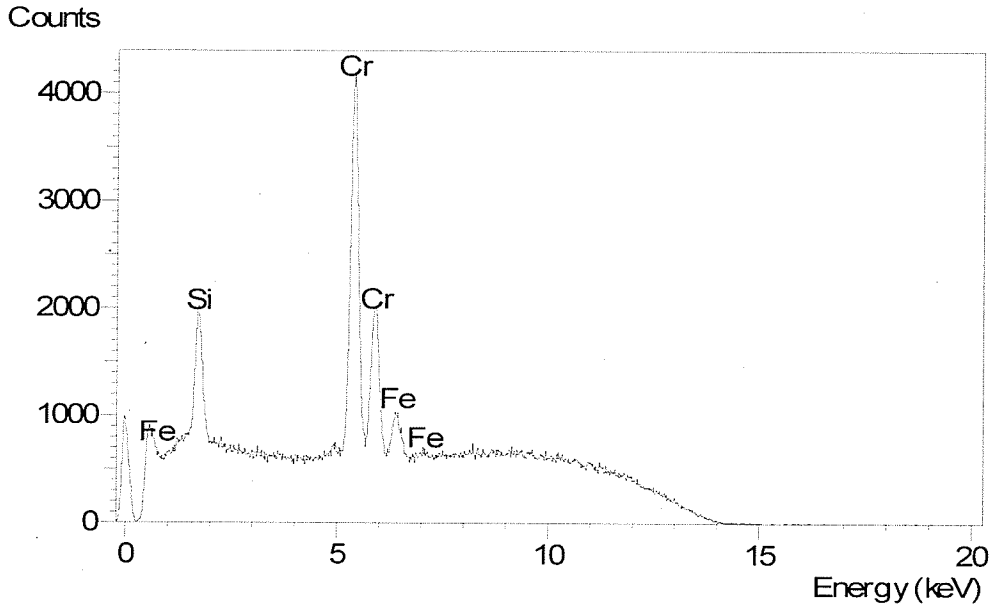

Figure 3.38: ED-XRF spectra of Area 6 from Figure 3.34.

Low-powered spark ablation (<1 A cm^{-2}) was performed for a 60 s period and investigated by SEM and ED-XRF. Figure 3.39 shows a distinct difference between this technique and high-powered spark ablation. Here, ablation appears to be more homogenous, and as a result sampling is probably better controlled. The pitting is less severe and distinctive ablation zones can be identified (Areas D through F). Sparking was concentrated around Area F. The vertical striations as seen on the right side of Area D in Figure 3.39, shows the direction of the filing pre-spark for surface preparation of the metal sample before sparking had occurred.

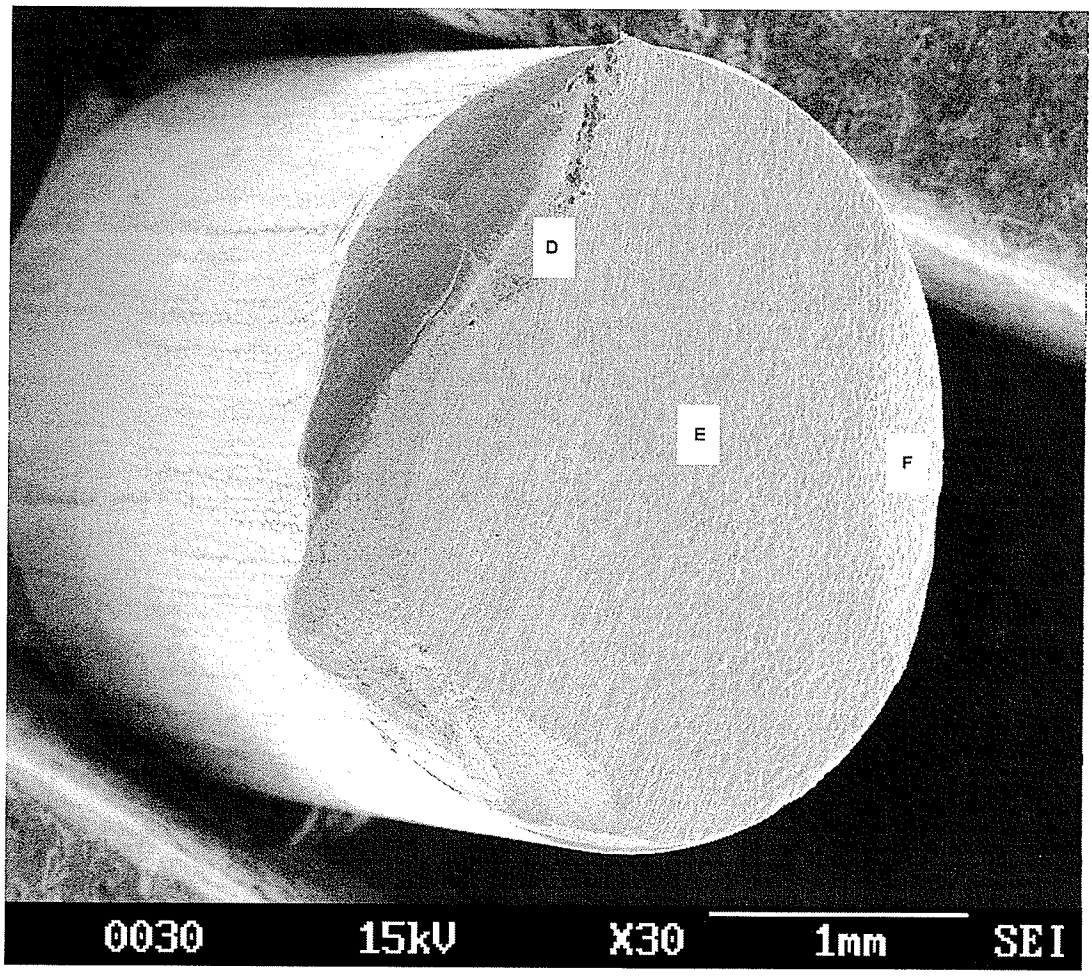

Figure 3.39: Low-powered spark ablation of alloy 308L.

Figure 3.40 is a higher magnification of Area D where 3 distinct interfaces can be seen. Area (i) is a boundary area between a non-sparked surface (dark region) where the metal was previously broken away, and the filed portion of the metal sample. Area (ii) is the boundary interface between the filed area of the metal and the area where sparking occurred.

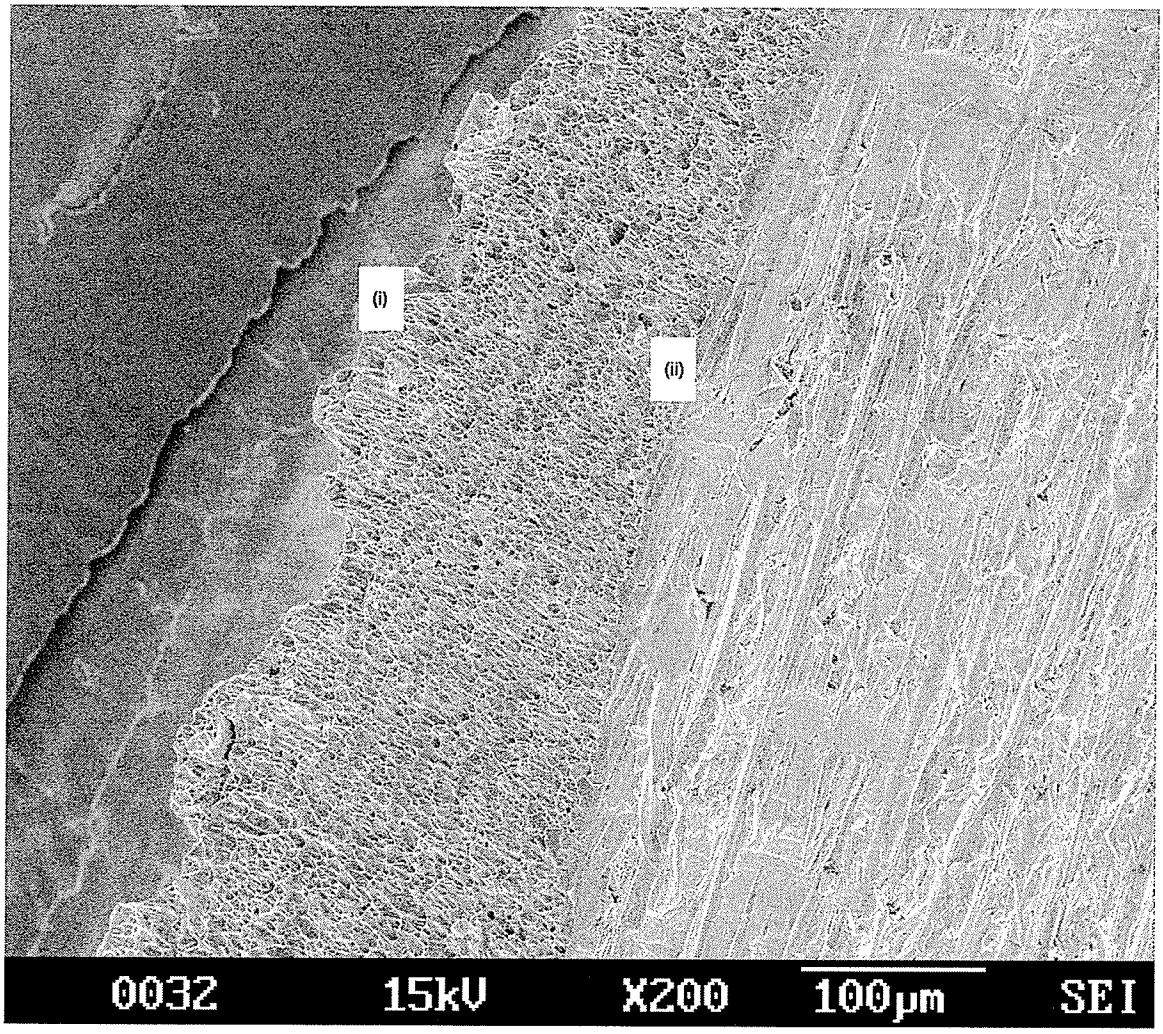

Figure 3.40: Higher magnification of Area D from Figure 3.39.

Figure 3.41 shows the boundary of the sparked region of area E from Figure 3.39 under higher magnification. By the various melted areas, this figure illustrates that there is not only one large crater, but many smaller craters.

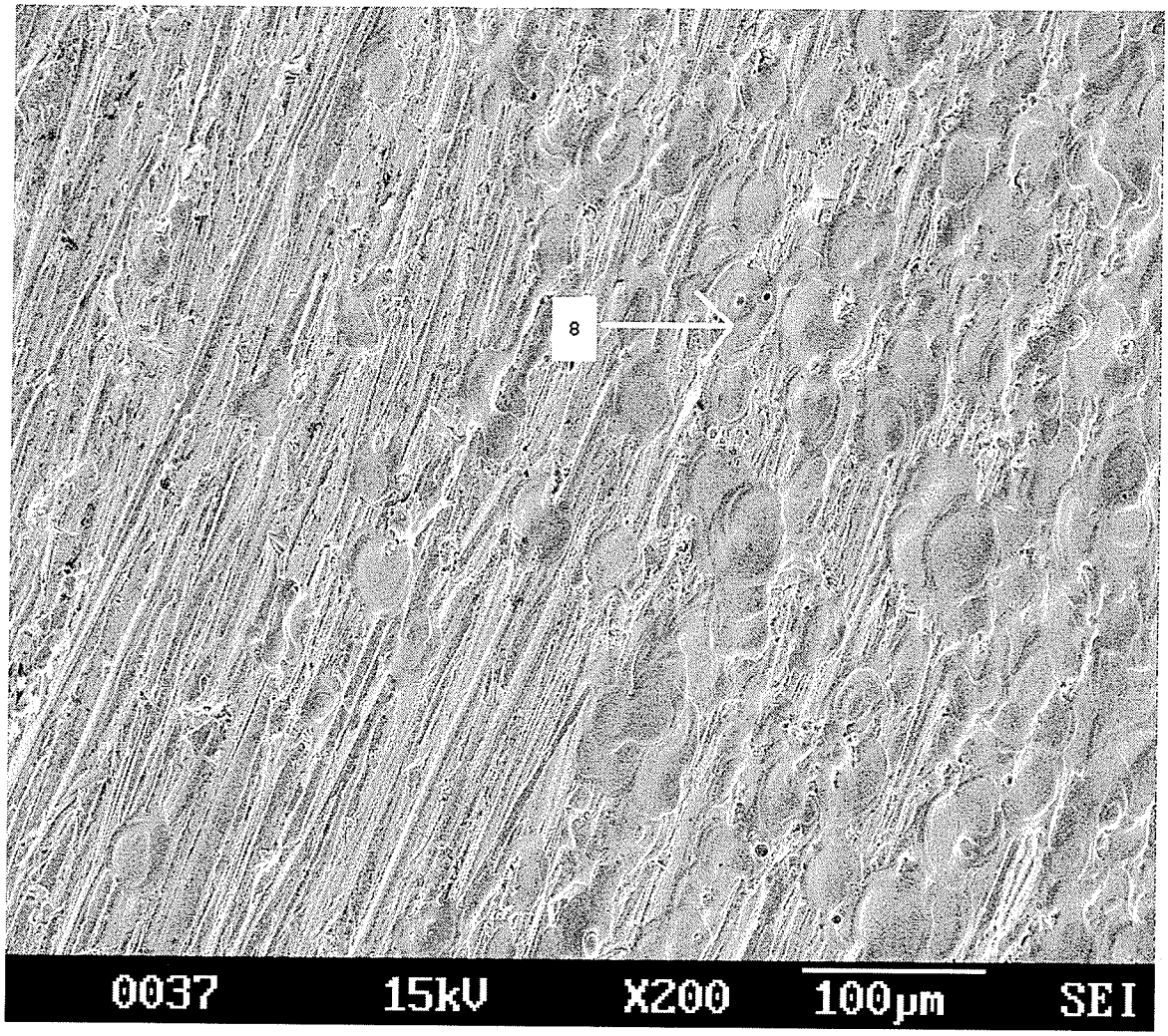

Figure 3.41: Higher magnification of area E from Figure 3.39.

Figure 3.42 shows low-powered spark ablation of alloy 308L, where the most concentrated region of sparking took place (Area F from Figure 3.39). This figure

demonstrates that although low-powered spark ablation was used, melting of the metal is likely occurring, though the pitting is not nearly as deep or severe as with a high-powered spark. Surface characteristics do not show jagged edges and cliffs as seen from high-powered ablation in Figure 3.34. The low-powered spark ablation (Figure 3.39) allows for a more homogeneous sampling of the metal surface, as shown in three distinct regions that have similar ED-XRF spectrographs (Area 8 from Figures 3.41 and 3.42).

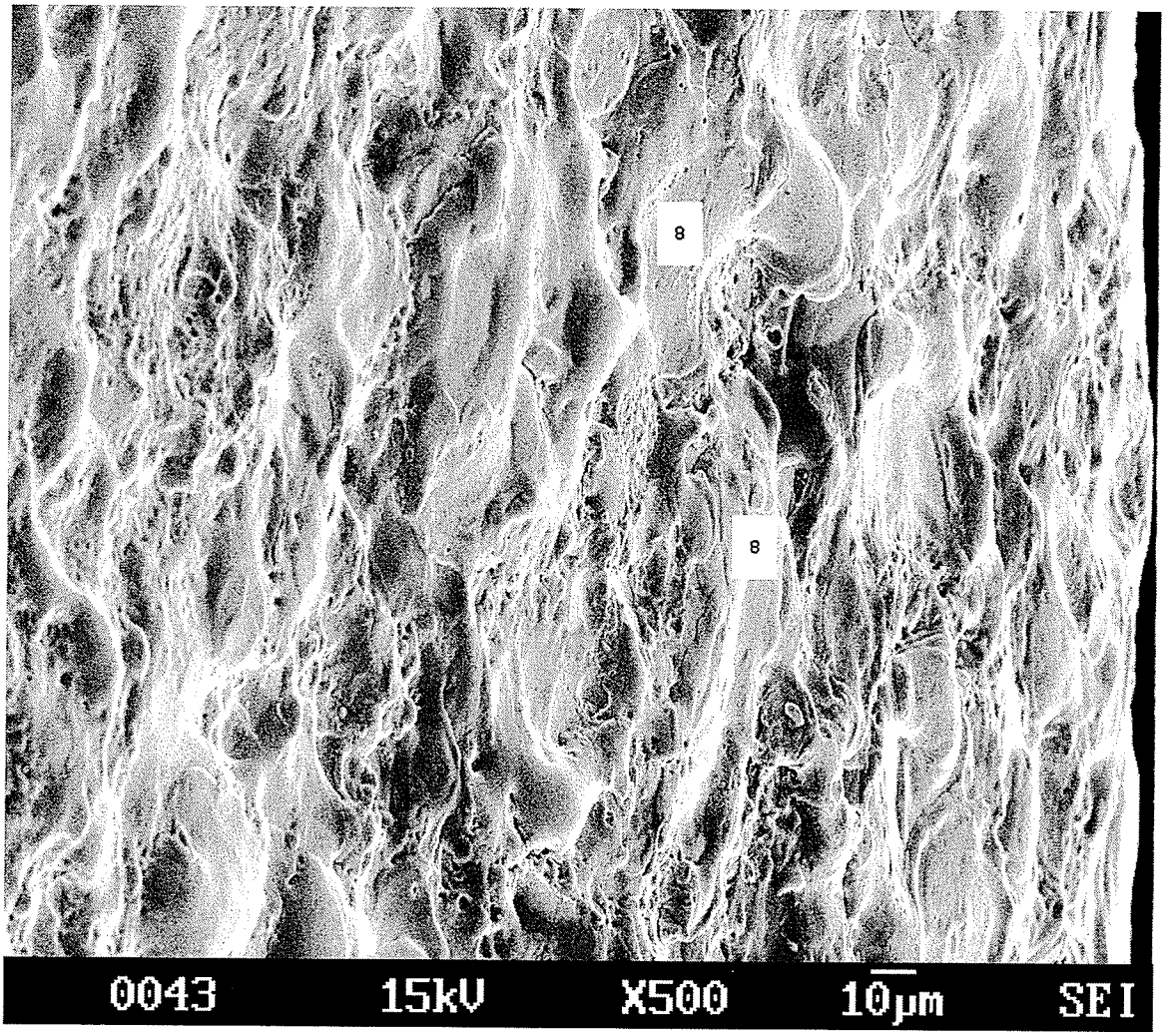

Figure 3.42: High resolution (10 µm) of Area F from Figure 3.3.12.

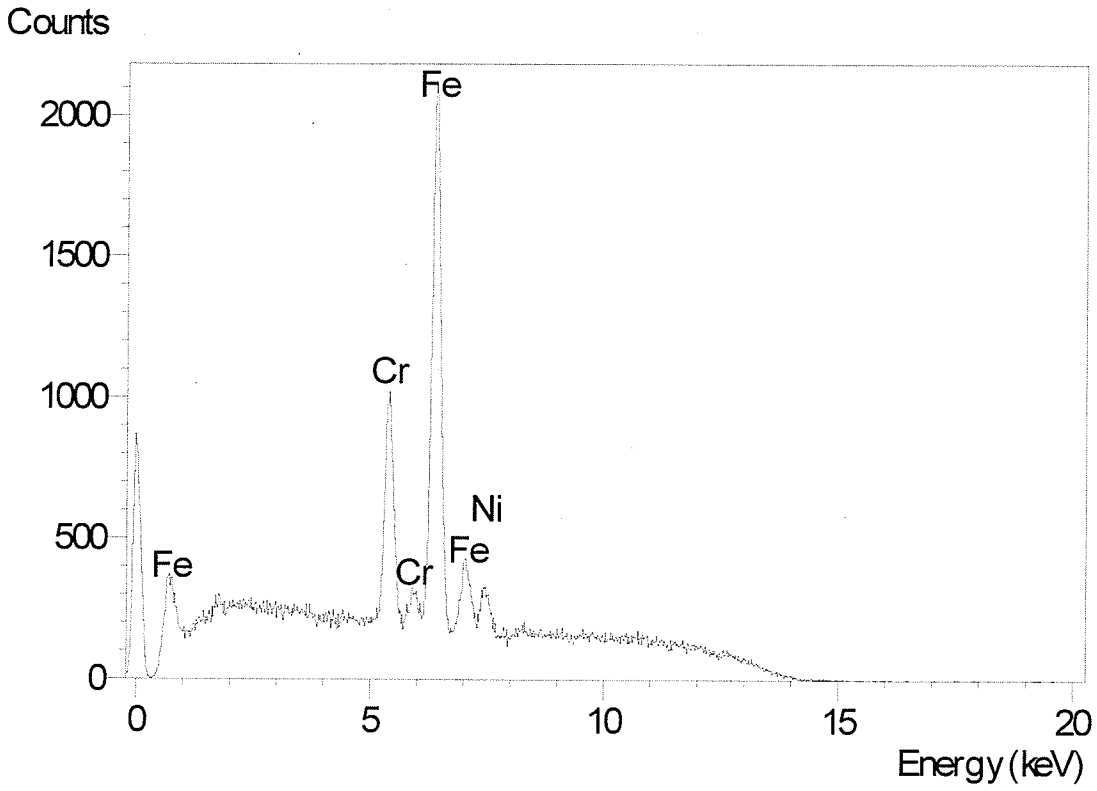

Figure 3.43: ED-XRF spectrogram of Areas 8 from Figures 3.41 and 3.42.

Electrocorrosion was performed on alloy 316L over a period of 5 s at a current of 2.5 A cm^{-2}. Figure 3.44 shows the distinct differences between this technique and spark ablation. Whereas spark ablation focuses energy on a discrete location, electrocorrosion erodes the entire submerged portion of the metal sample. The nature of elemental removal is also contrasted. Here, electrocorrosion removes metal predominantly by redox type reactions, leaving a porous (minute, micro pitting), almost flaky surface. Figure 3.45 shows in high magnification the pores left after electrocorrosion.

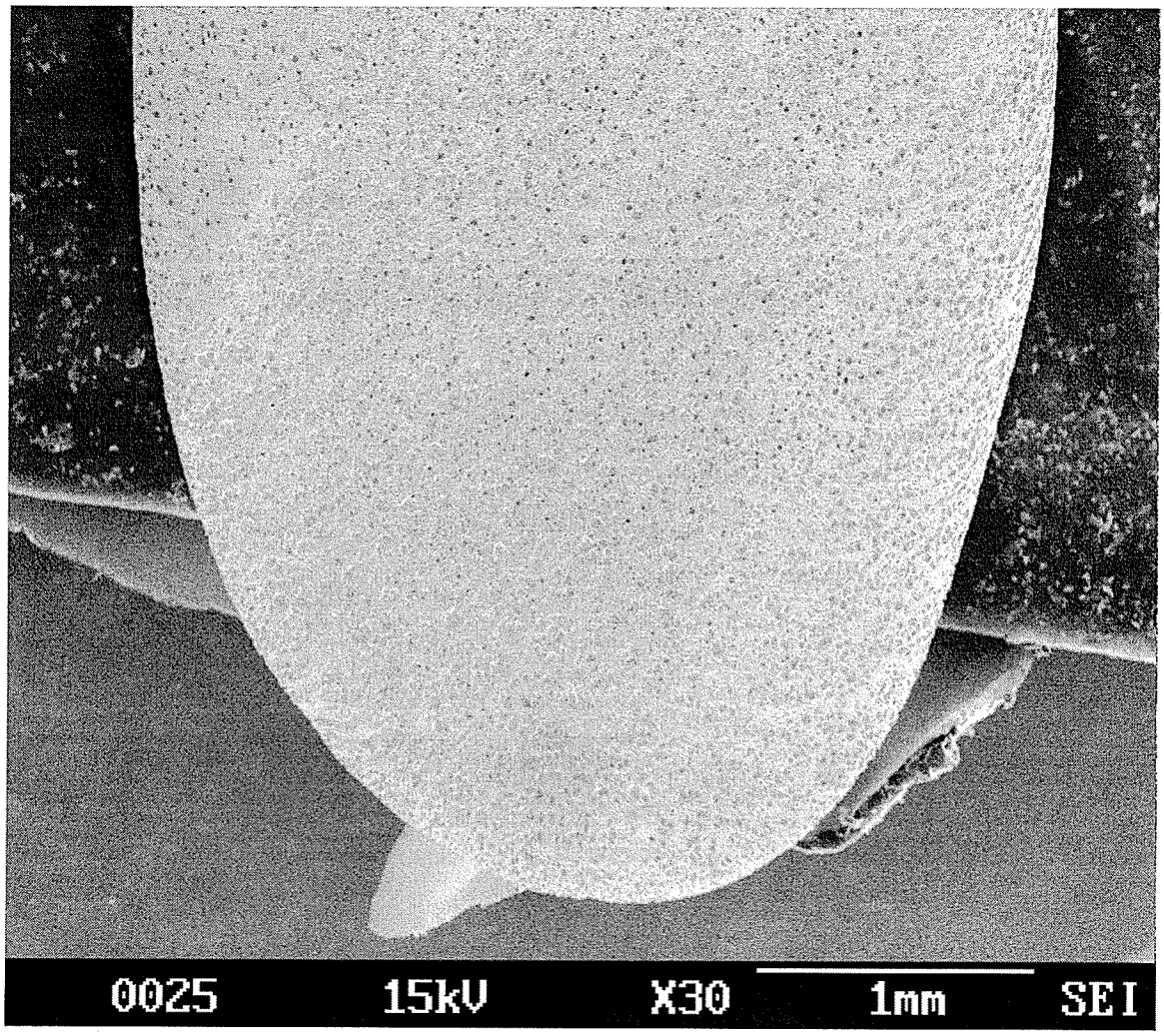

Figure 3.44: Tip of the metal sample (alloy 316L) after electrocorrosion.

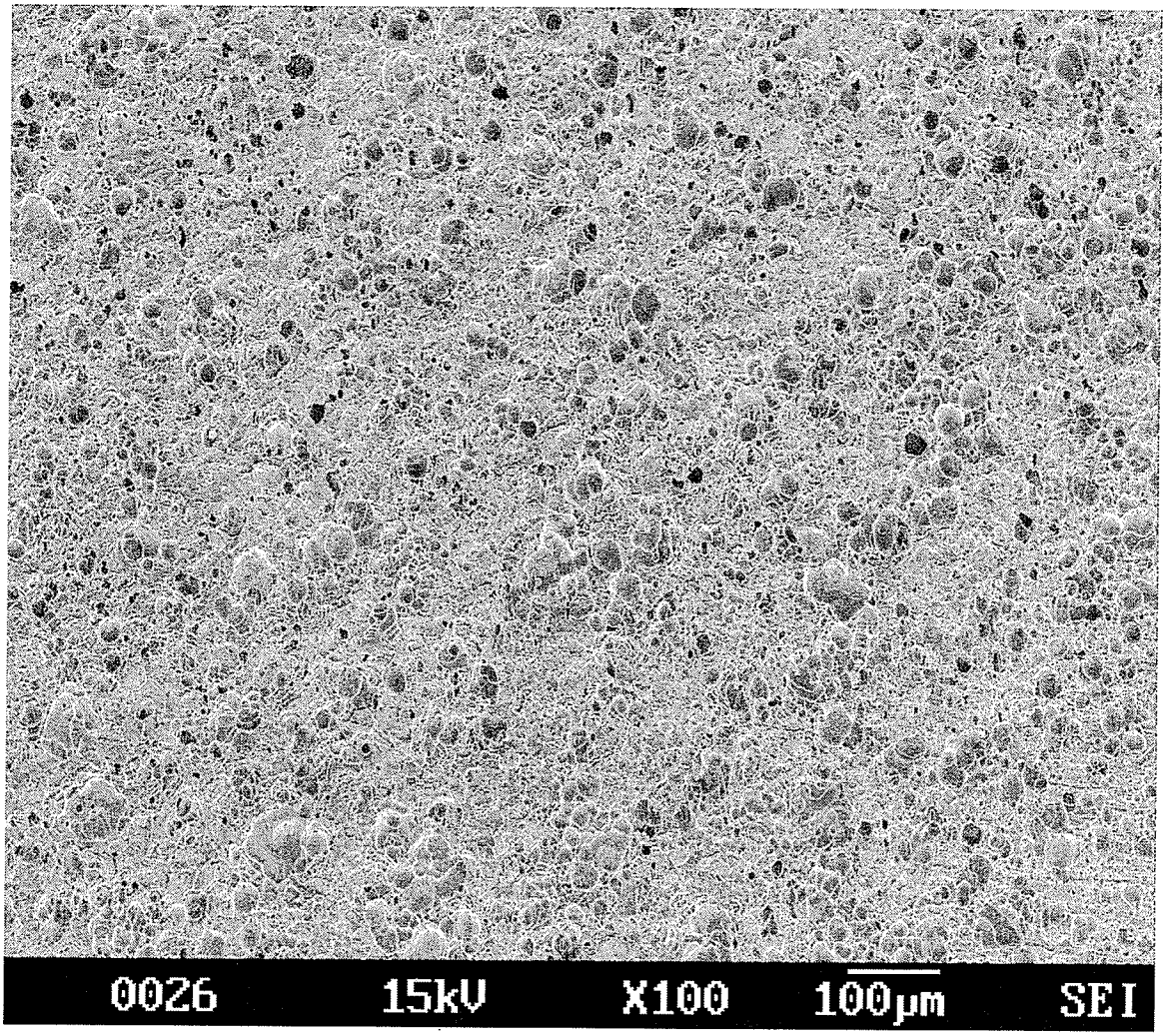

Figure 3.45: Higher magnification of Figure 3.44.

Figure 3.46 shows the highest resolution of Figure 3.44. The uniformity of the surface demonstrates the homogeneity of the sampling. ED-XRF spectra were taken on several different locations with the result shown in Figure 3.47. Due to their similarity, only one spectra, which is representative of all the ED-XRF spectra is shown. The similarity in the ED-XRF spectra of the corroded surface provides further proof of the homogeneous sampling of the metal surface relative to high-powered spark ablation.

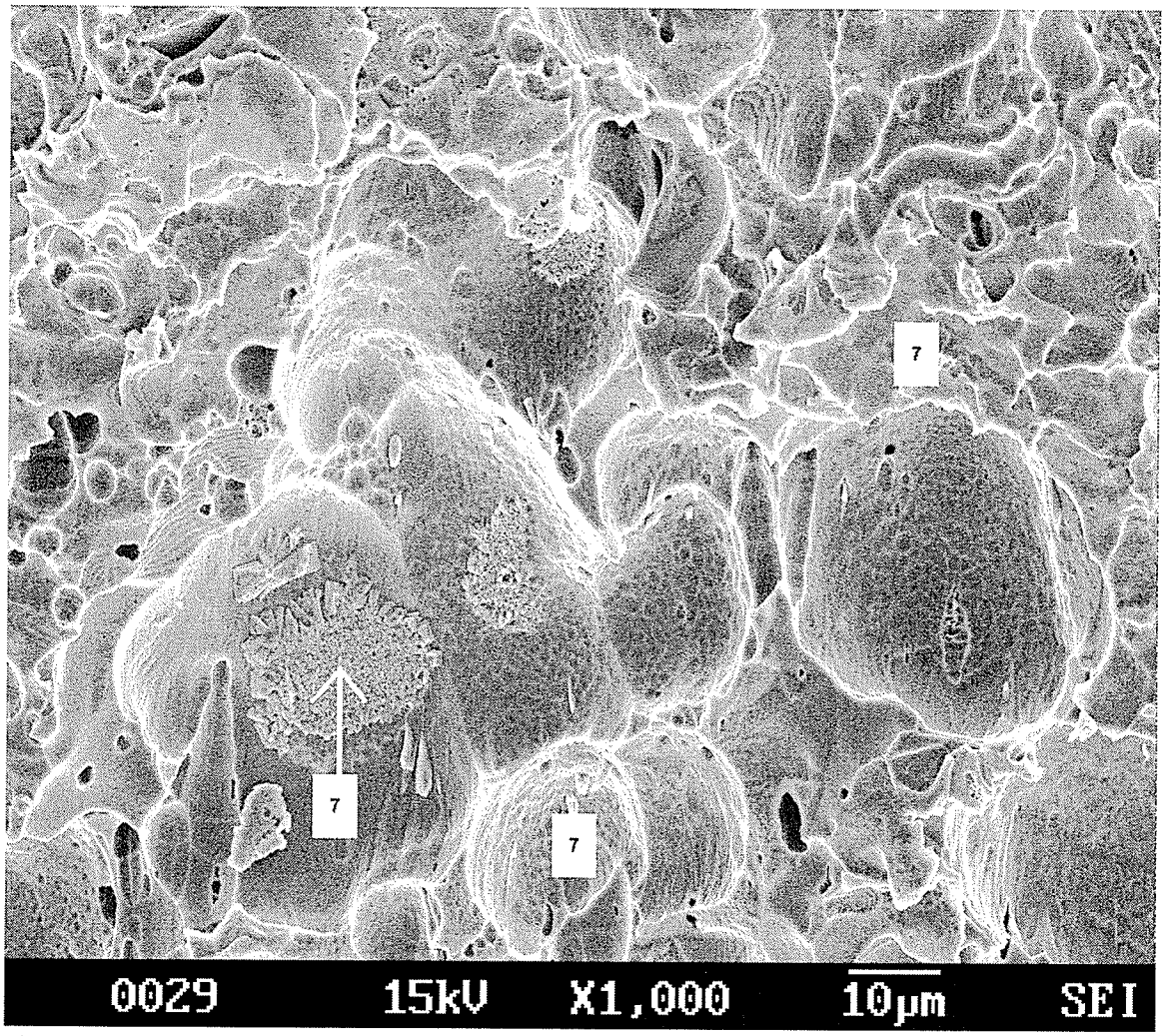

Figure 3.46: High resolution (10 µm) from Figure 3.44.

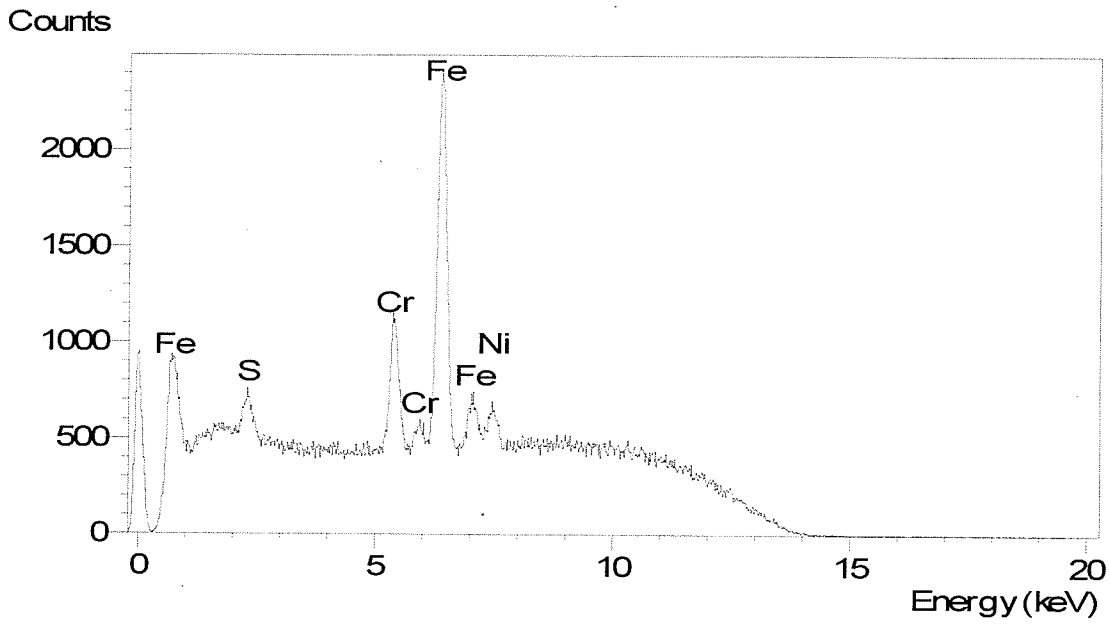

Figure 3.47: ED-XRF spectrograph of Area 7 from Figure 3.46.

Some final comparative observations can be made from the three different techniques. First, it is readily apparent from Figures 3.29 and 3.36 that spark ablation is focused in discrete areas, where ablation occurs primarily as a result of mechanical ablation from the current. Electrocorrosion occurs over the entire submerged portion of the metal sample, where corrosion is based on redox reactions. Metal sample disfiguration is much less apparent with electrocorrosion, especially if long periods of ablation/corrosion are required. Thus for samples where pitting may be prohibited, electrocorrosion may be the technique of choice. Electrocorrosion SEM images also indicate an increase in surface area due to the porosity of the metals surface. This could play a significant role with regards to corrosion rates. In cases where the need for

mechanical ablation is required (e.g. Au), spark ablation is able to ablate materials, and will provide minimal effects of pitting or discoloration.

4.0 Conclusion

Both electrocorrosion and spark ablation are useful alternatives to acid digestion for rapid metal sample preparation in aqueous solution. Electrocorrosion demonstrated deficiencies for corrosion of Au and Rh, as H_2O is easier to oxidize than either metal. Formation of passive layers on certain metals (Ni), could be accredited to the halides in solution. Surface properties of steel after electrocorrosion, as shown by SEM images, demonstrate less pitting and increased surface homogeneity when compared to high-powered spark ablation. Therefore, this technique could be used for samples where discoloration and disfigurement need to be avoided. Future research may focus on utilizing different conductive solutions to overcome passive layer formation on certain elements like Ni. This would make electrocorrosion a technique that can be applied universally to metals.

Spark ablation can be used to dissolve a wide variety of metals in aqueous solution. Quantification of Ag in Au was successfully accomplished by ablation followed by nitric acid addition and subsequent dilution before final analysis by GFAAS. SEM images confirm that large or bulk materials can be ablated in little time by high-powered spark ablation, though pitting and sample disfigurement are observed. Low-power spark ablation can be used for trace elemental work to ablate difficult to oxidize metals (e.g. Au, Rh) with less disfigurement.

5.0 References

1. Somenath M. *Sample Preparation Techniques in Analytical Chemistry* Wiley-Interscience Publisehers: New Jersey, 2003.

2. Whelam N. J. *Can. Metall. Quart.* 2001, **40**, 143.

3. Piippanen T., Jaatinen J., Tummavuori T. *Fresen. J. Anal. Chem.* 1997, **357**, 405. Micro ref.

4. Perez-Jordan D.C., Salvador, A., delaGuaria M. *Anal. Lett.* 1998, **31**, 867.

5. Chakraborty R., Das A.K., Cerva M.L., delaGuardia M. *Anal. Lett.* 1997, **30**, 283.

6. SenGupta J.G., Bertrand N.B. *Talanta.* 1995, **42**, 1947.

7. Wen X.H., Wu L.Z., Zhang Y., Chu Y. *Fresenius J. Anal. Chem.* 1997, **30**, 1111.

8. Fadda S., Rivoldini A., Cau I. *Geostand. Newslett.* 1995, **19**, 41.

9. Borszeki J., Halmos P., Gegus E. *Talanta.* 1994, **41**, 1089.

10. Hinds M.W., Littau S., Moulinie P. *Analyst.* 1990, **117**, 1089.

11. Berglund B., Fernando C. *Anal. Chim. Acta.* 1990, **236**, 399.

12. Granfors M., Gustavsson I. *J. Anal. At. Spectrom.* 2001, **16**, 1439.

13. Loretzen E.M.L., Kingston H.M. *Anal. Chem.* 1996, **68**, 4316.

14. Tuncel S.G., Yenisoy-Karakas S., Dogangun A. *Talanata* 2004, **63**, 273

15. Fujimoto K., Shimura M., Satoh S. *Tetsu. To. Hagane.* 2002, **88**, 285.

16. Yamaguchi H, Itoh S, Hasegawa S, Ide K, Kobayashi T *Tetsu. To. Hagane.* 2004, **90**, 48.

17. Alekseeva T.Y., Malyutina T.M., Karpov Y.A., Lvova T.V. *Indus. Lab.* 1990, **56**, 1181.

18. Potts P.J. *A Handbook of Silicate Rock Analysis*. Blackie Publishing: New York. 1987.

19. Skoog D., Holler F.J., Nieman T.A. *Principals of Instrumental Analysis*. Sauders Golden Publishing: Toronto. 1998.

20. Skoog D., West D.M. *Fundamentals of Analytical Chemistry*. Saunders Golden Publishing: Toronto. 1982.

21. Harris D.C. *Quantitative Chemical Analysis*. W.H. Freeman Publishing: New York. 2003.

22. Christian G.D. *Analytical Chemistry*. Wiley Publishing: Toronto. 1994.

23. Potts P.J. *A Handbook of Silicate Rock Analysis*. Blackie Publishing: New York. 1987.

24. Goltz, D. M., Kostic, G., Reinfelds, G. *Talanta.* 2000, **52**, 1131.

25. Goltz, D. M., Hinds, M., Coombs, J., Jagdeo, A., Craig, D. *J. Anal. Chem.* 2002, **17**, 395.

26. Maibusch R., Kuss H.M., Coedo A.G., Dorado T., Padilla I. *J. Anal. Atom. Spectrom.* 1999, **14**, 1155.

27. Nakamura Y. *Bunseki Kagaku.* 2000, **49**, 273.

28. Coedo A.G., Dorado T., Padilla I., Fernandez B.J. *Appl. Apectrosc.* 2000, **54**, 1032.

29. Jakubowski N., Feldman I., Stuewer D. *Spectrochim. Acta.* 1995, **50**, 639.

30. Pchelkin A.I., Kharlamov I.P., Gusinskii M.N., Shipova E.V. *Zh. Anal. Khim.* 1987, **42**, 1693.

31. Broekaert J.A.C., Browner R.F., Marcus R.K. *Spectrochim. Acta.* 1995, **50**, 549.

32. Bendicho C. *Fresenius J. Anal. Chem.* 1994, **348**, 353.

33. Coedo A.G., Dorado T., Padilla I., Fernandez B.J. *J. Anal. Atom. Spectrom.* 1195, **10**, 859.

34. Ghiglione M., Eljuri E., Cuevas C. *Appl. Spectrosc.* 1975, **30**, 320.

35. Human H.G.C., Scott R.H., Oakes A.R. West C.D. *Analyst.* **101**, 265.

36. L'vov B.V., Novichikhin A.V. *Atom. Spetrosc.* 1990, **11**, 1.

37. Karyakin V.Y., Kharlamov I.P., Pchelkin A.I. *Zavodsk. Lab.* 1986, **54**, 360.

38. Fowler R.G., Wolfe R.A. *J. Opt. Soc. America.* 1945, **35**, 170.

39. Witke T. Lenk A., Siemroth P. *IEEE T. Plasma. Sci.* 1997, **25**, 758.

40. Wang J., Carey J.M., Caruso J.A. *Spectrochim. Acta.* 1994, **49**, 193.

41. Fairman B., Hinds M.W., Nelms S.M., Penny D.M., Goodall P. *J. Anal. Atom. Spectrom.* 1998, **13**, 233.

42. Brenner I.B., Zander A. Kim S., Hollaway C. *Spectrocim. Acta.* 1995, **50**, 565.

43. Gunther D., Jackson S.E., Longrich H.P. *Spectrochim. Acta.* 1999, **54**, 381.

44. Jiang, S. J., Houk, R. S. *Anal. Chem.* 1986, 58, 1739.

45. Bergamin, H., Krug, F. J., Zagatto, E. A. G., Arruda, E. C., Courinho, C. A. *Anal. Chim. Acta.* 1986, **190**, 177.

46. Flock, J., Ohls, K. *Fresen. Z. Anal. Chem.* 1988, **331**, 408.

47. Tanaka, T., Shitan, H., Konda, H. *Bunseki Kagaku.* 2001, **50**, 855.

48. Gervaio, A. P. G., Caseri, de Luca, G., Meneario, A. A., Filho, H. B., Freire dos reis, B., Goncalves de Sousa, L. *Quim. Nova.* 1999, **22**, 669.

49. Goltz, D. M., Boileau, M. Reinfelds, G. *Spectrochim. Acta.* 2003, **58**, 1325.

50. Silva, J. B. B., Souza, I. G., Gervasio, A. P. G. *Quim. Nova.* 2000, **23**, 482.

51. Ogle, K., Weber, S. *J. Electrochem. Soc.* 2000, **147**, 1770.

52. Kondo, H., Aimoto, M., Ono, A., Chiba, K. *Anal. Chim. Acta.* 1999, **394**, 293.

53. Boileau, M., Goltz, D. M., Hinds, M. *Can. J. Anal. Sci. Spect.* 2004, **49**, 185.

54. Stansbury, E. E., Buchanan, R.A. *Fundamentals of Electrochemical Corrosion.* ASM International, Materials Park: Ohio, 2000.

55. Noel, M. *B. Electrochem.* 1999, **15**, 466.

56. Noel, M., Suryanarayanan, V., Krishnamoorthy, S. *B. Electrochem.*, 2002, **18**, 423.

57. Hummel, R. E., Smith, R. J. *Corros. Sci.*, 1990, **30**, 849.